EXPLORING THE REACTIVITY AND INTERACTIONS OF A POLY(FLUORENE-CO-TETRAZINE)-CONJUGATED POLYMER WITH SWNTS

EXPLORING THE REACTIVITY AND INTERACTIONS OF A POLY(FLUORENE-CO-TETRAZINE)-CONJUGATED POLYMER WITH SWNTS

BY

ALEXANDRA LY, B.SC.

A THESIS

SUBMITTED TO THE SCHOOL OF GRADUATE STUDIES

OF MCMASTER UNIVERSITY

IN PARTIAL FULFILMENT OF THE REQUIREMENTS

FOR THE DEGREE OF

M.SC. IN CHEMISTRY

M.Sc. of Chemistry (2023) McMaster University

(Chemistry and Chemical Biology) Hamilton, Ontario, Canada

TITLE: Exploring the Reactivity and Interactions of a Poly(Fluorene-*co*-Tetrazine)-Conjugated Polymer with SWNTs

AUTHOR: Alexandra Ly

B.Sc. (Integrated Sciences with Chemistry)

Western University, London, Ontario, Canada

SUPERVISOR: Professor Alex Adronov

NUMBER OF PAGES: XXIII, 138

Abstract

Conjugated tetrazine-containing polymers that undergo Inverse Electron Demand Diels-Alder (IEDDA) reactions with *trans*-cyclooctenes are interesting not only for their intrinsic optoelectronic properties, but also their interactions with π-conjugated surfaces. Here, we prepared a series of poly(fluorene-*co*-tetrazine) polymers and carried out IEDDA reactions to decorate them with hydroxyl, hexadecyl, or triethylene glycol side chains. The polymers were investigated pre- and post-IEDDA coupling in terms of their ability to disperse single-walled carbon nanotubes (SWNTs) in organic solvent. It was found that polymer molecular weight, side chain structure, and degree of conjugation all impacted the quality of SWNT dispersions. While the starting poly(fluorene-*co*-tetrazine) polymer produced concentrated dispersions, the post-IEDDA polymer containing dihydropyridazine groups did not produce dispersions of equal concentration. However, upon oxidation to the fully aromatic pyridazines, the polymers regained their ability to form concentrated dispersions. Furthermore, the post-IEDDA polymers exhibited increased selectivity toward metallic SWNTs relative to the starting polymer. In addition, due to the efficiency of the IEDDA reaction, it was possible to perform modification of the polymer-SWNT dispersion formed with poly(fluorene-*co*-tetrazine) to modify the polymer structure while on the SWNT surface. Overall, this work demonstrates the first use of reactive polytetrazines to disperse SWNTs and to rapidly modify the solubility of polymer-nanotube complexes.

Acknowledgements

First and foremost, I would like to thank my supervisor, Dr. Alex Adronov. He took a chance on me, gave me this opportunity, and helped me through a lot of my struggles throughout this degree. He was a constant calm and voice of reason, as well as an endless wealth of knowledge. I have learned so much from him, about chemistry and of life, and will bring many of the lessons I learned in his lab wherever I go. Thank you so much Alex for all your help, I really couldn't have achieved this without you.

Further, I would like to thank Dr. Katherine Bujold. She has been an inspiration to see around campus and wonderful person to have on my committee. Thank you so much for all your insight and the encouragement you brought to my degree.

Additionally, I would like to thank the Ontario Graduate Scholarship program for providing me with funding to make this work possible.

A humongous thanks goes to all of the members of the Adronov group, as well as my fourth-floor friends. From the Tim's runs to blasting music in the lab, the last two years would not be possible without the help and friendships I have forged at McMaster. A special shoutout goes to Billy Deng and Dr. Dialia Ritaine. Both of you have encouraged me and helped me through problems, in and out of the lab. Thank you from the bottom of my heart.

Other friends outside of the lab I want to thank are my best friend Sarah and my Haddon girls, Areeba, April, Noor, Beth, and Bella. Thank you for being there for me when I needed it most.

On a much more personal note, thank you Mom, Dad, Aaron, and Cooper for giving me unconditional love. Though it gets boring for me to rattle off about my research, you still pretended it was interesting and supported me through my university degrees. I could not have come this far without you.

And last but certainly not least, thank you to my love, Vinny. Words cannot begin to describe how thankful I am to have you in my life. But thank you for always being there for me, providing me with love and support. Thank you for patiently helping me with everything, big or small. And thank you for trying to stay awake whenever I worked until 5 am and for being beside me even when you couldn't!! I can't wait for the next chapter in our lives and our endless brunches in the future.

Table of Contents

List of Abbreviations

1D	One-Dimensional
2D	Two-Dimensional
3D	Three-Dimensional
θ	Chiral Angle
µm	Micrometer
AFM	Atomic Force Microscopy
Ar	Argon
BARAC	Biarylazacyclooctynone
BWF	Breit–Wigner–Fano
CD	Circular Dichroism
C_h	Chiral Vector
CH_2Cl_2	Dichloromethane
CP	Conjugated Polymer
CuAAC	Cu-catalyzed Alkyne-Azide Cycloaddition
CV	Column Volume
Đ	Dispersity
D-A	Donor-Acceptor
DGU	Density Gradient Ultracentrifugation
DI	Deionized
DIBAC	Dibenzoazacyclooctyne
DIBO	Dibenzocyclooctyne
DMSO	Dimethylsulfoxide
DNA	Deoxyribonucleic Acid

DOS	Density of States
DP	Degree of Polymerization
d_t	Diameter
EDG	Electron-Donating Group
EtOAc	Ethyl Acetate
EtOH	Ethanol
EWG	Electron-Withdrawing Group
FET	Field Effect Transistor
FTIR	Fourier Transform Infrared
GPC	Gel Permeation Chromatography
h	Hour
HiPco	High Pressure Carbon Monoxide
HOMO	Highest Occupied Molecular Orbital
Hx	Hexanes
IEDDA	Inverse Electron Demand Diels-Alder
LUMO	Lowest Occupied Molecular Orbital
m-SWNT	Metallic Single-Walled Carbon Nanotube
MeOH	Methanol
min	Minute
M_n	Number-Average Molecular Weight
M_W	Weighted-Average Molecular Weight
N_2	Nitrogen
nm	Nanometer

(n,m)	Integer Lattice Translations Indices for SWNTs
NMR	Nuclear Magnetic Resonance
OPV	Organic Photovoltaic
PL	Photoluminescence
PPP	Poly(p-phenylene)
PPV	Poly(phenylene vinylene)
PTFE	Polytetrafluoroethylene
RBM	Radial Breathing Mode
RRS	Resonant Rayleigh Scattering
rt	Room Temperature
sc-SWNT	Semiconducting Single-Walled Carbon Nanotube
S_NAr	Nucleophilic aromatic substitution
SPAAC	Strain-Promoted Alkyne-Azide Cycloaddition
SWNT	Single-Walled Carbon Nanotube
TCO	*trans*-Cyclooctenes
TEG	Triethylene Glycol
TGA	Thermogravimetric Analysis
THF	Tetrahydrofuran
UV-Vis-NIR	Ultraviolet Visible-Near-Infrared

List of Tables

List of Figures

List of Schemes

Chapter 1: Introduction

1.1. Introduction of Conjugated Polymers (CPs)

Synthetic polymers have been an ever growing and diverse field of innovation since the early 1900s.[1] Conjugated polymers (CPs), in particular, have been proven to be extremely relevant to many kinds of technologies and applications,[2] including organic photovoltaics (OPVs),[3,4] field effect transistors (FETs),[5,6] and sensors,[7,8] amongst many others. CPs may be defined as a class of polymers that exhibit an alternating sequence of single (σ) and double (π) bonds along their backbone.[9,10] The delocalized valence electrons within this π-conjugated system gives rise to the optoelectronic properties unique to CPs, and can be easily modified through structural changes, such as reduction and oxidation of the polymer chain.[11] Much of the focus and efforts regarding CPs has been around the development of structural diversity, expansion of synthetic approaches, and new applications. Further understanding of CP properties has been accomplished through exploration of novel polymer structures. However, it is limited by and tightly connected to the advancements of synthetic methods. The study of CPs has grown in complexity, as factors such as molecular weight and distribution contribute to both their mechanical and chemical properties. The already vast field of CPs only grew with the addition of heteroatoms to polymer composition where numerous studies have expanded these classes of CPs, such as polyaniline, polypyrrole, polycarbazole, and polythiophene. Meanwhile, other broad classes of CPs, such as poly(p-phenylene), poly(p-phenylene vinylene), polyacetylene, and polyfluorene, still garner much attention (Figure 1.1).[12] Their incorporation into flexible and stretchable materials such as thin films,[13,14] coatings,[15,16] and textiles[17–19] has allowed for the wide-spread usage of CPs in material sciences and industry.

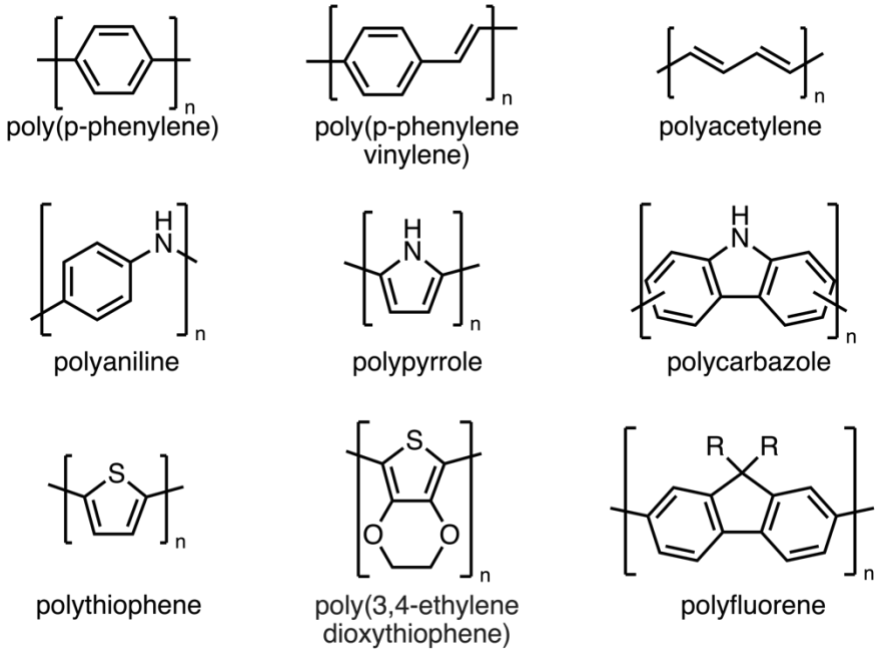

Figure 1.1. Structures of common conjugated polymers.

1.2. History and Classes of Conjugated Polymers

1.2.1. Discovery of Polyaniline

Though the start of synthetic polymers is often attributed to Bakelite, it is argued that the first fully synthetic polymer was also the first conjugated polymer, polyaniline.[20] The confusing and debated origins of CPs is due to the discovery of these materials predating the techniques necessary to elucidate their structure and the late acceptance of polymers as a concept in the 1920s.[1] Polyaniline was first prepared in the early 1800s as aniline salts through treatment of copper oxide or chromic acid and are readily produced through oxidative polymerization.[21] The earliest accreditation of polyaniline work goes to Friedlieb Ferdinand Runge in 1834 after he isolated aniline salts from a volatile oil from coal tar.[22] He further oxidized the material to obtain black insoluble dyes which would later be identified as polyaniline. Around the 1860s, Frederick Crace-Calvert, Samuel Clift, and their assistant Charles Lowe would commercialize Runge's findings, and oxidize aniline salts through potassium chlorate to yield dyes that could be altered

with the application of a base solution.[23] Towards the end of the 1860s, printers Wood and Wright would apply their methods and improve them to yield an almost black dye which would coincide with John Lightfoot's discovery of "aniline black", a term he coined for a black dye used in textiles.[21,24] It wouldn't be until the 1910s that the structure of polyaniline would be determined,[25,26] and an additional 50 years later for Jazefowics and coworkers to discover that polyaniline containing materials could be conductive, ranging from 10^{-5} to 10 S/cm.[9] Polyanilines remain a class of interest due to their highly conductive nature, simplicity of preparation, and easily modified properties.[27]

1.2.2. Discovery of Polypyrrole

Polypyrroles were another class of polymers disovered earlier in CP history. In 1915, Angelo Angeli worked on a dark precipitate he termed "pyrrole black" as it was the product of treating pyrrole with hydrogen peroxide/acetic acid mixtures.[28] He later found that pyrrole black was achievable through a variety of oxidizing agents and concluded it was in fact the result of pyrrole polymerization.[29] In 1921, Riccardo Ciusa thermally polymerized tetriodopyrrole to prepare a black graphitic-like material, however he only reported the appearance and elemental composition.[28] He never studied the resistivity of the pyrrole-based heterocyclic graphites, and 40 years would pass before Donald Eric Weiss would explore the conductivity of pressed polypyrrole pellets. He would find that polypyrroles outperformed all known non-pyrolyzed polymers at the time and would obtain a conductivity of 0.005 – 0.09 S/cm.[30] In the 1960s at the University of Parma, Luigi Chierici, Gian Piero Gardini, and Vittorio Bocchi would aim to further Angeli's previous work, leading to the formation of a laminar film of polypyrrole through electrolysis and obtaining conductivities of 7.54 S/cm.[31] Eventually, Arthur Diaz at IBM would pick up the torch

in the 1970s and through improvements on purity and quality of much thinner films, he would report conductivities ranging from 10 – 100 S/cm.[28]

1.2.3. Discovery of Polyacetylene

One of the most famous classes of CPs are polyacetylenes, though not without reason, as it would eventually lead to a Nobel Prize in 2000. Its discovery dates back to 1866, when the first known polymerization of acetylene was reported by Pierre Eugène Marcellin Berthelot as a three-dimensional material named *cuprene.*[32] Linear polyacetylene wouldn't be achieved until Giulio Natta in 1955 through the catalytic polymerization of gaseous acetylene with a triethylaluminum and titanium(IV) into a black crystalline material.[32–34] During the mid-1960s Masahiro Hatano and Sakuji Ikeda would develop methods to control cis/trans ratios through temperature modulation in an effort to produce highly crystalline polyacetylenes.[35] Hideki Shirakawa would join Ikeda's group in 1966, and in 1967 would unintentionally aid Hyung Chick Pyun in achieving Hatano and Ikeda's goal. A miscalculation of catalyst by 1000 fold would rapidly generate silvery plastic films at the air-solvent interface and vessel sidewalls.[35] This would lead to Shirakawa being able to reproduce these lustrous highly-crystalline films with conductivities of 10^{-9} – 10^{-4} S/cm. Later, he would collaborate with Alan Graham MacDiarmid and Alan Jay Heeger in 1976 to significantly improve the conductivity of these films through "chemical doping" by exposure to I_2 vapour.[36–38] The doped films would increase in conductivity by six orders of magnitude, rivaling metals in performance, and could be further improved if doped with AsF_5.[39] Shirakawa, MacDiarmid, and Heeger would eventually go on to win the 2000 Nobel Prize for *the discovery and development of electrically conductive polymers* in regards to their work on polyacetylene.[36]

1.2.4. Modern Developments of Conjugated Polymers

The impact of the Nobel prize winning work has led to the development of many more classes of conjugated polymers; from polythiophene in the 1980s to the modern CPs based on polyphenylenes, poly(phenylene vinylenes), polyfluorenes, polycarbazoles, and many other derivatives.[11,40,41] The discovery of these derivatives have been influenced by application development demands, with side chain and backbone engineering targeting different properties. Side chain design has mostly been focused in the alteration of mechanical properties or self-assembly packing of CPs.[42–48] Backbone modification developments are not only centered on tuning optoelectronic properties, such as bandgaps, absorption/emission wavelengths, and conductivity, but mechanical properties based on backbone packing and rigidity as well.[49–54] However, as discussed in Section 1.1, the development of CPs is tightly connected to the advancements of synthetic methods. Thus, the conversation within the field has been surrounding the enhancement of the polymer synthesis toolkit. Metal-mediated cross-coupling polymerization methods like Suzuki, Kumada, Sonogashira, Heck, and Stille couplings, as well as pseudo-living chain-growth polymerizations, have given us the ability to synthesize polymers of various backbones, structures, and properties.[55–61] With well-defined, block-copolymers, and regioregular polymers no longer out of reach, applications in photovoltaics, plastic electronics, and nanophotonics have only improved.[62–65]

1.2.5. Developments in New Conjugated Polymer Classes

The expansion of new CP classes developed from enhanced synthetic methods is vast, with designs and applications much more complicated than the original polyaniline, polypyrrole, and polyacetylene. The most popular of the modern conjugated polymer classes are polythiophene,

poly(p-phenylene), poly(phenylene vinylene), and polyfluorene.[66] Polythiophene is of great interest in device applications and has been extensively studied using theoretical and experimental approaches.[67–72] The ability to substitute side chains and improve solubility has allowed for the preparation of processable high molecular weight polythiophenes.[73,74] Studies have also been focused in improving the regioregularity of the side chains or to impart self-assembly, as both factors heavily improve electronic and optical functionalities.[75,76] Kobayashi and coworkers found that a regioregular poly(3-alkylthiophene-2,5-diyl) film was 15 times more conductive than its regiorandom counterpart.[77] Due to its outstanding conductivity, amongst other notable properties, polythiophene has been used in conductive coatings,[78,79] sensors,[80–82] and field effect transistors.[83,84]

Poly(p-phenylene) (PPP) and poly(phenylene vinylene) (PPV) are another two classes of polymers that have excited the interests of the polymer community.[85–89] PPP are rigid, highly stable polymers that are insoluble if not functionalized. However, developments in solubility with side chain engineering and the discovery of metal-catalyzed Suzuki aryl coupling has allowed for the preparation of high molecular weight polymers. PPV addresses the stability issues of polyacetylene and extreme rigidity of PPP, as it can be considered the structural intermediate class of the two. PPV-based materials exhibit both p and n doping properties, and the optical properties can be influenced by conformational factors. Given its fluorescence, electron-donor character, and hole transporting ability, PPV has been used in sensors with carbon nanostructures,[89–91] photovoltaic devices,[92] and light-emitting diodes.[93]

Another class of polymers of interest is polyfluorenes. It is a prototypical “hairy-rod” conjugated polymer as it contains a rigid backbone with a dense system of side chains.[94,95] This is due to its ability to undergo a facile substitution at the bridging methylene group, thus introducing

alkyl groups and other side chains without influencing the conjugation of the polymer chain. They are typically prepared by Suzuki–Miyaura-type polycondensations and are the most promising polymer class in light emitting diodes. The rigid biphenyl backbone enhances conjugation, resulting in a large bandgap and imparting interesting optical properties.[96–99] It is mainly the tunability of the emission that makes this easily modified class of polymers applicable towards light emitting diodes. Interestingly, polyfluorenes have recently garnered interest with applications concerning single-walled carbon nanotubes (SWNTs). The separation, purification, and processability of SWNTs poses a significant challenge for their use in electronics. The dispersion of SWNTs using CPs has potential in addressing these issues and been accomplished with PPV and poly(3-dodecylthiophene) derivatives.[89,100] Polyfluorenes in particular have demonstrated superior selectivity for sc-SWNTs when mixed with HiPCO SWNTs.[101,102] Further research and development in the scalable purification of SWNTs remains an important topic in the polymer community.

1.3. Introduction to Single-Walled Carbon Nanotubes (SWNTs)

Since their discovery 30 years ago, interest in single-walled carbon nanotubes has continued to skyrocket.[103] SWNTs are cylindrical one-dimensional carbon allotrope with unique optoelectronic[104,105] and physical properties, such as high conductivity[106–108] and mechanical strength.[109,110] They notably have a high-aspect ratio with diameters (d_t) on the nanometer scale and lengths on the micrometer scale. The diameters can range from ~0.4 – 3 nm depending on the method of production. Their wide variety of applications span from transparent flexible electronics,[111] nanoprobes and sensors,[112] conductive inks,[113,114] and field-effect transistors,[111,115,116] to numerous others. The distinction of *single-walled* carbon nanotube arises

from the distinction of these nanostructures from other nanotube species, namely the significantly larger multi-walled carbon nanotubes.[117]

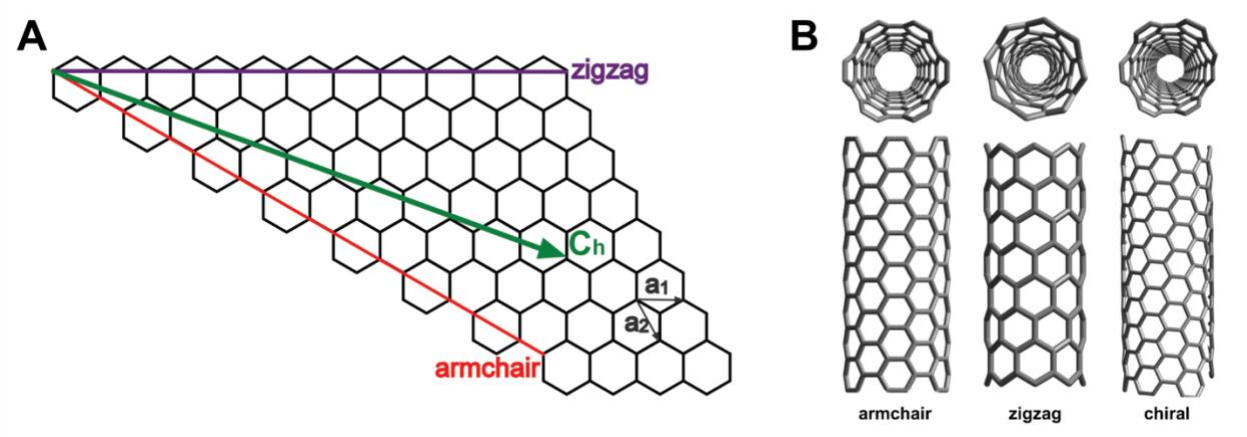

Figure 1.2. A) Graphene template with labelled chiral vector (C_h green), chiral angle (θ, blue), unit vectors a_1 and a_2 (black). a_1 and a_2 with the n and m integer values define the C_h. Armchair and zigzag SWNT are labeled in red and purple, respectively. B) Nanotube species and cross-sections.

The structure of SWNT can be described as a seamless cylinder resulting from a 2D sheet of graphene being rolled up. Different species of SWNTs will arise according to the "rolling" direction (Figure 1.2). The chiral vector (C_h, green arrow) connects the two endpoint carbons together as if they are superimposed upon each other. In conjunction with the chiral angle (θ, blue arrow), the C_h represents the circumference and chirality of a SWNT species.[118] The C_h is determined by the unit cell vectors, a_1 and a_2, of the rolled graphene sheet where they are defined by using integer values n and m (n,m) per Equation 1.1.

$$C_h = na_1 + ma_2 = d_t\pi \quad (1.1)$$

Except for two cases, all SWNTs are chiral. This is due to the hexagonal symmetry in the graphene lattice. The chiral angle lies between 0 – 30° with the two extremes representing a

completely symmetrical SWNT at m = 0 (θ = 0°) or n = 0 (θ = 30°). The former is known as a "zigzag" nanotube, while the latter is an "armchair" nanotube. Both names refer to the symmetrical edge pattern of the SWNT.[119]

The electronic properties change drastically based on the nanotube species, where they can either be classified as metallic (m) or semiconducting (sc). The separation between the top of the valence π band (HOMO) and the bottom of the conduction π* band (LUMO), changes with the diameter and chirality of the SWNT.[120] This is because the nanotube diameter is small enough that its quasi 1D structure results in the quantum confinement effect of its electrons.[121] Therefore, the electrons can only exist in discrete energy levels, known as the van Hove singularities, within the density of states (DOS) (Figure 1.3).[122]

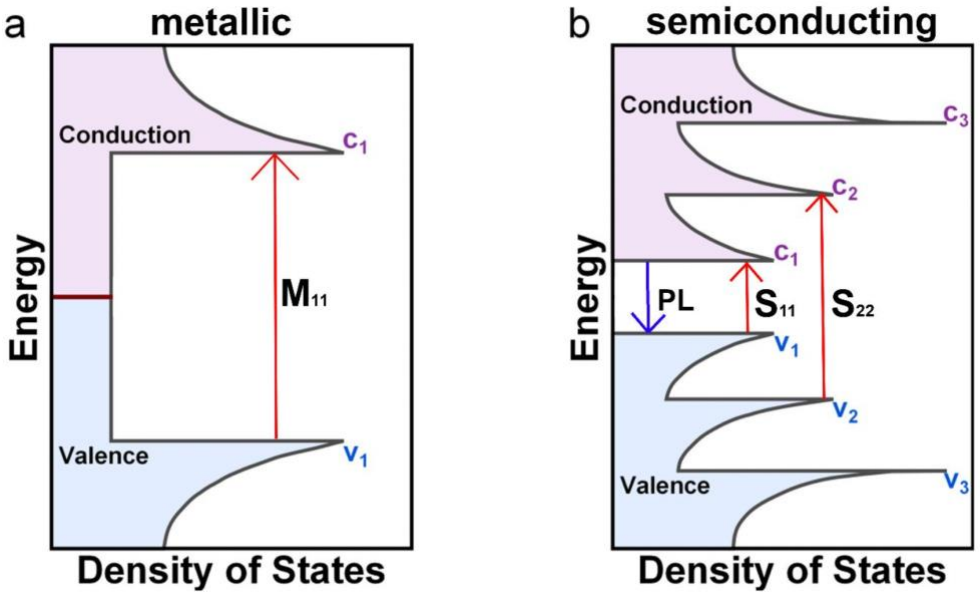

Figure 1.3. Simplified depictions of density of states (DOS) plots for a) metallic and b) semiconducting SWNTs with arrows indicating absorption and photoluminescence transitions between the valence and conduction bands. Reproduced with permission from [Bodnaryk, W.J. Purification of Semiconducting and Metallic Single-Walled Carbon Nanotubes Using Conjugated Polymers, McMaster University, 2020].[123] Copyright 2020.

There is no HOMO-LUMO band gap with metallic SWNTs, whereas in semiconducting carbon nanotubes, the band gap lies between ~0.5 – 1.0 eV and is inversely proportional to the diameter.[120] SWNTs are considered semi-metallic when the band-gap is ~1 − 100 meV and the (n,m) values adhere to the equation $|n-m|=3j$ where j is a non-zero integer. Semi-metallic nanotubes possess similar characteristics and properties as metallic nanotubes, therefore they will be classified as metallic to prevent confusion moving forward. Statistically, one third of SWNT structures are metallic SWNTs, while the remaining two thirds are semiconducting SWNT.

1.4. Covalent and Non-Covalent Functionalization of SWNTs

As previously mentioned, SWNTs have widespread potential applications, however commercial methods of synthesizing nanotubes result in a heterogeneous mixture of both electronic species of various diameters and lengths. The nanotubes also exhibit strong van der Waals interactions, thus causing them to form bundles and leading to poor solubility and processability.[124] The majority of applications mentioned in Section 1.3 require purification of all non-SWNT impurities, as well as solubilization and sorting of the electronic species. Methods to covalently and non-covalently functionalize SWNT sidewalls have been extensively studied as a way to impart solubility, and purify SWNTs by electronic type, diameter, and (n,m) chiral indices.[125–127]

1.4.1. Covalent Functionalization

Covalent functionalization of SWNTs refers to the direct modification of the SWNT surface to impart solubility. Most commonly, it requires a reactive species forming covalent adducts to pre-existing or intentionally added defects of the nanotube sidewall and ends. Though

there are naturally occurring defects upon formation of the nanotube, ultrasonic treatment, shear mixing, and strong oxidizing agents are typically used to introduce more reactive sites.[128] Chemical oxidation of nanotubes can be achieved using oxidizing agents under harsh conditions in both the liquid and gaseous phase, such as HNO_3, H_2SO_4, $KMnO_4$, HCl, hydrogen peroxide, carbon dioxide, water vapor, oxygen and ozone.[129] The resultant carboxy, ester, and quinone defects can be further functionalized with a multitude of groups like amines,[130,131] silanes,[132,133] and thiols,[134] thus promoting solubility in water or organic solvents. Other methods like the direct cycloaddition or fluorination then alkylation of the sidewall are also effective in solubilizing SWNTs.[135–137] Though covalent functionalization of SWNTs is stable and can modify functionality, the defects introduced throughout the structure interrupts the π -conjugated network and drastically affects optoelectronic and mechanical properties.[138]

1.4.2. Non-Covalent Functionalization

Non-covalent functionalization is typically used to impart solubility onto SWNTs where applications require the preservation of optoelectronic and mechanical properties. This is achieved by sonicating bundled SWNTs with dispersants to form supramolecular dispersant-SWNT complexes that prevent reaggregation.[139,140] These dispersants may entail biomacromolecules,[141–144] surfactants,[145–150] small aromatic molecules,[151–153] and conjugated polymers.[154–158]

A scalable and cost-efficient method of dispersing carbon nanotubes in aqueous solutions is by using surfactants. The nanotubes are mechanically separated through sonication, allowing the hydrophobic tail of the surfactant to adsorb to the nanotube surface, while the hydrophilic head facilitates dissolution.[159] Some examples of surfactants used to exfoliate carbon nanotubes are sodium dodecyl sulfate,[159,160] sodium dodecylbenzene sulfonate,[161–163] and Triton X-100.[164–166]

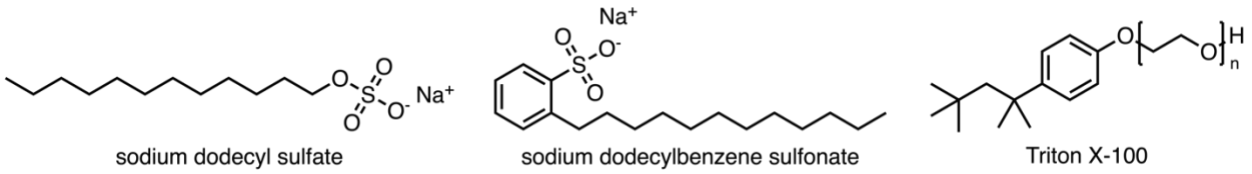

Figure 1.4. Commonly used surfactants for dispersing carbon nanotubes in aqueous solutions.

Although there are some surfactants that are able to selectively disperse SWNTs based on diameter or electronics, they must be enhanced through very specific conditions.[167,168] The majority of surfactants are unable to distinguish nanotubes based on species. To purify SWNTs after imparting solubility, other secondary techniques are often used in tandem, such as conventional or density gradient ultracentrifugation (DGU), gel, size-exclusion or ion-exchange chromatography, and electrophoresis.[169] DGU was originally developed to isolate biomacromolecules, sub-cellular components, and sequences of DNA by buoyant densities. In the mid-2000s, Arnold et al. began investigating DGU as a method for enriching SWNTs.[170,171] The technique requires adding a surfactant-SWNT dispersion to a non-ionic density gradient medium, iodixanol, then centrifuging at 174,000 *g* or 207,000 *g* between 9 and 24 hours. The unique density of each surfactant-coated SWNT species allows it to travel through a density gradient under the applied force of centrifugation. The nanotube species will eventually reach an equilibrium position and accumulate in coloured bands. Ghosh and coworkers would significantly improve this technique in 2010 by using carefully prepared nonlinear density gradients with optimized conditions to achieve sorting of individual SWNT species (Figure 1.5).[172]

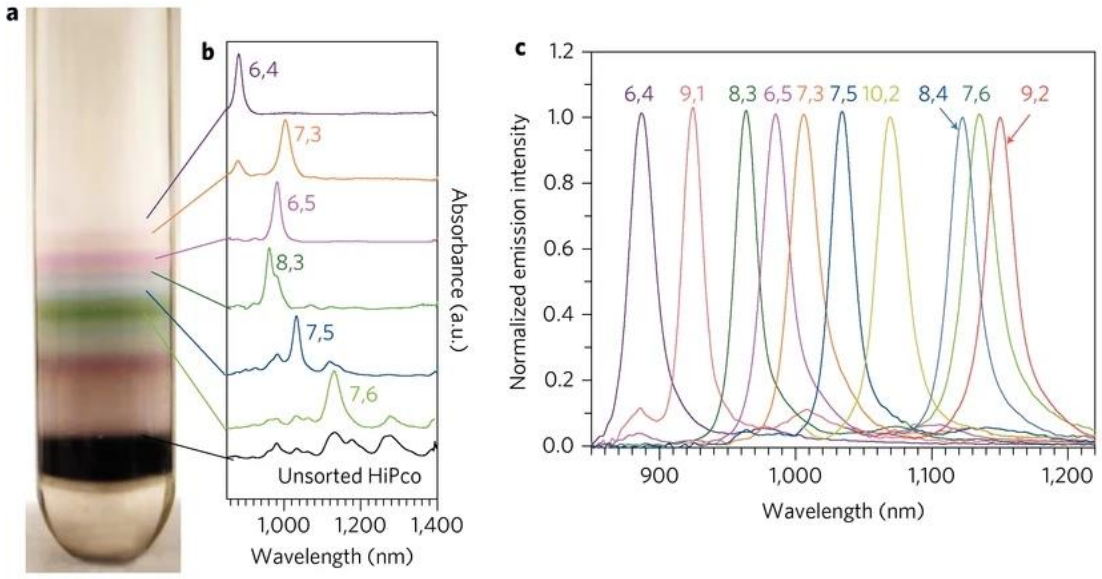

Figure 1.5. A) Image of centrifuge tube containing DGU sorted HiPco SWNTs with localized distinct coloured bands of different SWNT species. B) Near-infrared absorption spectra from the different isolated bands after DGU. C) Photoluminescence spectra of separated fractions. Reproduced with permission.[172] Copyright Nat. Nanotechnol., 2010.

Agarose gel chromatography and two-phase extraction are two other approaches of separating surfactant-treated SWNTs by species.[173–176] Although DGU and gel chromatography purification of surfactant-coated SWNTs are techniques currently used to purify commercially available nanotubes, they are not efficient and produce less than a milligram of purified aqueous soluble material, despite combining numerous batches.

Single-stranded DNA can also be used to separate SWNTs through the π-π interactions of the nucleotides with the SWNT π-system.[177] Zheng et al. were able to isolate highly specific single-stranded DNA sequences that were able to produce dispersions of single (n,m) species when combined with ion exchange chromatography. However, the method of purification is once more

reliant on a secondary technique and is afflicted with low yields. It should also be noted that the preparation of the highly specific sequences of DNA is costly and not suitable for industry scale.

1.5. Supramolecular Interactions Between CPs and SWNTs

An alternative approach to enriching carbon nanotubes is by using conjugated polymers. Dispersing SWNTs with CP addresses the strain in scalability, cost, and post-processing techniques required of other purification methods. The π-conjugated backbone of CPs interacts with SWNTs through π-π stacking. The supramolecular complexes of CP-wrapped nanotubes are soluble in organic solvents compatible with the polymer.[178] In this process, the van der Waals forces between the individual nanotubes are disrupted, thus preventing reaggregation. The selectivity in CP-SWNT dispersions was first realized by Nicholas and coworkers in 2007, where they demonstrated the discrimination between nanotube species by diameter or chiral angle using commercially-available polymers.[179] Ever since, interest in CPs for the separation of SWNTs has drastically increased, with many studies exploring polyfluorenes, polycarbazoles, polythiophenes, donor–acceptor (D-A) polymers, and many other CPs in dispersing SWNTs.[101,157,180–185]

The efficacy and selectivity of CPs dispersing SWNTs is highly dependent on dispersing conditions, molecular weight, backbone rigidity, electron density, and backbone and side chain composition.[186] Typically, CP-SWNTs dispersions are prepared by sonicating, centrifuging, then filtering SWNTs in the presence of CPs and a solvent of choice. Each polymer system will require the optimization of sonication time, power, and temperature,[187,188] CP:SWNT mass ratio,[189] solvent choice,[190] and centrifugation speed,[191] depending on the desired application and requirements of the dispersion. Solvent choice in particular can have drastic effects, as the polymer must be soluble but the solvent must be less than the buoyant density of a typical aggregate (1.3 g/mL).[189] THF,

toluene, o-xylene, m-xylene, tetralin, and decalin have all been used to disperse SWNTs, with considerations of their viscosity, polarity, and dielectric constant aiding to produce stable and selective dispersions.

Despite purification of SWNTs using CPs being so promising, much of the fundamental principles dictating selectivity, stability, and efficacy of forming CP-SWNT complexes has yet to be explored. Though efforts have been made in designing conjugated polymers for the purification of specific individual (n,m) species, this has yet to be achieved. A large barrier in attaining this goal is in the challenge of accomplishing miniscule and precise changes to the structure without affecting other macromolecular properties, such as molecular weight and polydispersity. As both factors heavily change the efficiency of CP-SWNT interactions, it is difficult to compare a library of functionalized polymers without the use of well-controlled and strenuous specialized polymerization methods.[65,192–194] To establish a consistent and defined understanding of polymer-SWNT interactions, control over length and dispersity is required while polymer electronics, sterics, and other structural features can be systematically varied.

1.5.1. Post-Synthetic Modification of CPs

Post-synthetic modification of polymers has been explored as a route towards the facile design and comparable preparation of conjugated polymers. A parent conjugated polymer is functionalized to prepare numerous daughter polymers with negligible change to the length and dispersity. Either the side chains or backbone may be modified to suit its applications. Modification of CP side chains is often performed to achieve more solution-processable polymers. However, side chains can also have a profound impact on the molecular dynamics, optoelectronic, and physical properties of a polymer.[46] Although there are various classes of side chains to impart

different properties onto CPs, alkyl, oligoether, and conjugated side chains are amongst the most common.

Alkyl chains, both branched and linear, are often used to impart solubility in organic solvents, with the former improving solubility more efficiently when comparing the same molecular formula. However, branched chains have more steric bulk, thus will exhibit more interchain interdigitation. On the other hand, oligoether side chains have demonstrated imparting hydrophilicity onto select CPs, like PPV, polyfluorene, and propylenedioxythiophene. Unlike alkyl and oligoether side chains, conjugated chains are not grafted with the purpose of modifying solubility, but to modify the HOMO/LUMO levels of the CP, therefore fine tuning the optoelectronic properties.[22]

Though it is more challenging, significant change to the optoelectronic properties of CPs is better achieved through backbone modification. In 2012, Dichtel and coworkers reported the $Cu(OTf)_2$-catalyzed benzannulation of phenylene ethynylenes to achieve sterically demanding polyarylenes and demonstrated the first efficient cycloaddition reaction of a CP backbone.[196] Nucleophilic aromatic substitution (S_NAr) has also been useful in post-polymerization functionalization. The S_NAr of aryl fluoride derivatives on benzothiadiazole monomer units with a series of thiols and alcohols was reported in 2014.[197] The authors prepared fluorescent mono and multifunctional semiconducting polymer nanoparticles of varying optical properties. The authors also demonstrated control over the degree of substitution and the possible introduction of orthogonal functional groups on the side chains for further functionalization.

Rapid and efficient "click" chemistry is a concept that has come to fruition in recent years.[198] In 2001, Karl Barry Sharpless, Hartmuth Kolb, and M.G. Finn coined the term "click chemistry" which utilized "spring-loaded" reactions that were rapid and highly selective towards a single

product. Sharpless would go on to win a Nobel prize "for the development of click chemistry and bioorthogonal chemistry" alongside Carolyn R. Bertozzi and Morten Meldal in 2022. His stringent criteria of click reactions required the reaction be versatile, have high yields, produce only "inoffensive byproducts", be stereospecific, have simple reaction conditions, utilize readily available starting materials, be in easily removed solvent, and simple in product isolation/purification. The four classes of transformations Sharpless had originally deemed to fit the criteria were cycloadditions of unsaturated species, S_N2 ring-opening reactions of strained heterocyclic electrophiles, carbonyl chemistry of the "non-aldol" type, and additions to carbon–carbon multiple bonds. The orthogonality of click reactions, high yield, and facile purification would make them particularly attractive for post-polymerisation functionalization.

1.5.2. Alkyne-Azide Cycloadditions (SPAAC & CuAAC)

Alkyne-Azide "Click", a [3+2] cycloaddition reaction, has been explored as a possible route for polymer backbone functionalization. Cu-catalyzed alkyne-azide cycloadditions (CuAAC) have a facile workup and rapid reaction times with a rate constant of 10 – 100 M^{-1} s^{-1} (Table 1.1).[199] Another alkyne-azide click reaction, Strain-Promoted Alkyne-Azide Cycloaddition (SPAAC), circumvents the need for cytotoxic Cu(I) catalysts through the use of strained-cyclooctyne. Strained-cyclooctyne units incorporated in a CP backbone allow for the formation irreversible triazole linkages and subsequent post-synthetic functionalization when reacted with an azide derivative. The bond angle deformation of the acetylene from 180° to 163° stores approximately 18 kcal/mol of ring strain.[200,201] Thus, the reaction proceeds without the need of catalysts or high temperatures, though at a slower rate than CuAAC (~0.1– 60 M^{-1} s^{-1}).[202] Many dibenzoannulated derivatives for SPAAC reactions have been investigated, such as

dibenzocyclooctyne (DIBO), dibenzoazacyclooctyne (DIBAC), and biarylazacyclooctynone (BARAC).[203]

Table 1.1. Common click reactions with rate constants and considerations. Reproduced with permissions.[204] Copyright Chem. Sci., 2019.

Name	Representative reaction	k (M^{-1} s^{-1})	Pros/cons
CuAAC	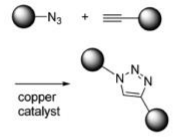	~10–100 (with 20 μM Cu(I))[8]	- Both small structures - Cheap price - Toxic copper catalyst - High second order reaction rate constant
SPAAC	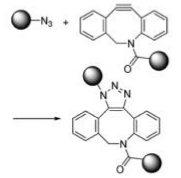	~1–60 (M^{-1} s^{-1})[9]	- One small and one large structure - Moderate second order reaction rate constant - No catalyst
iEDDA	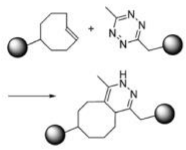	~1–10^6 (M^{-1} s^{-1})[10]	- Two large structures - Very high second order reaction rate constant - No catalyst

[a] CuAAC: copper-catalyzed [3 + 2] azide–alkyne cycloaddition; SPAAC: strain-promoted azide–alkyne cycloaddition; iEDDA: inverse-electron-demand Diels–Alder reaction.

SPAAC reactions with DIBO-containing conjugated polymer proved to be a possible route for backbone functionalization for CPs.[205,206] However, the CPs were not suitable for dispersing SWNTs as issues with kinked conformations, hydrolytic stability, arduous synthesis, and intolerance to cross coupling conditions arose. This highlights a large set-back for SPAAC for post-synthetic modification of backbones. Transition-metal catalyzed cross-coupling reactions for step-growth polymerization are incompatible with strained alkynes. Strained-cyclooctynes will form metallocyclopropene in the presence of transition metals and deactivate the catalyst, making high-molecular weight polymers containing the strained-cyclooctyne moiety unattainable.[207–209]

1.5.3. Inverse Electron Demand Diels-Alder (IEDDA)

The inverse electron demand Diels-Alder (IEDDA) reaction was introduced by Blackman et al. in 2008 in response to the bioincompatible CuAAC and SPAAC reactions and was deemed the fastest bioorthogonal reaction with a rate constant between $1–10^6$ M^{-1} s^{-1}.[210] Not unlike a normal demand Diels-Alder reaction, IEDDA reactions are a concerted [4+2] cycloaddition involving a 4π electron system (diene) and a 2π electron system (dienophile) to form a 6-membered ring. However, the two reactions differ in the HOMO-LUMO interactions between the diene and dienophile. In a normal demand Diels-Alder reaction, an electron-rich diene (HOMO) reacts with an electron-poor dienophile (LUMO), but in the inverse, the electron-poor diene (LUMO) will react with an electron-rich dienophile (HOMO) (Figure 1.6).[211] Based on frontier molecular orbital theory, IEDDA reaction kinetics are determined by the HOMO–LUMO energy gap of the reactants. Thus, tuning the reactivity of IEDDA can be accomplished through the substituents. Electron-donating groups (EDG) will raise both HOMO and LUMO energy, whereas electron-withdrawing groups (EWG) will lower the levels. Therefore, any pairs of diene and dienophile resulting in a smaller energy gap would increase the rate of the IEDDA reaction.

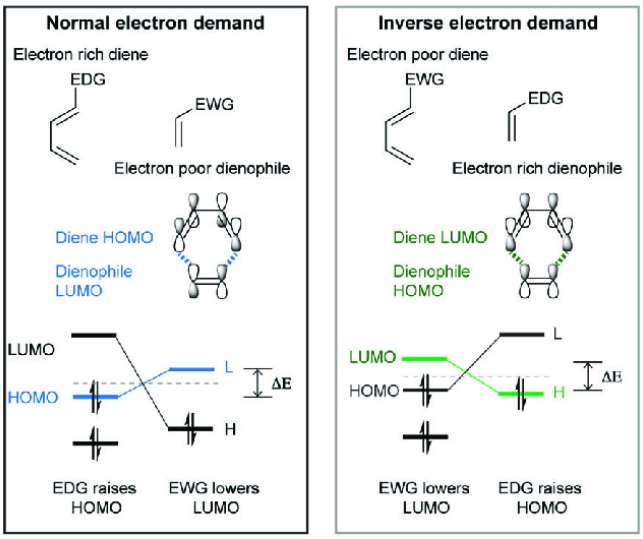

Figure 1.6. Frontier molecular orbital of normal- (left) and inverse-demand (right) Diels-Alder reactions. Reproduced with permission.[211] Royal Society of Chemistry, 2017.

1,2,4,5-Tetrazines, or *s*-Tetrazines are notable for undergoing a rapid IEDDA reaction with *trans*-cyclooctenes (TCO), cyclooctynes, and norbornenes.[212–215] They attracted attention for *in vivo* applications due to their properties, including stability, bio-orthogonality, and tolerance to Suzuki polymerization conditions. With regard to post-polymerization modification, Kardelis et al. incorporated an *s*-tetrazine moiety into a poly(furyltetrazine-*co*-hexadecylfluorene) conjugated polymer.[216] The authors were able to successfully demonstrate the rapid (1.25 ± 0.07 M^{-1} s^{-1}) click-functionalization with a series of TCO derivatives onto the backbone without impacting planarity of the polymer or the average degree of polymerization. Despite its rapid functionalization and suitability for dispersing SWNTs, studies with conjugated polytetrazines and SWNTs have not been conducted before.

1.6. Characterization of SWNT Dispersions

As the purity and functionality of SWNT plays such a large role in its applicability, it is imperative to fully characterize polymer-SWNT complexes. Assignment of (n,m) chirality can be achieved through both optical and non-optical methods, consisting of resonant Raman scattering, absorption, photoluminescence (PL), resonant Rayleigh scattering (RRS), and circular dichroism (CD) spectroscopies, scanning tunneling microscopy, transmission electron microscopy and electron diffraction.[178] Absorption spectroscopy, photoluminescence (PL) mapping, and Raman spectroscopy have become the most widely used of these methods as they are rapid, facile, and non-destructive. All three techniques take advantage of the differences in the density of states between each unique species of SWNT to characterize and elucidate the necessary information from a polymer-SWNT dispersion.

1.6.1. UV-Vis-NIR Absorption Spectroscopy

UV-Vis-Near-Infrared (UV-Vis-NIR) absorption spectroscopy is a fundamental and facile method for the quantification and qualitative analysis of SWNT dispersions. It can be used to determine the quality, purity, and concentration of SWNTs within a dispersion.[217] As previously mentioned in Section 1.3, each species of SWNT possesses unique electronic transitions due to differences in diameter and chirality, which can be characterized through optical spectroscopic techniques like UV-Vis-NIR absorption spectroscopy.[218,219] Qualitative analysis of the spectrum can indicate how well the SWNTs have been separated and exfoliated. Good resolution of the Van Hove singularities indicated individualized nanotubes, whereas unsorted and bundled SWNTs will exhibit broad peaks.[219] sc- and m-SWNTs can be categorized into defined regions of the UV-Vis-NIR spectrum by band gap (Figure 1.3). For HiPco SWNTs the three distinct electronic transition

regions are observed at 830 to 1600 nm for semiconducting regions S_{11}, 600 to 800 nm for S_{22}, and 440 to 645 nm for metallic region M_{11} (Figure 1.7.).[217]

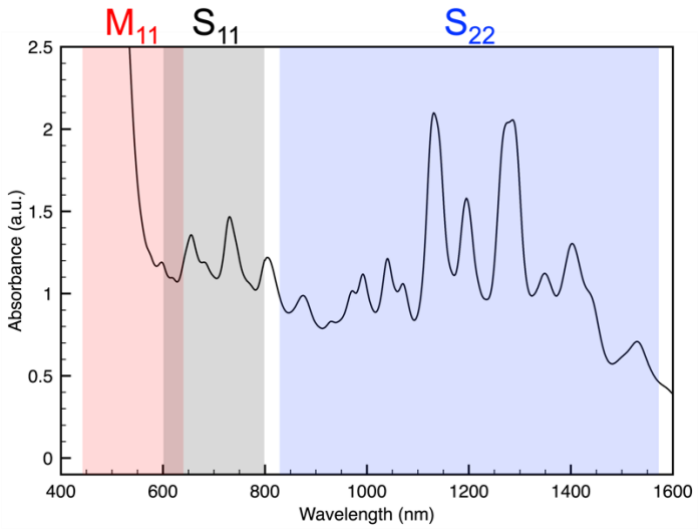

Figure 1.7. UV-Vis-NIR absorption spectrum of HiPco SWNTs dispersed using a tetrazine containing polymer in THF with labelled metallic (M_{11}), and semiconducting (S_{11}, and S_{22}) regions.

It should be noted that there is overlap between the S_{22} and M_{11} regions, therefore complicating the evaluation of electronic purity and sc- and m-SWNTs ratios. Analysis of electronic purity is better achieved through qualitative measures as quantitative analysis loosely assumes that each polymer-SWNT species has an identical extinction coefficient. For true depiction and accurate characterization of a polymer-SWNT dispersion, a full suite of analysis consisting of photoluminescence mapping, Raman, and UV-Vis-NIR spectroscopy is required.

1.6.2. Resonance Raman Spectroscopy

Raman spectroscopy is a method of characterization utilizing vibrational energy and provides another route to evaluating polymer-SWNT dispersions. It is a powerful and versatile

tool in characterizing the abundance of the different (n, m) species present in a sample.[220] This non-destructive technique may be performed on individualized and unsorted SWNTs, and is instrumental in determining the electronic purity, as well as defect density, of the nanotube population.[221] Upon excitation with powerful incident light source, the photons absorbed interact with molecular vibrational modes, as well as one or more phonons, and scatter before being emitted. Raman spectroscopy is the measure of intensity of scattered photons with respect to the Raman shift.[222]

Resonance Raman spectroscopy significantly outperforms non-resonance Raman spectroscopy with enhanced signals that can detect singular tubes.[223] With the former spectroscopic technique, the incident or scattered light is in resonance with the electronic transitions of SWNTs, thus dramatically enhancing the observed signal.[224] Thereby tuning the laser excitation wavelengths to overlap with the van Hove singularities present in the 1D DOS, the signals observed are enhanced and can be distinguished.[220] As the electronic transitions and van Hove singularities of each SWNT species is dependent on chirality and diameter, it is necessary to use varying excitation wavelengths to differentiate the nanotubes present in a sample.[225] 532 nm, 633 nm, and 785 nm excitation wavelengths have been determined to be reasonable wavelengths to probe and distinguish m- and sc- HiPco SWNTs.

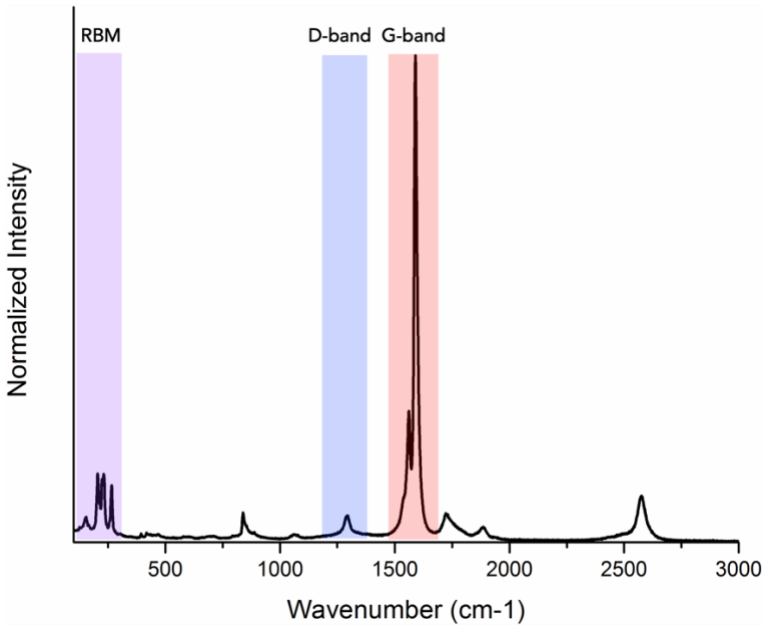

Figure 1.8. An example of a typical Raman spectrum of HiPco SWNTs with RBM (purple box), D-band (blue box), and G-band (red box) regions.

Typically we analyze three regions of a Raman spectrum: the *G*-band (~1590 cm^{-1}), the *D*-band (~1290 cm^{-1}), and the radial breathing mode (RBM) region (~100 – 400 cm^{-1}) (Figure 1.8).[226–228] The *D*-band, or the disordered band, arises from the presence of sp^3-hybridized carbons due to defects and is used to determine the structural integrity of a carbon nanotube. The *G*-band is a feature in Raman spectra of graphitic structures and pertains to the resonance of sp^2-hybridized carbons. It consists of a lower-frequency G^- and a higher-frequency G^+ peak. The G^- band arises from vibration along the axial direction, while the G^+ arises from vibrations in the circumferential direction (Figure 1.9).[229] The *G* band shape and position can be used to determine the species of nanotubes present in a sample. As depicted in Figure 1.10, a sample with mostly sc-SWNTs will exhibit a *G* band with a Lorentzian line shape.[230] In contrast, for m-SWNTs, the G^- will have a broader Breit–Wigner–Fano (BWF) line shape.

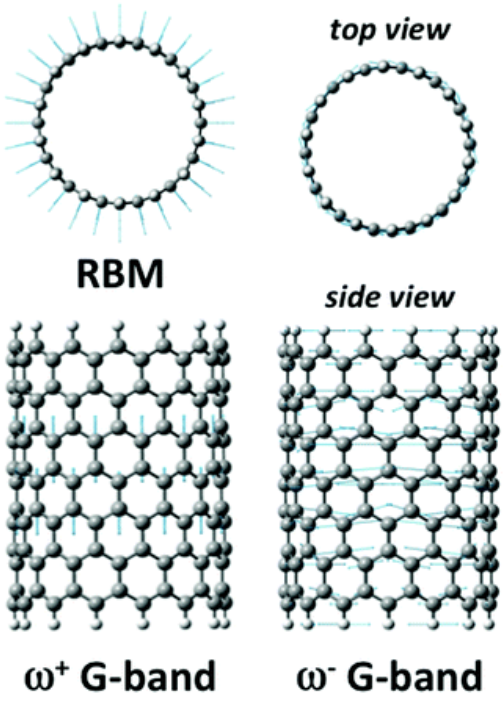

Figure 1.9. Diagram depicting the molecular motions for RBM, G^- and G^+ bands. Reproduced with permission.[231] Copyright Phys.Chem.Chem.Phys., 2016.

The radial breathing mode is unique to SWNTs and corresponds to the radial vibrations of the carbon nanotube, as if the tube is "breathing" (Figure 1.10). The RBM is attributed to the position of signals in the lower-frequency region of the Raman spectrum.[227] Depending on the excitation wavelength, both m- and sc-SWNTs can be separately probed and identified, with 532 nm, 633 nm, and 785 nm proven to be suitable for HiPco SWNTs.[218,225,232] m-SWNTs are primarily in resonance when excited at 532 nm (~215–300 cm^{-1}).[233] When excited at 633 nm, both m-SWNT (~170–230 cm^{-1}) and sc-SWNTs (~240–300 cm^{-1}) are in resonance.[217] Lastly, sc-SWNTs are primarily in resonance when excited at 785 nm (175–280 cm^{-1}). For complete evaluation of every nanotube species of different diameters present in the sample, it would be necessary to utilize more than the three wavelengths discussed here. However, in combination with

G-band analysis the electronic character of SWNTs can be accurately determined, especially in conjunction with UV-Vis-NIR absorption spectroscopy.

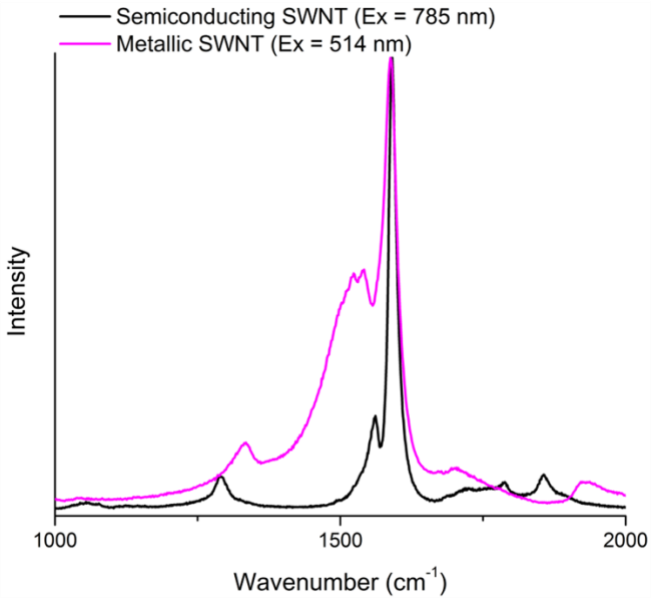

Figure 1.10. Comparison of different G-band line shapes, the Lorentzian line shape of a mostly semiconducting SWNT sample (black) and a BWF line shape of a mostly metallic SWNT sample (magenta). Reproduced with permission from [Rice, N. A. Separation of Single-Walled Carbon Nanotubes By Electronic Type Using Conjugated Polymers, McMaster University, 2015].[123] Copyright 2015.

1.6.3. Photoluminescence (PL) Mapping

Photoluminescence (PL) mapping is a technique specific to semi-conducting SWNTs and can provide insight on emission properties and identification of sc-SWNT species within a sample.[234] Nanotube fluorescence can be determined at significantly lower concentrations than absorption spectroscopy and provides a more detailed insight into the species present in a heterogeneous sample of SWNTs. Semi-conducting SWNTs exhibit a unique infrared PL upon

excitation due to the band gap between the conductive and valence bands. For sc-SWNT, the DOS will determine how an excited electron radiatively relaxes from c_1 to v_1 then emits a photon.[235] The resulting photoluminescence will be unique to each (n,m) SWNT. As metallic SWNTs do not possess a band gap and have a continuous DOS, an excited electron would relax through non-radiative pathways rather than through photoluminescence. Therefore, it is necessary to use this technique on samples with low concentrations of m-SWNTs as their presence drastically quenches sc-SWNT PL. A 3D map can be built from exciting and collecting the dispersion at multiple wavelengths where individual sc-SWNT species can be identified by their PL maximum.[235] The (n,m) values of SWNTs have been empirically determined and can be overlaid onto the PL map to assign chiralities to the PL maxima (Figure 1.11).[218]

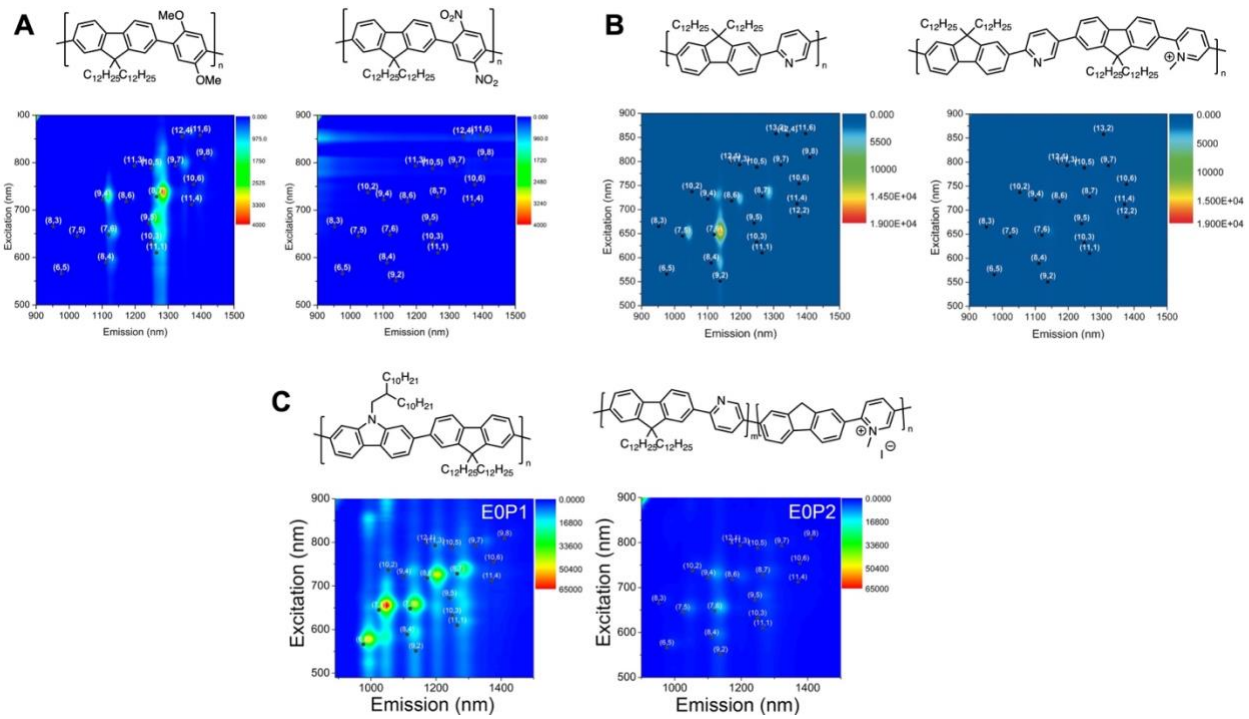

Figure 1.11. PL maps with labelled empirical (n,m) values from studies of selectivity using electron-rich/electron-poor polymer-SWNT dispersions of A) poly(fluorene-*co*-phenylene)

derivatives,[102] B) poly(fluorene-*co*-pyridine) derivatives,[236] and C) a combination of poly(fluorene-*co*-carbazole) and poly(fluorene-*co*-pyridine) derivatives[237] demonstrating PL quenching in the presence of metallic SWNTs. Reproduced with permissions. Copyright 2015, Macromolecules. Copyright 2016, Chem. Eur. J. Copyright 2018, ACS Omega.

Quantitative analysis of carbon nanotube dispersions using PL mapping remains a challenge due to complications with concentration, purity, and efficiency of the tubes. As mentioned previously, any presence of m-SWNT will quench the fluorescence of sc-SWNTs, but defects in the nanotube will also result in disturbed emission.[238–240] Thus, pristine and sorted SWNTs are necessary to accurately quantify nanotubes in a sample. De-bundling of SWNTs is also required as any aggregate of three or more nanotubes will statistically contain a m-SWNT as ~33% of SWNTs are metallic in nature. Furthermore, it has been reported that SWNT quantum yields are not equal and vary depending on the diameter, chiral angle, modulus, and length of the tube.[241,242] Therefore, PL mapping is better suited to qualitative evaluation of dispersions. Previously Rice et al. in 2015,[102] Fong et al. in 2016,[236] and Bodnaryk et al. in 2018[237] evaluated the metallic character within samples by comparison of fluorescence maxima (Figure 1.11) as the presence of more metallic SWNTs would have lower PL maxima.

1.7. Summary

In summary, the understanding of the underlying principles governing interactions between conjugated polymers and SWNTs remains largely unexplored. Given the tools of “click” chemistry, the work in this thesis aims to investigate the interactions of tetrazine-containing polymers with SWNTs and how those interactions change based on the post-synthetic modification

of the backbone. Through my thesis, I aim to demonstrate how solubility, aromaticity, and molecular weight all play a large role in the efficacy of forming CP-SWNT complexes. To date, this is the first study of tetrazine-based polymers interacting with SWNTs, and the first demonstration of IEDDA for post-dispersion modification of a polymer backbone.

Chapter 2: Preparation, Modification, and Characterization of Poly(Fluorene-*co*-Tetrazine)-Conjugated Polymer

2.1. Overview

Conjugated polymers (CP) adsorb to the surface of SWNTs through π- π interactions, and can be easily modified through the introduction of varying functional groups.[243] However, the electronic, chemical, and physical properties, namely solubility, of CPs are highly dependent on the structure of the polymer backbone, and their modification requires the preparation and synthesis of an entirely new polymer.[1,60,244–246] Thus, with the exception of a few well-controlled specialized polymerization methods, it is often difficult to directly compare a library of functionalized polymers without affecting other macromolecular properties.[65,192–194]

Post-synthetic modification of CP backbones has been widely considered a solution, though few efficient methods of CP backbone modification have been published.[50,51,196] Many post-polymerization modified CPs demonstrated in the literature are plagued with issues of stability,[206,247] utilize synthetically challenging monomers,[191,205] or adopt a kinked conformation post-modification.[248,249] Recently, our attention turned to a class of molecules known as 1,2,4,5-tetrazines, or *s*-tetrazines, which are notable for undergoing a rapid inverse-electron-demand Diels-Alder (IEDDA) reaction with trans-cyclooctenes, cyclooctynes, and norbornenes.[212–215] Due to its stability, bio-orthogonality, and tolerance to Suzuki polymerization conditions, we have previously incorporated an *s*-tetrazine moiety into a poly(fluorene-*co*-tetrazine) conjugated polymer.[216] We successfully demonstrated this polymer's ability to undergo efficient IEDDA reaction with a series of *trans*-cyclooctene (TCO) derivatives without impacting planarity or the average degree of polymerization. Despite their rapid functionalization and potential suitability for dispersing SWNTs, studies of conjugated polytetrazines and SWNTs have not been previously conducted.

The main objective of Chapter 2 is to prepare the poly(fluorene-*co*-tetrazine) at two molecular weights and modify the backbone through IEDDA. The synthetic approach involves the preparation of a *s*-tetrazine-Br_2 monomer and a bis(pinacolato)boronate ester fluorene comonomer and generating the polymers through a Suzuki polycondensation reaction. The reactive tetrazine moieties are modified with TCO derivatives to graft a hydroxyl, hexadecyl, and triethylene glycol functional group. The modified polymers were then further oxidized to regain continuous conjugation of the backbone. A full suite of characterization confirms the complete post-synthetic functionalization of the polymer. The conjugated polymers were used to prepare the polymer-SWNT complexes in Chapter 3.

2.2. Synthesis of Tetrazine-Containing Polymers

We began with the preparation of two reactive *s*-tetrazine containing conjugated polymers with differing molecular weights by following a literature procedure (see Supporting Information for details).[216] *s*-Tetrazine **1** was synthesized *via* a modified Pinner reaction with commercially available 2-furonitrile, followed by an oxidation with isoamyl nitrite (Scheme 2.1A).[250] Bromination of *s*-tetrazine **1** with *N*-bromosuccinimide yielded *s*-tetrazine-Br_2 monomer **2**. Commercially available fluorene was also brominated with *N*-bromosuccinimide, then alkylated under phase-transfer conditions with 1-bromohexadecane to produce compound **4** (Scheme 2.1B). The bis(pinacolato)boronate ester comonomer **5** was prepared from **4** using the Miyaura borylation reaction. Monomers **2** and **5** were copolymerized via Suzuki polycondensation at 50 °C for varying times (30 min and 1.5 h) to afford low and high number average molecular weight (M_n) polymers, $\mathbf{P1_{13k}}$ and $\mathbf{P1_{24k}}$ (Scheme 2.1C). The M_n and dispersity ($Đ$) of the polymers were determined by gel permeation chromatography (GPC), with $\mathbf{P1_{13k}}$ having an M_n of 13.0 kDa and a $Đ$ of 2.9, and

P1$_{24k}$ having an M_n of 23.7 kDa and $Đ$ of 3.4. The polymers were also end-capped with *p*-anisole pinacolato boronate ester **6** to provide an NMR handle that enables calculation of M_n through ^{1}H-NMR end-group analysis. Comparison of the distinct methoxy group signal at ~3.86 ppm with the polymer backbone signals allowed confirmation of the M_n for **P1$_{13k}$** and **P1$_{24k}$**, which was 22.9 kDa and 46.4 kDa and corresponded to a degree of polymerization (DP) of 28 and 56, respectively (Figures S14 and S15). The discrepancy between the GPC and NMR M_n data can be attributed to the polystyrene standards used for GPC calibration, which result in errors associated with the GPC measurement. Thermogravimetric analysis (TGA) under Ar atmosphere was used to determine the thermal decomposition profiles of the polymers, which indicated two distinct decomposition events. For both low and high molecular weight tetrazine polymers, the first mass loss of 7% occurs at ~260 °C, corresponding to the loss of N_2 from the polymer backbone, and the second loss occurs at ~400 °C, corresponding to the loss of the hexadecyl side chain on the fluorene unit.

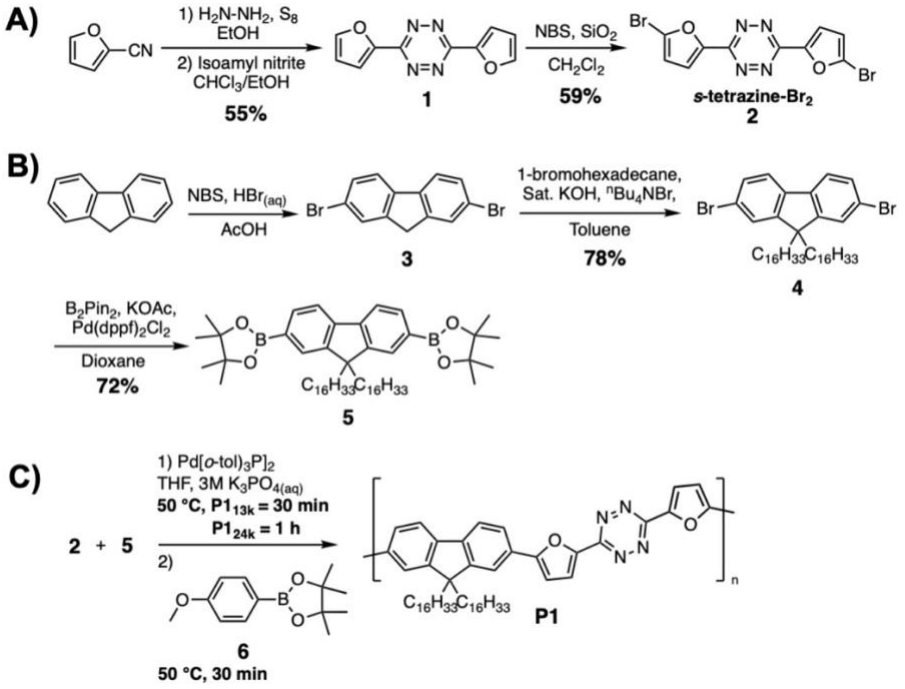

Scheme 2.1. Synthesis of A) *s*-tetrazine-Br$_2$ monomer, B) bis(pinacolato)boronate ester comonomer, and C) hexadecylfluorene-*co*-tetrazine conjugated polymers **P1$_{13k}$** and **P1$_{24k}$**.

2.3. Preparation of the TCO Derivatives

Three derivatives of *trans*-cyclooctene (TCO) were prepared to undergo the IEDDA reaction with **P1$_{13k}$** and **P1$_{24k}$**. rel-(1*R*, 4*E*, p*R*)-Cyclooct-4-enol (TCO-OH) **5** was prepared *via* photoisomerization of the cis isomer,[251] and subsequently activated with nitrophenyl chloroformate to yield activated TCO **6** (Scheme 2.2). The activated TCO underwent substitution with hexadecyl amine or α-amino-ω-methoxy triethylene glycol to produce TCO derivatives **7a** and **7b**, respectively (Scheme 2.2). To prevent any thermal isomerization of the products, **7a** and **7b** were stored at −20 °C prior to their utilization.

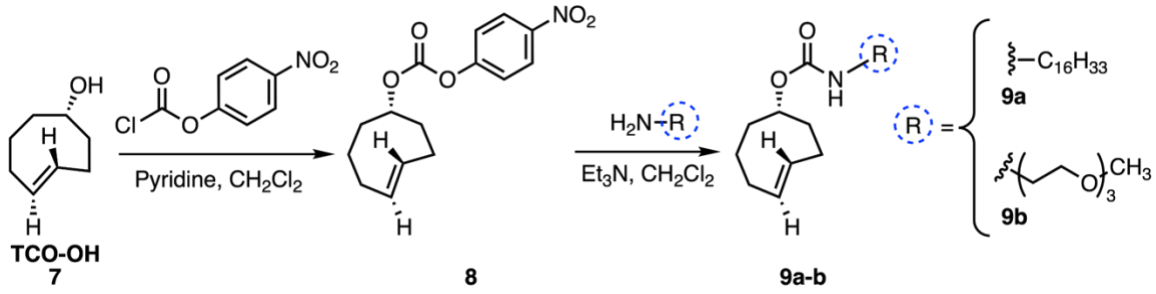

Scheme 2.2. Synthesis of *trans*-cyclooctene (TCO) derivatives.

2.4. Preparation of P2 Polymer Series

With both components for the IEDDA reaction in hand, we proceeded to prepare a series of post-polymerization modified polymers with our desired functional groups. **P1$_{13k}$** and **P1$_{24k}$** were allowed to react with TCO derivatives **7** and **9a-b** at room temperature for 30 min in tetrahydrofuran, resulting in gas evolution and rapid onset of fluorescence. The reaction was monitored by UV-Vis spectroscopy, as the polymer undergoes a significant hypsochromic shift (see spectrum for **P2$_{24k}$-b** in Figure 2.1A) of 42 to 75 nm (see Supporting Information for other polymers, Figures S31-S34, Table S1). The λ_{max} of **P1** at ~450 nm shifts to an average λ_{max} of ~395 nm for the **P2** polymer series, which is in accordance with a decrease in conjugation length. In

addition to UV-Vis spectroscopy, FTIR spectroscopy was used to confirm the completion of the reaction. A decrease in the stretch at ~1535 cm^{-1} was observed as the tetrazine containing polymer reacts with each TCO derivative (Figure 2.1B, Figures S51-55), most likely correlating to the N_2 stretch that is lost upon the IEDDA reaction.[252] Furthermore, a strong carbonyl stretch from the carbamates appears at ~1715 cm^{-1} (Figure S53-S55). ^{1}H NMR spectroscopy confirms quantitative conversion to the 1,4-dihydropyridazine with the complete disappearance of signals at ~7.05 and ~7.90 ppm. This corresponds with the furyl protons adjacent to the tetrazine heterocycle shifting to a lower frequency post-click (see spectrum for **P2$_{24k}$-c** in Figure 2.2, and other polymer ^{1}H NMR spectra in Supporting Information, Figures S14-29). In addition, a proton signal between 8 and 8.5 ppm appears in the product polymer spectra, corresponding to the N-H group in the 1,4-dihydropyridazine unit. Based on NMR, the degree of polymerization and the subsequent M_n remained comparable and indicated no chain scission had occurred post-modification. The apparent molecular weight observed by GPC analysis only indicated small or insignificant changes with the addition of functional groups, except for **P2$_{13k}$-a** and **P2$_{24k}$-a** (Supporting Information, Figures S45-50, Table S2). These polymers, clicked with the hydroxyl-TCO **7,** demonstrated a sharp decrease in M_n, most likely due to interactions with the stationary phase of the GPC column delaying the elution time of the polymer and giving the appearance of a much lower apparent molecular weight. Additionally, as previously noted, a significant change in fluorescence is observed post-IEDDA. **P1$_{13k}$** and **P1$_{24k}$,** which exhibited no fluorescence prior to the reaction, exhibited strong emission centered around 485 nm after the IEDDA reaction, regardless of the TCO derivative used (Figure 2.2 and Figures S35-S44).

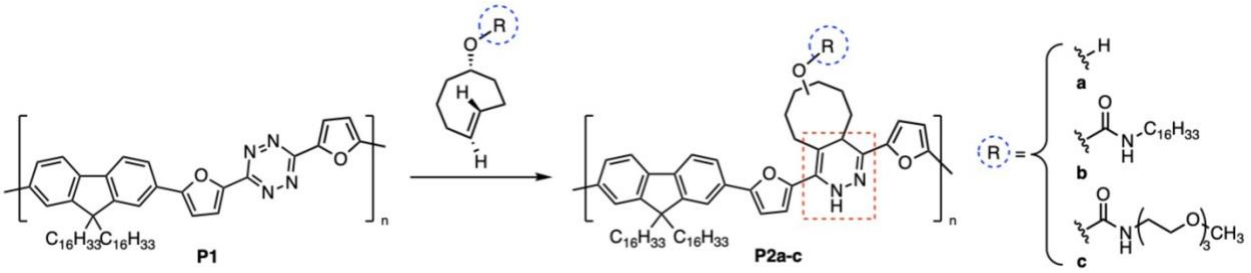

Scheme 2.3. Preparation of **P2** polymer series with TCO derivatives.

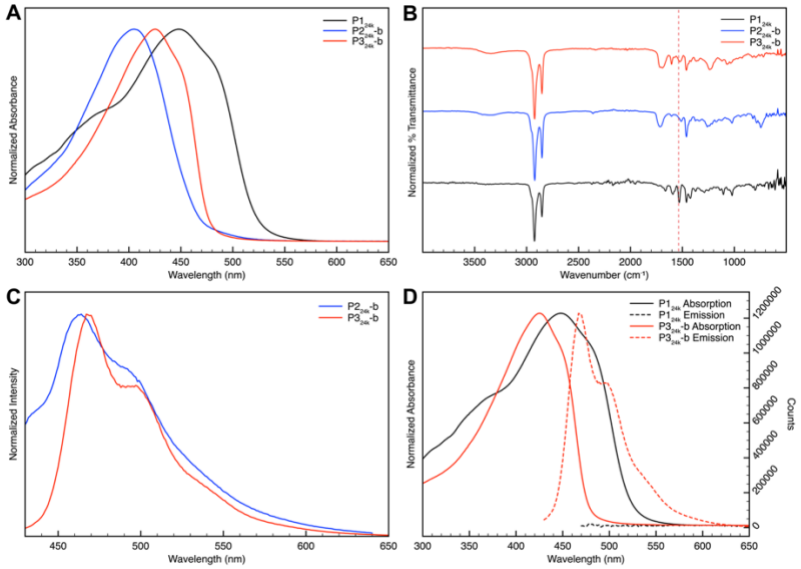

Figure 2.1. A) Overlayed UV-Vis absorption spectra of **P1$_{24k}$** (black), **P2$_{24k}$-b** (blue), and **P3$_{24k}$-b** (red) demonstrating the hypsochromic shift upon IEDDA with TCO (thus breaking conjugation), and subsequent bathochromic shift post-oxidation. B) IR data illustrating the decrease in the N_2 stretch at 1535 cm^{-1} post-click. C) Fluorescence data for **P2$_{24k}$-b** and **P3$_{24k}$-b**. D) Comparison of absorption and emission spectra for **P1$_{24k}$** and **P3$_{24k}$-b**.

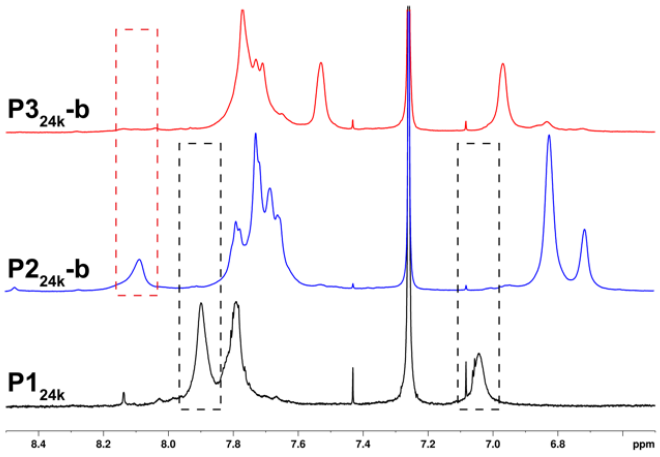

Figure 2.2. ^{1}H-NMR spectral overlay of **P1$_{24k}$** (black), **P2$_{24k}$-b** (blue), and **P3$_{24k}$-b** (red) illustrating the disappearance of furyl protons upon the IEDDA reaction, then disappearance of N-H resonance of dihydropyridazine upon oxidation.

2.5. Preparation of P3 polymer series

Conjugation length of the polymer plays a large role in the efficient dispersion of the SWNTs as non-convalent functionalization is accomplished through π- π interactions. Thus, it was necessary to oxidize the dihydropyridazine **P2** polymer series and fully aromatize the backbone to form the pyridazine **P3** polymer series (Scheme 4). This was accomplished using 2,3-dichloro-5,6-dicyano-1,4-benzoquinone (DDQ), which was added to a solution of polymer in THF at room temperature and stirred for 1 h, producing **P3$_{13k}$-a-c** and **P3$_{24k}$-a-c**. Once again, the reaction may be monitored by UV-Vis spectroscopy as the polymer exhibits a bathochromic shift of 19 to 45 nm upon oxidation (Figure 2.1A for **P3$_{13k}$-b** and Figure S31-S34, Table S1). This shift indicates an increase in conjugation length upon regaining aromaticity throughout the backbone, however, the λ_{max} of **P3** does not return to the same λ_{max} as the original **P1** tetrazine polymer. It should be noted that despite the significant change in the UV-Vis spectrum, the IR spectrum did not change

appreciably from the dihydropyridazine to the pyridazine (Figure 2.1B, Figures S51-55). Oxidation of the polymer backbone was confirmed by the complete disappearance of the signal arising from the dihydropyridazine N-H group in the ^{1}H-NMR spectrum (Figure 2.2, Figures S14-29). When comparing NMR and GPC results of the oxidized to the unoxidized polymers, there was no significant change in the apparent molecular weights, indicating that the polymers did not undergo chain scission in the oxidation process (Figures S45-50, Table S2). Further comparison of the **P1$_{24k}$** tetrazine polymer to the oxidized **P3$_{24k}$-c** polymer in Figure 2.1D demonstrates the sharp increase in fluorescence post-IEDDA and oxidation.

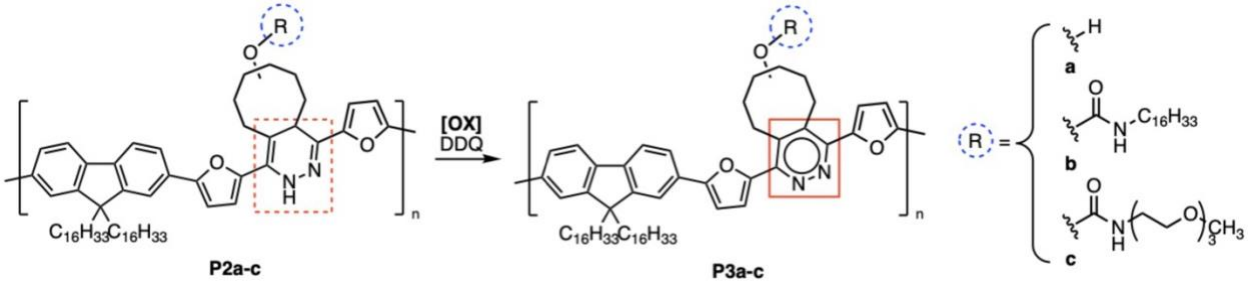

Scheme 2.4. Oxidation of **P2** polymer series, yielding the **P3** polymer series.

2.6. Conclusions

After the multi-step synthesis of a *s*-tetrazine-Br_2 monomer and a bis(pinacolato)boronate ester fluorene comonomer, the preparation of poly(tetrazines) of two molecular weights were prepared through a Suzuki polycondensation reaction. Post-synthetic backbone modification of the polymers was accomplished *via* an IEDDA reaction with select number of TCO derivatives. Completion of the reaction was monitored and confirmed through UV-Vis, FTIR, fluorescence, NMR spectroscopy, and TGA. The polymer was oxidized with DDQ to regain full conjugation of the backbone. GPC and end-group analysis through NMR spectroscopy confirmed the polymer

did not undergo chain-scission in the oxidation process. Following the work presented in this chapter, the polymers were used to prepare polymer-SWNT complexes in Chapter 3.

Chapter 3: Preparation and Characterization of Polymer-SWNT Complexes

3.1. Overview

Since their discovery 30 years ago, interest in single-walled carbon nanotubes (SWNTs) has flourished.[103] Their popularity can be attributed to their unique optoelectronic[104,105] and physical properties, such as high conductivity[106–108] and mechanical strength.[109,110] Some of their applications include use in transparent flexible electronics,[111] nanoprobes and sensors,[112] conductive inks,[113,114] and field-effect transistors.[111,115,116] However, carbon nanotubes have been plagued with difficulties in processing and poor solubility in organic solvents due to their tendency to aggregate.[124] Methods to covalently and non-covalently functionalize SWNT sidewalls are often performed to impart solubility.[125–127] Though covalent functionalization methods, such as fluorination-alkylation[135] or cycloaddition of the sidewall[136] are effective in solubilizing SWNTs, they introduce sp^3-hybridized carbon defects throughout the structure. Consequently, conjugation of the sp^2-hybridized carbons is disturbed, and many of the desired optoelectronic properties are disrupted.[126] Non-covalent methods utilize dispersants to form supramolecular dispersant-SWNT complexes that prevent reaggregation.[139,140] These dispersants include biomacromolecules,[141–144] surfactants,[145–150] small aromatic molecules,[151–153] and conjugated polymers.[154–158]

Conjugated polymers (CP) adsorb to the surface of SWNTs through π- π interactions, and can be easily modified through the introduction of varying functional groups.[243] Chapter 3 focuses on the preparation of polymer-SWNT complexes with the polymers prepared in Chapter 2. Solubility, conjugation of the backbone, and molecular weight were all systematically varied in this investigation to study how these structural factors affect the polymer efficiency in dispersing SWNTs. Modification on a polymer-SWNT complex was also explored and monitored through

UV-Vis-NIR absorption spectroscopy in this chapter to study the possibility of backbone modification post-dispersion.

3.2. Preparation and Exploration of Polymer-SWNT Dispersions

With all polymers in hand, we set out to study their interactions with SWNTs. Following literature procedures, we prepared the polymer-SWNT complexes by first probe sonicating a mixture of 7.5 mg of the respective polymer and 5.0 mg of HiPCo SWNTs in 10 mL of THF for 30 min. The resultant opaque black dispersion was centrifuged at 8346 *g* for 30 min, and the supernatant was carefully isolated and passed through a cotton plug. To remove excess polymer, the dispersion was filtered through a 0.2 µm pore diameter Teflon membrane and washed with THF until the filtrate was colorless and did not fluoresce when excited with a hand-held UV lamp at 365 nm. The film was then redispersed in 10 mL of THF by bath sonication for 3 h.

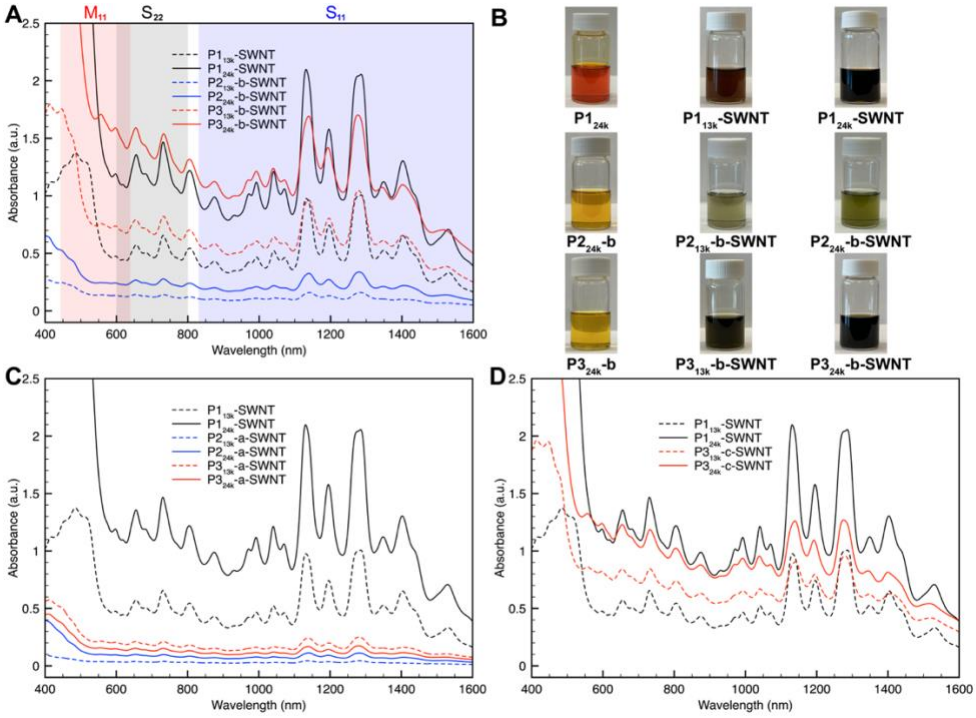

Figure 3.1. A) Photographs of dispersions prepared using high and low molecular weight polymers pre- and post-IEDDA/oxidation, illustrating the differences in opacity post-transformation and oxidation. B) Overlayed UV-Vis-NIR absorption spectra of dispersions prepared with tetrazine-containing polymers (black), unoxidized (blue), and oxidized (red) polymers reacted with hexadecylamine-TCO **7a**. C) Overlayed UV-Vis-NIR absorption spectra of dispersions prepared with polymers clicked with hydroxyl-TCO **5**. D) Overlayed UV-Vis-NIR absorption spectra of dispersions prepared with polymers clicked with TEG-TCO **7b**.

Figure 3.1A illustrates the distinct differences between the different polymer-SWNT dispersions as a result of the different molecular weights and polymer structures used for their preparation. When the pre-IEDDA polymer (**P1**) was used, it was observed that the higher molecular weight structure (24 kDa) resulted in a more concentrated nanotube dispersion than what was obtained with the lower molecular weight (13 kDa) polymer. This is consistent with previous reports indicating that low molecular weight polymers are less effective than higher molecular weight analogs.[243] Upon reaction with any of the TCO derivatives, it was found that the intermediate dihydropyridazine structures produce significantly less concentrated dispersions relative to those with unreacted polymers. This decreased concentration likely results from the fact that the dihydropyridazine structures are not fully conjugated and exhibit a non-planar structure, hindering the interaction with the SWNT sidewall. However, upon oxidation of the polymer backbone and rearomatization of the pyridazines (**P3**), it was found that the dispersions regain their dark color and are nearly equal in concentration to those with the unreacted polymers (**P1**). Thus, both molecular weight and conjugation of the polymer backbone are important factors dictating the interactions with SWNTs.

The UV−Vis−Near-Infrared (UV-Vis-NIR) absorption data allows the quantification of these observations (Figure 3.1B-D). Dispersions made with HiPCo SWNTs can be characterized through UV-Vis-NIR spectroscopy to determine the quality of the dispersion, concentration, and selectivity toward SWNT species in the sample.[217] For all the polymers investigated, the spectra indicate well-dispersed SWNTs as all peaks were sharp and intense. Using the spectra in Figure 3.1, we can confirm the impact of molecular weight on the concentration of SWNTs in a dispersion as in almost all cases the higher molecular weight polymer disperses more carbon nanotubes. It should be noted that **P3$_{13k}$-a-SWNT** and **P3$_{24k}$-a-SWNT** do not follow this trend. However, this is likely due to the lower solubility of the 24 kDa hydroxyl-functionalized polymer in THF affecting the solubility of the final dispersion. Solubility plays a large role in producing higher concentration SWNT dispersions, as seen when comparing the polymers containing the hexadecyl chain and the hydroxyl cycloadducts (Figure 3.1B–C). Both unoxidized, **P2-b-SWNT**, and oxidized, **P3-b-SWNT** dispersions resulted in a higher SWNT concentration when compared to their tetrazine and hydroxyl cycloadduct polymer counterparts, **P1-SWNT**, **P2-a-SWNT**, and **P3-a-SWNT**. The importance of uninterrupted conjugation of the polymer backbone is also highlighted, as the unoxidized **P2** polymers consistently produce dispersions of lower SWNT concentration than the oxidized **P3** polymers, regardless of side chain structure. Finally, we investigated the influence of side-chain polarity on the dispersion quality and concentration utilizing the TEG-containing polymers (Figure 3.1D). The concentration of SWNTs in **P3c-SWNT** is notably lower than that of **P3-b-SWNT**, however still comparable or more concentrated than **P1-SWNT**.

To further investigate the selectivity of the pre- and post-IEDDA polymers toward specific SWNT species, we analyzed normalized UV-Vis-NIR spectra. Three distinct electronic transition

regions are observed with HiPCo SWNTs: semiconducting regions S_{11} (830 to 1600 nm), and S_{22} (600 to 800 nm), and the metallic region M_{11} (440 to 645 nm).[217] The pre-IEDDA polymer **P1** did not demonstrate significant selectivity toward either sc- or m-SWNTs when dispersed in THF (Figure 3.2). However, post-IEDDA, all dihydropyridazine (**P2**) and pyridazine (**P3**) polymers produced dispersions with increased relative concentrations of m-SWNTs, as seen in the M_{11} region, and decreased concentrations of sc-SWNTs in the S_{11} region, indicating less selectivity toward sc-SWNTs than **P1** in THF. The exact reason for this small difference in selectivity between the pre- and post-clicked polymers is not clear, but the fact that the polymer structures are identical in length and nearly identical in structure allows us to probe the small structural changes that give rise to the difference in selectivity. One significant difference that results from IEDDA is the change from the tetrazine to the pyridazine structure. The tetrazine is symmetrical, and therefore exhibits a small dipole moment, whereas the pyridazine structure is not symmetrical, with the two nitrogens attracting electron density and creating a dipole. Polar solvents are known to interact more strongly with the more polarizable m-SWNTs than non-polar solvents,[113] therefore the more dipolar pyridazine-containing polymers may similarly exhibit a preferential interaction with the m-SWNTs.

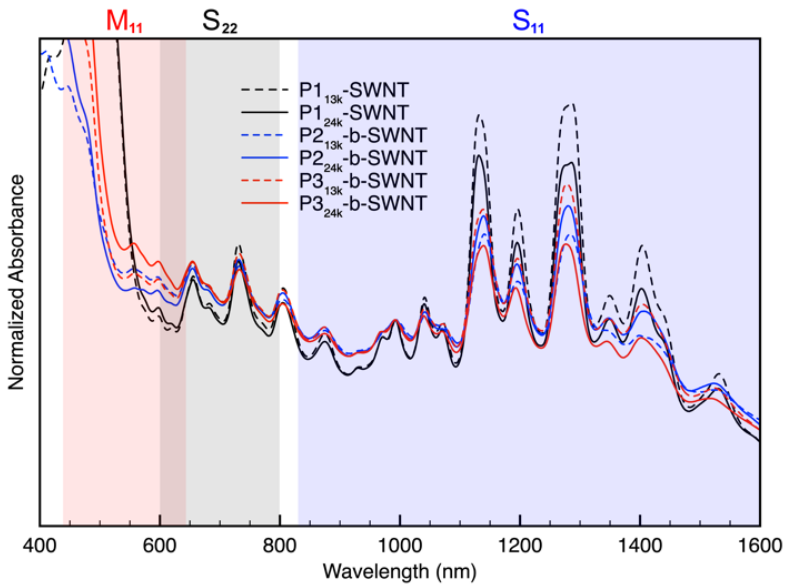

Figure 3.2. Normalized absorption data of **P1-SWNT**, **P2-b-SWNT**, **P3-b-SWNT** illustrating an increase in absorbance in the M_{11} region and a decrease in the S_{11} region.

Photoluminescence (PL) maps provide insight into the population of sc-SWNT species that are present in a dispersion, as their individual emission peaks can be resolved.[218] Comparing the PL map of the nanotube dispersion with **P1$_{24k}$** (Figure 3.3A) to the post-IEDDA sample with **P3$_{24k}$** (Figure 3.3B), it is clear that there is little difference in selectivity for any specific semiconducting (n,m) species. However, the PL data indicates an increase in m-SWNT concentration, which quenches nanotube fluorescence, as there is a significant decrease in the emission intensity for the **P3$_{24k}$-b-SWNT** sample compared to the **P1$_{24k}$-SWNT** sample (compare intensity scales in Figure 3.3). This observation is consistent with the UV-Vis-NIR absorption data (Figure 3.2), which also indicated an increase in m-SWNT content when the post-IEDDA polymer was used to disperse SWNTs. In addition, the intense fluorescence observed at ~1125 nm and ~1275 nm when **P1$_{24k}$-SWNT** is excited at ~525 nm disappears in the **P3$_{24k}$-b-SWNT** sample, which is consistent with the other post-IEDDA polymers (Figures S77–S80). These signals in the NIR region are likely

caused by energy transfer from the poly(fluorene-*co*-tetrazine), which exhibits an absorption tail up to 550 nm (Figure 2.1A), to the SWNT, followed by emission from the (8,4), (7,6) and (9,4) species at ~1125 nm, and the (10,3), (9,5), and (8,7) species at ~1275 nm. Upon reaction with the TCO derivatives, the hypsochromic shift to the polymer's absorption spectrum removes this ability to absorb excitation wavelengths above 500 nm, thus the sensitized nanotube emission cannot occur.

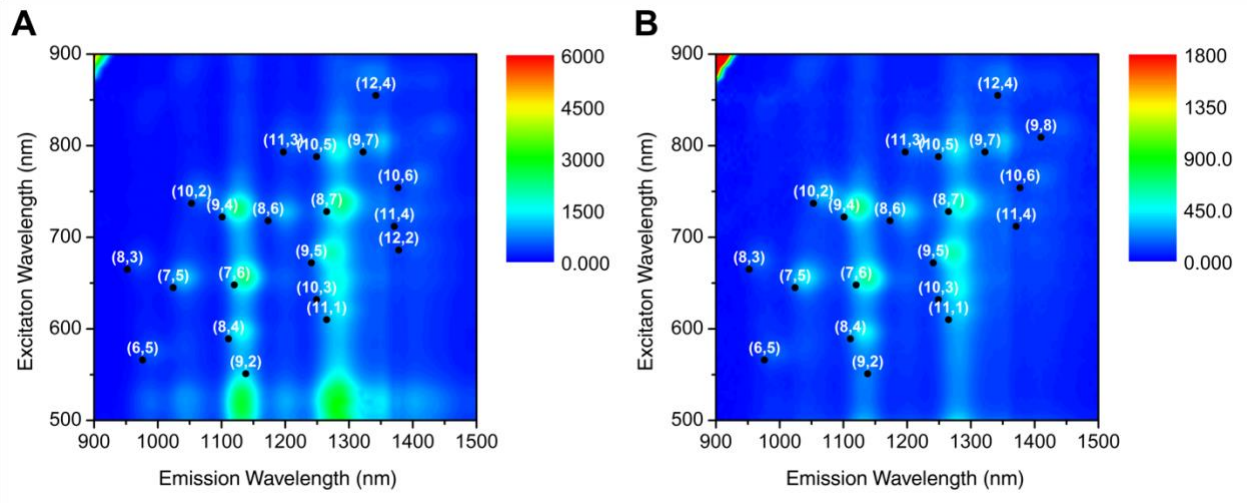

Figure 3.3. PL maps of **P1$_{24k}$-SWNT** (A) and **P3$_{24k}$-b-SWNT** (B) in THF.

Additional characterization by resonance Raman spectroscopy allowed further investigation of polymer-SWNT dispersions.[220,225] 532 nm, 633 nm, and 785 nm were used to identify m- and sc-SWNTs within the samples.[232] All samples were prepared by drop-casting the polymer-SWNT dispersions onto a clean silicon wafer and allowing the sample to evaporate at room temperature. Raw HiPCo SWNTs were sonicated in THF and similarly prepared for Raman spectroscopy. Figure 3.4A-C depicts the Raman spectra of raw SWNTs, **P1-SWNT**, **P2-b-SWNT**, and **P3-b-SWNT** excited at 532 nm, 633 nm, and 785 nm respectively. For all samples, it was found that the relative intensity of the D-band (~1290 cm^{-1}) remains negligible, indicating that

disperson with the polymers does not introduce defects on the SWNT structure. In most cases, it was also found that the G-band exhibited a Lorentzian line shape, which is consistent with the presence of mostly sc-SWNTs. However, when **P3-b-SWNT** was excited at 532 nm (Figure 3.4A), a broad G^- band having a Breit-Wigner-Fano (BWF) line shape was observed, indicating that this sample contains a higher relative m-SWNTs content than the other samples. This observation is again consistent with the UV-Vis-NIR spectra (Figure 3.2) and the PL maps (Figure 3.3) discussed above. Additionally, the line pattern for **P1-SWNT** when excited at 532 nm is unusual, with numerous intense signals between 700 and 1600 cm^{-1} (Figure 3.4A). These signals do not appear when longer excitation wavelengths are used and are also not present in the post-IEDDA dispersions. Furthermore, these signals are not observed for the polymer alone, indicating that they arise from vibrations of the polymer structure that only occur when it is bound to the nanotube surface. Considering that **P1** exhibits absorption intensity between 500 and 550 nm (while **P2** and **P3** do not), it is not surprising that the observed vibrations are only seen with 532 nm excitation, and only with this polymer.

Figures 3.4D shows the normalized radial breathing mode (RBM) data of **P1-SWNT**, **P2-b-SWNT**, and **P3-b-SWNT**, excited at 532 nm where m-SWNTs are primarily in resonance (~215–300 cm^{-1}).[233] These spectra indicate an increase in m-SWNT content within the samples prepared with post-IEDDA polymers, further confirming our observations from the UV-Vis-NIR spectra (Figure 3.2). When excited at 633 nm, both m-SWNT (~170—230 cm^{-1}) and sc-SWNTs (~240—300 cm^{-1}) are in resonance (Figure 3.4E).[217] From these spectra, we again observe an increase in m-SWNT content post-IEDDA. Lastly, excitation at 785 nm is primarily in resonance with sc-SWNTs, and the spectra are consistent with the presence of semiconducting species. Additionally, this excitation wavelength allows investigation of nanotube bundling in the samples,

which can be identified by the presence of a peak at 265 cm^{-1} corresponding to bundled (10,2) SWNTs (the "bundling" peak, Figure 3.4F). This bundling peak is clearly present in the raw SWNT sample but have very low intensity in all the polymer-SWNT dispersions, indicating that SWNTs are well dispersed by the polymers.

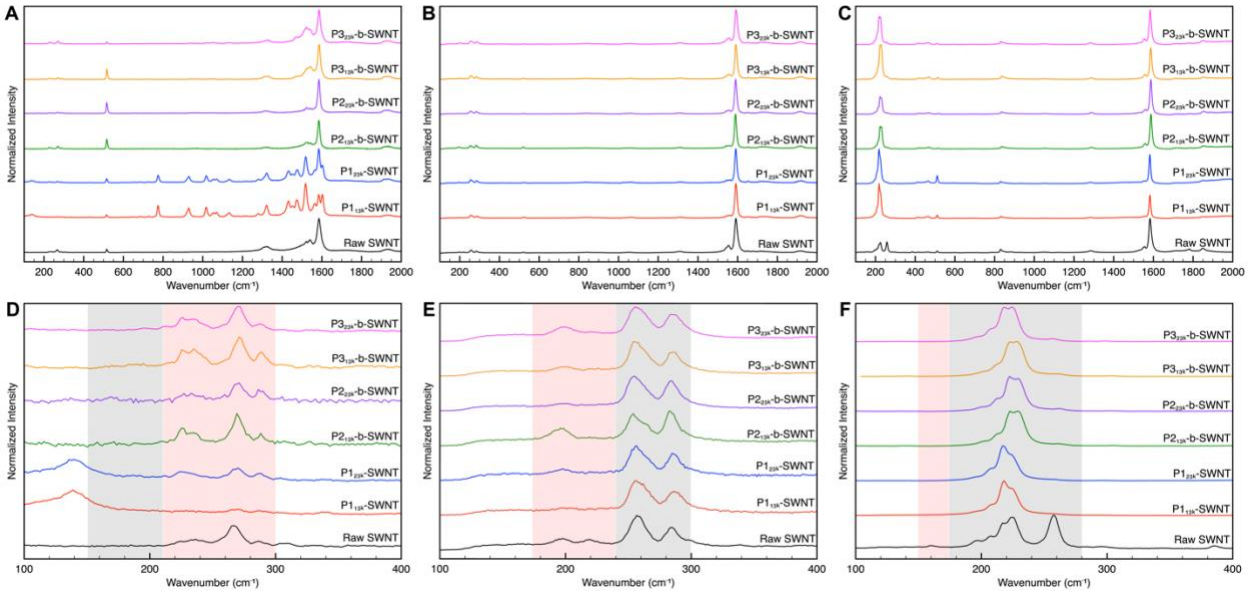

Figure 3.4. Full Raman spectra of raw SWNTs, **P1-SWNT**, **P2-b-SWNT**, and **P3-b-SWNT** at A) λ_{ex} = 532 nm, B) λ_{ex} = 633 nm, and C) λ_{ex} = 785 nm, and of the RBM region at D) 532 nm, E) 633 nm, and F) 785 nm. The signal at 520 cm^{-1} arises from the silicon substrate.

We used atomic force microscopy (AFM) to qualitatively assess the dispersions and to measure the height profiles of the polymer-SWNT complexes (Figure 3.5). **P1$_{24k}$-SWNT** appears to form a uniform coating on the nanotube surface, with only miniscule amounts of detectable excess polymer in the images (Figure 3.5A,B). In contrast, when **P3$_{24k}$-b** was used for SWNT dispersion, numerous features resembling aggregates of polymer associated with nanotubes, as well as possible SWNT bundles, were observed (Figure 3.5C,D). These aggregates were observed consistently with all post-IEDDA polymers (Figures S71–S76) and are likely caused by increased

intermolecular interactions that result from an increase in polarity of the polymer backbone. The height profiles of the polymer-SWNT complexes remain consistent across all the samples, irrespective of the IEDDA reaction. As an example, the **P1$_{24k}$-SWNT** sample had an average height of 2.43 ± 1.23 nm, while the post-IEDDA **P3$_{24k}$-b-SWNT** sample exhibited a height of 1.98 ± 0.77 nm, illustrating very minute changes in the height of polymer-SWNT complexes between all the samples (data provided in the Supporting Information, Tables S3–S10).

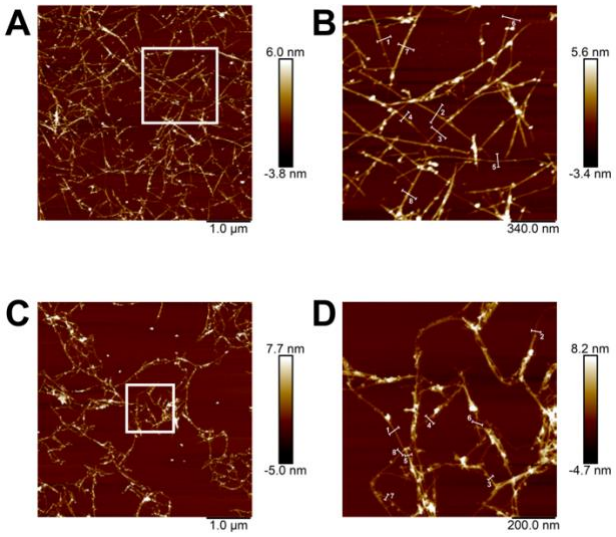

Figure 3.5. AFM images of **P1$_{24k}$-SWNT** (A) and **P3$_{24k}$-b-SWNT** (C) spin-coated on a mica substrate, as well as the respective magnified regions (**P1$_{24k}$-SWNT** (B) and **P3$_{24k}$-b-SWNT** (D)) illustrated with a white box. Height profiles were measured at locations where individual SWNTs were present; these locations are depicted with white lines.

3.3. IEDDA transformation on Polymer-SWNT dispersion

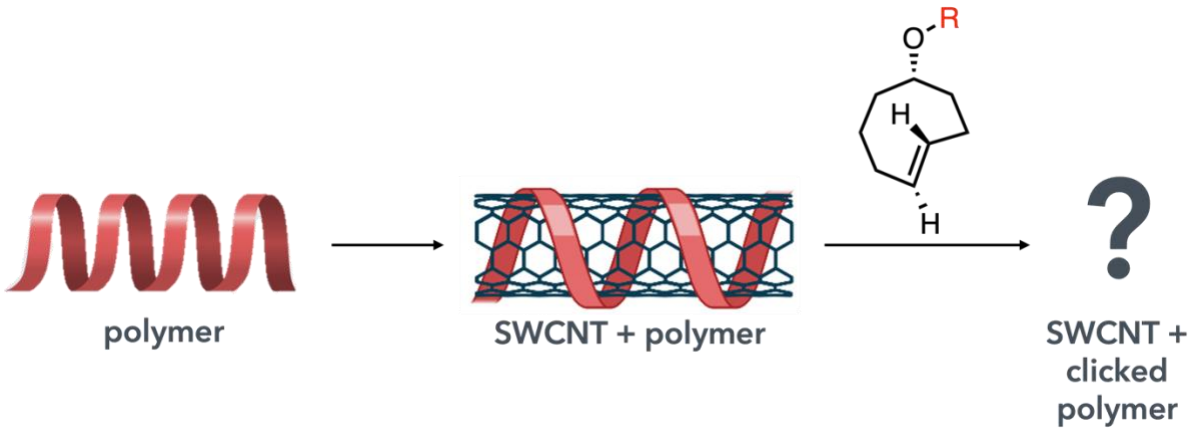

Considering that the IEDDA reaction is highly efficient on the poly(fluorene-*co*-tetrazine) in solution, we set out to explore the possibility of performing this reaction on the nanotube-bound polymer (i.e., the polymer-SWNT dispersion). The dispersions were prepared with **P1$_{13k}$** and **P1$_{24k}$** following the previous procedure. As there is a significant hypsochromic shift in the polymer absorption upon IEDDA with TCO derivatives (Figure 2.1), we utilized UV-Vis absorption spectroscopy to monitor the reaction. We chose to carry out the reaction with hexadecylamine-TCO **9a** as the resulting polymer is highly soluble and led to stable nanotube dispersions when used directly. The polymer-SWNT dispersions were prepared as described above and subsequently treated with 1.5 eq of **9a** (relative to the tetrazine repeat unit) under vigorous stirring. 200 μL aliquots were sampled from the dispersion and diluted to 800 μL prior to UV-Vis absorption measurement. Figure 3.6A illustrates the absorption spectra from the reaction of **9a** with **P1$_{24k}$-SWNT** collected at various time points over the course of 9 h. A clear hypsochromic shift in the absorption spectrum was observed, consistent with the polymer in solution (Figure 2.1). The spectral shift was found to stop changing after 8 h, indicating the end of the reaction. The dispersion remained mostly stable and dark in color over the course of the reaction (see images in Figure 3.6B), but it should be noted that small amounts of particulate were observed to sediment

after the IEDDA reaction. Oxidation of the dispersion was achieved by treatment with 1.5 eq of DDQ (relative to the original tetrazine repeat units in the polymer) followed by stirring for 6 h at room temperature. The dispersion was rinsed of excess DDQ by filtration through a Teflon membrane and washing with excess THF. The resulting film was redispersed in 10 mL of THF using bath sonication. UV-Vis absorption spectroscopy of the final dispersion showed the expected bathochromic shift of ~30-60 nm after oxidation (Figure 3.6C), consistent with what was observed for the polymer alone.

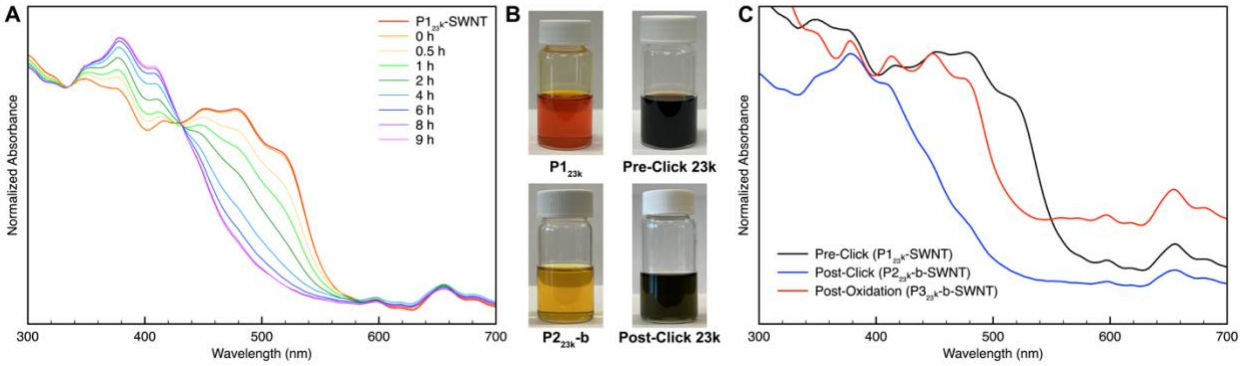

Figure 3.6. A) UV-Vis absorption data of the monitored IEDDA reaction between hexadecylamine-TCO **9a** and the **P1$_{24k}$-SWNT** dispersion. B) Photographs of **P1$_{24k}$** and **P1$_{24k}$-SWNT** pre- and post-IEDDA. C) UV-Vis absorption data of **P1$_{24k}$-SWNT** pre-IEDDA, post-IEDDA, and post-oxidation, normalized at 378 nm.

Raman analysis of the dispersions pre- and post-IEDDA and oxidation showed that the D-band retained a negligible relative intensity, indicating that the post-dispersion chemistry did not introduce defects within the nanotube structure (Figures 3.7 and S89-S91). In all spectra, the G-band retains a sharp, Lorentzian lineshape, indicating that the samples are mostly composed of sc-SWNTs. However, when excited at 532 nm, the post-IEDDA samples show a small increase in the

G^- band, corresponding to the presence of m-SWNTs. This is corroborated by the RBM signals, where an increase in signals arising from m-SWNTs (205-300 cm^{-1}) is observed upon excitation at 532 nm. Considering that the IEDDA chemistry was performed on a pre-dispersed sample of SWNTs, the increase in m-SWNT intensity can only arise if sc-SWNTs selectively precipitate during the reaction. This is consistent with the small change in selectivity toward m-SWNTs that was observed when post-IEDDA polymers were used to prepare dispersions. Excitation at 633 nm also indicates that m-SWNTs are present at higher concentration post-IEDDA, especially with the higher molecular weight polymer (**P2$_{24k}$**). Lastly, 785 nm excitation shows that the bundling peak is almost undetectable, again indicating that the samples are well dispersed and did not aggregate after the IEDDA reaction.

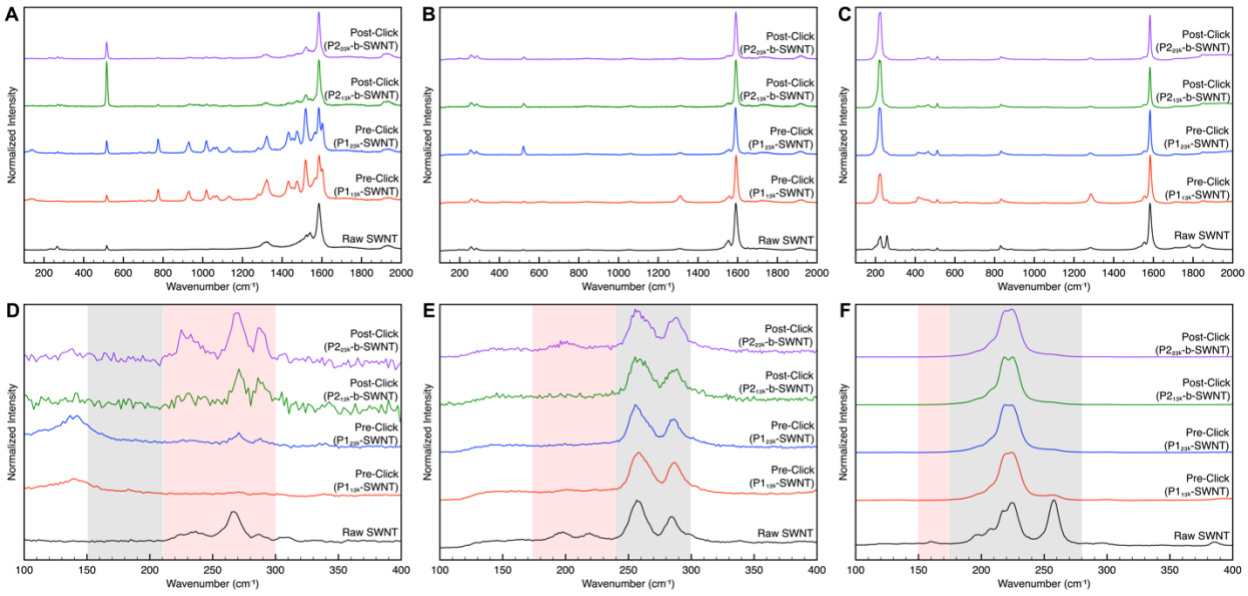

Figure 3.7. Full Raman spectra of raw SWNTs, and **P1-SWNT** pre- and post- IEDDA at A) λ_{ex} = 532 nm, B) λ_{ex} = 633 nm, and C) λ_{ex} = 785 nm, and of the RBM region at D) 532 nm, E) 633 nm, and F) 785 nm. The signal at 520 cm^{-1} arises from the silicon substrate.

Interestingly, AFM analysis of the post-IEDDA dispersions (spin coated onto mica) shows a significant amount of aggregation upon sample drying (Figure 3.8). This aggregation is consistent with what was observed when the post-IEDDA polymer was used to disperse SWNTs, and again indicates that the dispersed polymer-SWNT complexes have a greater tendency to interact with one another upon conversion of tetrazines to pyridazines and introduction of the hexadecyl sidechains. It is likely that the increased polarity of the pyridazines relative to tetrazines introduces dipole-dipole interactions that promote sample aggregation upon drying on the mica surface. Height analysis of features that represent individual nanotubes (Figure 3.8B) resulted in an average height of 2.75 ± 0.62 nm, which is consistent with a single tube wrapped by polymer (individual values for each analyzed feature are provided in the Supporting Information, Table S12).

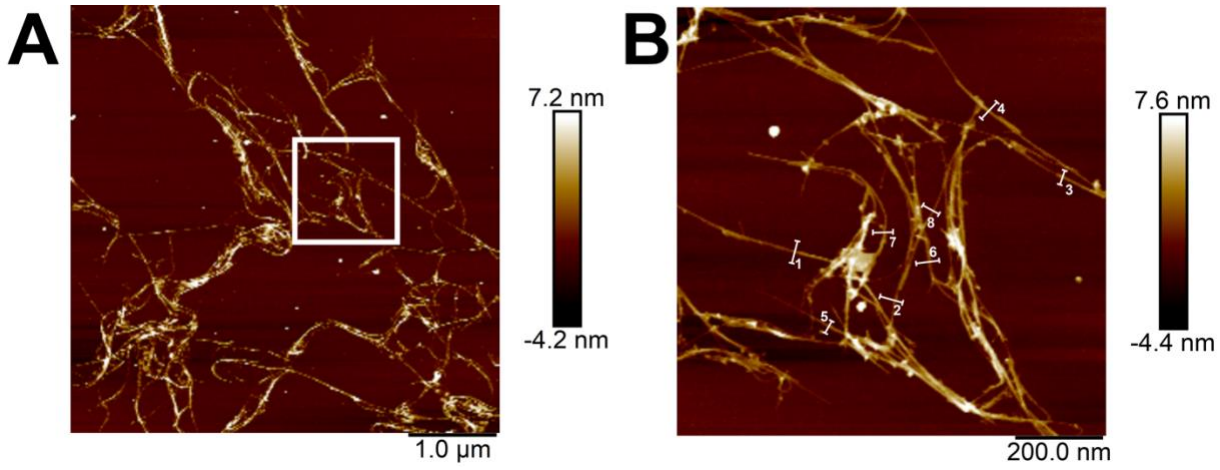

Figure 3.8. AFM images of **P1$_{24k}$-SWNT** after undergoing IEDDA and oxidation, spin-coated on a mica substrate (A), as well as the respective magnified region illustrated with a white box (B). Height profiles were measured at locations where individual SWNTs were present; these locations are depicted with white lines.

3.4. Conclusions

The polymers were used to prepare dispersions and characterized through AFM, UV-Vis-NIR, Raman, and PL mapping, indicating that **P1** uniformly coated the SWNTs and produced high concentration dispersions composed of mostly sc-SWNTs. Selectivity towards m-SWNTs increases post-IEDDA, as suggested by the Raman and normalized absorption data. Comparison of the **P2** and **P3** polymer series suggests dispersion concentration is dependent on conjugation. Solubility of the polymer plays an important role in the dispersion of SWNTs as demonstrated by comparison of functional groups. Lastly, a model study using a hexadecylamine-TCO on **P1-SWNT** dispersions shows that quantitative functionalization of the polymer can be achieved post-dispersion while still preserving the structure and properties of the SWNTs.

Chapter 4: Overall Conclusions and Recommendations For Future Work

4.1. Overall Conclusions

SWNTs represent a cylindrical one-dimensional carbon allotrope with unique optoelectronic and physical properties, such as high conductivity and mechanical strength. Though there are extensive studies of their interactions with conjugated polymers, studies to understand the fundamental principles of non-covalent functionalization with CPs are few and far between. To establish an understanding would require control over length and dispersity while exploring polymer electronics, sterics, and other structural features. In the effort to achieve this understanding, the work in this thesis successfully explores the interactions of a reactive tetrazine-containing conjugated polymer with SWNTs.

In Chapter 2, we demonstrated two tetrazine-containing polymers of low and high molecular weight undergoing rapid transformation and functionalization with a select number of TCO derivatives to generate dihydropyridazine polymers. From there, the polymers were then oxidized to produce fully conjugated pyridazine polymers. Full characterization of the polymers was achieved through UV-Vis, FTIR, NMR, and fluorescence spectroscopy, as well as GPC and TGA.

The polymers were used to prepare SWNT dispersions in Chapter 3. Characterization through AFM, UV-Vis-NIR, Raman, and PL mapping indicate uniform coating of the SWNTs with the tetrazine-containing polymers, producing high concentration dispersions with mostly sc-SWNTs. UV-Vis-NIR spectroscopy of the dihydropyridazine polymer series suggests dispersion concentration is heavily reliant on aromaticity as an increase in concentration is observed when dispersed with the oxidized pyridazine polymers. Solubility also plays a large role in dispersion efficiency as the hexadecyl and triethylene glycol grafted polymers consistently outperformed the

hydroxyl grafted polymers in THF. The normalized absorption data suggests the clicked polymers disperse more m-SWNTs than the tetrazine-containing polymers, which was further corroborated with Raman spectroscopy.

The most significant contribution of this thesis lies in the possibility of backbone modification on polymer-SWNT complexes. A model study demonstrates that polymer-SWNT complexes are able to undergo post-synthetic functionalization *via* IEDDA. Completion of the reaction was monitored through the UV-Vis absorption spectroscopy. Backbone modification can be accomplished while preserving the structure and properties of the SWNTs. This shows promising applications for the rapid functionalization of carbon nanotubes dispersed with tetrazine-based polymers in the future.

4.2. Recommendations for Future Works

This thesis is the first example of reactive poly(tetrazines) dispersing carbon nanotubes, thus many potential avenues remain open to exploration. For one, the exploration of different comonomers should be exploited, as the backbone structure greatly alters the electronic properties, reactivity, and solubility of the overall polymer. The IEDDA reaction is governed by the substituents on the diene and dienophile. Tetrazines with electron-withdrawing groups have shown improved reactivity but also demonstrate lower stability.[212] Thus, it is worthwhile to investigate the balance between improved reactivity and stability with different comonomers. Further exploration into the utilization of EWG and EDG comonomers to improve the selectivity toward m- or sc-SWNTs would also be beneficial in understanding polymer-SWNT interactions.

Another potential direction to explore is improving the solubility of the tetrazine monomer. The tetrazine polymer described in this work demonstrated low solubility. To improve solution

processability of the tetrazine polymers, it would be interesting to prepare moieties with alkyl chains on the furyl ring.

This work demonstrated the first backbone modification of tetrazine polymers within a polymer-SWNT complex. It would be a missed opportunity to not investigate different TCO derivatives to exploit this ability. Rapid functionalization of polymer-SWNT dispersions with *bis*-functionalized poly(ethylene glycol) TCO derivatives could potentially be used to prepare a crosslinked carbon nanotube-loaded material. Other studies involving the comparison of TCO derivatives to cyclooctynes and norbornenes, while still using the same progenitor polymer, should be investigated to evaluate backbone functionality. It is also possible to be selective toward different diameters of carbon nanotubes by altering the functional group on the TCO. This would be an opportunity to systematically study the effects of side chain steric bulk on SWNT selectivity using this system. There is additional potential with the system described in this thesis to further the understanding of polymer interactions with carbon nanotubes by investigating the effects of small structural changes on the polymer that impart specific changes to its polarity or electronic nature. The advancement of this knowledge will aid in the future designs of conjugated polymers for SWNT applications.

References

(1) Feldman, D. *Des. Monomers Polym.* **2008**, *11* (1), 1.
(2) Lu, H.; Li, X.; Lei, Q. *Front. Chem.* **2021**, *9* (732132).
(3) Zhan, X.; Zhu, D. *Polym. Chem.* **2010**, *1* (4), 409.
(4) Zheng, B.; Huo, L.; Li, Y. *NPG Asia Mater.* **2020**, *12* (1), 3.
(5) Zou, X.; Cui, S.; Li, J.; Wei, X.; Zheng, M. *Front. Chem.* **2021**, *9* (671294).
(6) Sirringhaus, H.; Tessler, N.; Friend, R. H. *Science* **1998**, *280* (5370), 1741.
(7) Lu, S.; Jia, C.; Duan, X.; Zhang, X.; Luo, F.; Han, Y.; Huang, H. *Colloids Surf. Physicochem. Eng. Asp.* **2014**, *443*, 488.
(8) Inal, S.; Rivnay, J.; Suiu, A.-O.; Malliaras, G. G.; McCulloch, I. *Acc. Chem. Res.* **2018**, *51* (6), 1368.
(9) Rasmussen, S. C. *ChemPlusChem* **2020**, *85* (7), 1412.
(10) Skotheim, T. A. *Handbook of Conducting Polymers: Second Edition, Revised and Expanded*; CRC Press: Boca Raton, 1997.
(11) Müllen, K.; Scherf, U. *Macromol. Chem. Phys.* **2023**, *224* (3), 2200337.
(12) Lakard, B. *Appl. Sci.* **2020**, *10* (18), 6614.
(13) Zhang, S.; Ocheje, M. U.; Luo, S.; Ehlenberg, D.; Appleby, B.; Weller, D.; Zhou, D.; Rondeau-Gagné, S.; Gu, X. *Macromol. Rapid Commun.* **2018**, *39* (14), 1800092.
(14) Gumyusenge, A.; McNutt, W.; Mei, J. In *Conjugated Polymers: Properties, Processing, and Applications*; Reynolds, J. R., Thompson, B. C., Skotheim, T. A., Eds.; CRC Press: Boca Raton, 2019; p 25.
(15) Zeng, W.; Deng, Z.; Wang, H.; Zhang, H.; Zhou, Q. *Dyes Pigments* **2019**, *164*, 198.
(16) Choudhary, K.; Chen, A. X.; Pitch, G. M.; Runser, R.; Urbina, A.; Dunn, T. J.; Kodur, M.; Kleinschmidt, A. T.; Wang, B. G.; Bunch, J. A.; Fenning, D. P.; Ayzner, A. L.; Lipomi, D. J. *ACS Appl. Mater. Interfaces* **2021**, *13* (43), 51436.
(17) Lund, A.; Van Der Velden, N. M.; Persson, N.-K.; Hamedi, M. M.; Müller, C. *Mater. Sci. Eng. R Rep.* **2018**, *126*, 1.
(18) Lee, D.; Sang, J.; Yoo, P.; Shin, T.; Oh, K.; Park, J. *Polymers* **2018**, *11* (1), 16.
(19) Andrew, T. L.; Zhang, L.; Cheng, N.; Baima, M.; Kim, J. J.; Allison, L.; Hoxie, S. *Acc. Chem. Res.* **2018**, *51* (4), 850.
(20) Geni, E. M.; Boyle, A.; Lapkowsky, M.; Tsintavis, C. *Synth. Met.* **1990**, *36* (2), 139.
(21) Rasmussen, S. C. *Subst. Int. J. Hist. Chem.* **2017**, *1* (2), 99.
(22) Kränzlein, G. *Angew. Chem.* **1935**, *48* (1), 1.
(23) Crace-Calvert, F.; Revely, H. W. *J. Soc. Arts* **1862**, *10* (481), 167.
(24) Rasmussen, S. C. *Ambix* **2018**, *65* (4), 356.
(25) Green, A. G.; Wolff, S. *Berichte Dtsch. Chem. Ges.* **1911**, *44* (3), 2570.
(26) Green, A. G.; Woodhead, A. E. *Berichte Dtsch. Chem. Ges.* **1912**, *45* (2), 1955.
(27) Abu-Thabit, N. Y. *J. Chem. Educ.* **2016**, *93* (9), 1606.
(28) Rasmussen, S. C. *Bull. Hist. Chem.* **2015**, *40* (1).
(29) Zhang, Z.; Rouabhia, M.; Moulton, S. E. *Conductive Polymers: Electrical Interactions in Cell Biology and Medicine*; CRC Press: Boca Raton, 2018.
(30) Bolto, B. A.; McNeill, R.; Weiss, D. E. *Aust. J. Chem.* **1963**, *16* (6), 1090.
(31) Sasso, C.; Beneventi, D.; Zeno, E.; Chaussy, D.; Petit-Conil, M.; Belgacem, N. *BioResources* **2011**, *6* (3), 3585.
(32) Rasmussen, S. C. *Bull. Hist. Chem.* **2017**, *42* (1).

(33) Natta, G.; Mazzanti, G.; Corradini, P. In *Stereoregular Polymers and Stereospecific Polymerizations*; Natta, G., Danusso, F., Eds.; Pergamon: Oxford, 1967; pp 463–465.
(34) Natta, G.; Pasquon, I.; Giachetti, E. *Angew. Chem.* **1957**, *69* (7), 213.
(35) Rasmussen, S. C. *Substantia* **2021**, *5* (1).
(36) MacDiarmid, A. G. *Angew. Chem. Int. Ed.* **2001**, *40* (14), 2581.
(37) Shirakawa, H.; Louis, E. J.; Macdiarmid, A. G.; Chiang, C. K.; Heeger, A. J. *J. Chem. Soc. Chem. Commun.* **1977**, No. 16, 578.
(38) Chiang, C. K.; Fincher, C. R.; Park, Y. W.; Heeger, A. J.; Shirakawa, H.; Louis, E. J.; Gau, S. C.; MacDiarmid, A. G. *Phys. Rev. Lett.* **1977**, *39* (17), 1098.
(39) Rasmussen, S. C.; Rasmussen, S. *Bull Hist Chem* **2014**, *39* (1).
(40) Rasmussen, S. C. In *100+ Years of Plastics. Leo Baekeland and Beyond*; Strom, E. T., Rasmussen, S. C., Eds.; American Chemical Society: Washington, 2011; Vol. 1080, pp 147–163.
(41) Le, T.-H.; Kim, Y.; Yoon, H. *Polymers* **2017**, *9* (12), 150.
(42) Chueh, P.-H.; Chang, C.-Y.; Lin, Y.-C.; Chen, W.; Chueh, C.-C. *J. Taiwan Inst. Chem. Eng.* **2022**, *140*, 104566.
(43) Root, S. E.; Savagatrup, S.; Printz, A. D.; Rodriquez, D.; Lipomi, D. J. *Chem. Rev.* **2017**, *117* (9), 6467.
(44) Luo, N.; Ren, P.; Feng, Y.; Shao, X.; Zhang, H.-L.; Liu, Z. *J. Phys. Chem. Lett.* **2022**, *13* (4), 1131.
(45) Mei, J.; Bao, Z. *Chem. Mater.* **2014**, *26* (1), 604.
(46) He, Y.; Kukhta, N. A.; Marks, A.; Luscombe, C. K. *J. Mater. Chem. C* **2022**, *10* (7), 2314.
(47) Son, S. Y.; Kim, Y.; Lee, J.; Lee, G.-Y.; Park, W.-T.; Noh, Y.-Y.; Park, C. E.; Park, T. *J. Am. Chem. Soc.* **2016**, *138* (26), 8096.
(48) Zhao, H.; Shanahan, J. J.; Samson, S.; Li, Z.; Ma, G.; Prine, N.; Galuska, L.; Wang, Y.; Xia, W.; You, W.; Gu, X. *Macromol. Rapid Commun.* **2022**, *43* (24), 2200533.
(49) Galuska, L. A.; McNutt, W. W.; Qian, Z.; Zhang, S.; Weller, D. W.; Dhakal, S.; King, E. R.; Morgan, S. E.; Azoulay, J. D.; Mei, J.; Gu, X. *Macromolecules* **2020**, *53* (14), 6032.
(50) Rimmele, M.; Glöcklhofer, F.; Heeney, M. *Mater. Horiz.* **2022**, *9* (11), 2678.
(51) Creamer, A.; Wood, C. S.; Howes, P. D.; Casey, A.; Cong, S.; Marsh, A. V.; Godin, R.; Panidi, J.; Anthopoulos, T. D.; Burgess, C. H.; Wu, T.; Fei, Z.; Hamilton, I.; McLachlan, M. A.; Stevens, M. M.; Heeney, M. *Nat. Commun.* **2018**, *9* (1), 3237.
(52) Yin, J.; Choi, S.; Pyle, D.; Guest, J. R.; Dong, G. *J. Am. Chem. Soc.* **2023**, *145* (34), 19120.
(53) Dong, C.-S.; Meng, B.; Liu, J.; Wang, L.-X. *Chin. J. Polym. Sci.* **2023**, *41* (1), 108.
(54) Leclerc, N.; Chávez, P.; Ibraikulov, O.; Heiser, T.; Lévêque, P. *Polymers* **2016**, *8* (1), 11.
(55) Woods, E. F.; Berl, A. J.; Kalow, J. A. *ChemPhotoChem* **2021**, *5* (1), 4.
(56) Lo, C. K.; Wolfe, R. M. W.; Reynolds, J. R. *Chem. Mater.* **2021**, *33* (13), 4842.
(57) Campeau, L.-C.; Hazari, N. *Organometallics* **2019**, *38* (1), 3.
(58) Amna, B.; Siddiqi, H. M.; Hassan, A.; Ozturk, T. *RSC Adv.* **2020**, *10* (8), 4322.
(59) Inzelt, G. *Conducting Polymers: A New Era in Electrochemistry*, 1st ed.; Monographs in Electrochemistry; Springer Berlin Heidelberg: Berlin, 2008.
(60) *Conjugated Polymers: Theory, Synthesis, Properties, and Characterization*, 3rd ed.; Skotheim, T. A., Reynolds, J., Eds.; CRC Press: Boca Raton, 2006.
(61) Liu, J.; Baek, J.-B.; Dai, L. In *Encyclopedia of Polymeric Nanomaterials*; Kobayashi, S., Müllen, K., Eds.; Springer: Berlin, 2021; pp 1–7.
(62) Kang, S.; Kim, G.-H.; Park, S.-J. *Acc. Chem. Res.* **2022**, *55* (16), 2224.

(63) Stefik, M.; Guldin, S.; Vignolini, S.; Wiesner, U.; Steiner, U. *Chem. Soc. Rev.* **2015**, *44* (15), 5076.
(64) Ying, L.; Huang, F.; Bazan, G. C. *Nat. Commun.* **2017**, *8* (1), 14047.
(65) Ye, S.; Cheng, S.; Pollit, A. A.; Forbes, M. W.; Seferos, D. S. *J. Am. Chem. Soc.* **2020**, *142* (25), 11244.
(66) Li, J.; Hou, J. In *Introduction to Organic Electronic and Optoelectronic Materials and Devices*; Sun, S.-S., Dalton, L. R., Eds.; CRC Press: Boca Raton, 2016.
(67) Mehmood, U.; Al-Ahmed, A.; Hussein, I. A. *Renew. Sustain. Energy Rev.* **2016**, *57*, 550.
(68) Kaloni, T. P.; Giesbrecht, P. K.; Schreckenbach, G.; Freund, M. S. *Chem. Mater.* **2017**, *29* (24), 10248.
(69) Jayasundara, W. J. M. J. S. R.; Schreckenbach, G. *J. Phys. Chem. C* **2020**, *124* (32), 17528.
(70) Mousavi, S. M.; Hashemi, S. A.; Bahrani, S.; Yousefi, K.; Behbudi, G.; Babapoor, A.; Omidifar, N.; Lai, C. W.; Gholami, A.; Chiang, W.-H. *Int. J. Mol. Sci.* **2021**, *22* (13), 6850.
(71) Kumar, A.; Buyukmumcu, Z.; Sotzing, G. A. *Macromolecules* **2006**, *39* (8), 2723.
(72) Singh, N.; Singh, S.; Kumar, P.; Riaz, U. *RSC Adv.* **2020**, *10* (61), 37456.
(73) Vanossi, D.; Cigarini, L.; Giaccherini, A.; Da Como, E.; Fontanesi, C. *Molecules* **2016**, *21* (1), 110.
(74) McCullough, R. D. *Adv. Mater.* **1998**, *10* (2), 93.
(75) Yamamoto, T. *NPG Asia Mater.* **2010**, *2* (2), 54.
(76) Faïd, K.; Leclerc, M. *Chem. Commun.* **1996**, No. 24, 2761.
(77) Kobayashi, T.; Endo, T.; Shinke, W.; Nagase, T.; Murakami, S.; Naito, H. *Jpn. J. Appl. Phys.* **2011**, *50* (7R), 072601.
(78) Widge, A. S.; Jeffries-El, M.; Cui, X.; Lagenaur, C. F.; Matsuoka, Y. *Biosens. Bioelectron.* **2007**, *22* (8), 1723.
(79) Zhang, Q.; Weng, Z.; Wu, K.; Chen, W.; Lu, M. *J. Phys. Chem. C* **2020**, *124* (46), 25202.
(80) Harding Lepage, P.; Peytavi, R.; Bergeron, M. G.; Leclerc, M. *Anal. Chem.* **2011**, *83* (21), 8086.
(81) Li, C.; Shi, G. *ACS Appl. Mater. Interfaces* **2013**, *5* (11), 4503.
(82) Wang, F.; Gu, H.; Swager, T. M. *J. Am. Chem. Soc.* **2008**, *130* (16), 5392.
(83) *P3HT Revisited – From Molecular Scale to Solar Cell Devices*, 1st ed.; Ludwigs, S., Ed.; Advances in Polymer Science; Springer Berlin Heidelberg: Berlin, 2014; Vol. 265.
(84) Murphy, A. R.; Liu, J.; Luscombe, C.; Kavulak, D.; Fréchet, J. M. J.; Kline, R. J.; McGehee, M. D. *Chem. Mater.* **2005**, *17* (20), 4892.
(85) Wegnerc, G. *Mol. Cryst. Liq. Cryst.* **1993**, *235* (1), 1.
(86) K, N.; Rout, C. S. *RSC Adv.* **2021**, *11* (10), 5659.
(87) Blayney, A. J.; Perepichka, I. F.; Wudl, F.; Perepichka, D. F. *Isr. J. Chem.* **2014**, *54* (5–6), 674.
(88) Remmers, M.; Müller, B.; Martin, K.; Räder, H.-J.; Köhler, W. *Macromolecules* **1999**, *32* (4), 1073.
(89) Bobrowska, D. M.; Gdula, K.; Breczko, J.; Basa, A.; Markiewicz, K. H.; Winkler, K. *J. Nanoparticle Res.* **2022**, *24* (11), 222.
(90) Yang, C.; Wohlgenannt, M.; Vardeny, Z. V.; Blau, W. J.; Dalton, A. B.; Baughman, R.; Zakhidov, A. A. *Phys. B Condens. Matter* **2003**, *338* (1–4), 366.
(91) Ago, H.; Shaffer, M. S. P.; Ginger, D. S.; Windle, A. H.; Friend, R. H. *Phys. Rev. B* **2000**, *61* (3), 2286.
(92) Tajima, K.; Suzuki, Y.; Hashimoto, K. *J. Phys. Chem. C* **2008**, *112* (23), 8507.

(93) Chen, J.-T.; Hsu, C.-S. *Polymer* **2013**, *54* (16), 4045.
(94) Stepanyan, R.; Subbotin, A.; Knaapila, M.; Ikkala, O.; Ten Brinke, G. *Macromolecules* **2003**, *36* (10), 3758.
(95) Liu, B.; Li, T.; Zhang, H.; Ma, T.; Ren, J.; Liu, B.; Liu, B.; Lin, J.; Yu, M.; Xie, L.; Lu, D. *J. Phys. Chem. C* **2018**, *122* (26), 14814.
(96) Zhang, Q.; Wang, P.-I.; Ong, G. L.; Tan, S. H.; Tan, Z. W.; Hii, Y. H.; Wong, Y. L.; Cheah, K. S.; Yap, S. L.; Ong, T. S.; Tou, T. Y.; Nee, C. H.; Liaw, D. J.; Yap, S. S. *Polymers* **2019**, *11* (5), 840.
(97) He, B.; Li, J.; Bo, Z.; Huang, Y. *Polym. J.* **2007**, *39* (12), 1345.
(98) Huyal, I. O.; Ozel, T.; Koldemir, U.; Nizamoglu, S.; Tuncel, D.; Demir, H. V. *Opt. Express* **2008**, *16* (2), 1115.
(99) Zhao, Q.; Liu, S.-J.; Huang, W. *Macromol. Chem. Phys.* **2009**, *210* (19), 1580.
(100) Wang, H.; Koleilat, G. I.; Liu, P.; Jiménez-Osés, G.; Lai, Y.-C.; Vosgueritchian, M.; Fang, Y.; Park, S.; Houk, K. N.; Bao, Z. *ACS Nano* **2014**, *8* (3), 2609.
(101) Mirka, B.; Fong, D.; Rice, N. A.; Melville, O. A.; Adronov, A.; Lessard, B. H. *Chem. Mater.* **2019**, *31* (8), 2863.
(102) Rice, N. A.; Subrahmanyam, A. V.; Coleman, B. R.; Adronov, A. *Macromolecules* **2015**, *48* (15), 5155.
(103) Manikandan, N.; Suresh Kumar, V. P.; Siva Murugan, S.; Rathis, G.; Vishnu Saran, K.; Shabariganesh, T. K. *Mater. Today Proc.* **2021**, *47*, 4682.
(104) Kataura, H.; Kumazawa, Y.; Maniwa, Y.; Umezu, I.; Suzuki, S.; Ohtsuka, Y.; Achiba, Y. *Synth. Met.* **1999**, *103* (1–3), 2555.
(105) Gangoli, V. S.; Godwin, M. A.; Reddy, G.; Bradley, R. K.; Barron, A. R. *C — J. Carbon Res.* **2019**, *5* (4), 65.
(106) Terrones, M. *Annu. Rev. Mater. Res.* **2003**, *33* (1), 419.
(107) Kaskela, A.; Laiho, P.; Fukaya, N.; Mustonen, K.; Susi, T.; Jiang, H.; Houbenov, N.; Ohno, Y.; Kauppinen, E. I. *Carbon* **2016**, *103*, 228.
(108) Peng, L.-M.; Zhang, Z.; Qiu, C. *Nat. Electron.* **2019**, *2* (11), 499.
(109) Treacy, M. M. J.; Ebbesen, T. W.; Gibson, J. M. *Nature* **1996**, *381* (6584), 678.
(110) Coleman, J. N.; Khan, U.; Blau, W. J.; Gun'ko, Y. K. *Carbon* **2006**, *44* (9), 1624.
(111) Wu, Z.; Chen, Z.; Du, X.; Logan, J. M.; Sippel, J.; Nikolou, M.; Kamaras, K.; Reynolds, J. R.; Tanner, D. B.; Hebard, A. F.; Rinzler, A. G. *Science* **2004**, *305* (5688), 1273.
(112) Eatemadi, A.; Daraee, H.; Karimkhanloo, H.; Kouhi, M.; Zarghami, N.; Akbarzadeh, A.; Abasi, M.; Hanifehpour, Y.; Joo, S. W. *Nanoscale Res. Lett.* **2014**, *9* (1), 1.
(113) Wang, H.; Hsieh, B.; Jiménez-Osés, G.; Liu, P.; Tassone, C. J.; Diao, Y.; Lei, T.; Houk, K. N.; Bao, Z. *Small* **2015**, *11* (1), 126.
(114) Chun, K.-Y.; Oh, Y.; Rho, J.; Ahn, J.-H.; Kim, Y.-J.; Choi, H. R.; Baik, S. *Nat. Nanotechnol.* **2010**, *5* (12), 853.
(115) Mirka, B.; Rice, N. A.; Williams, P.; Tousignant, M. N.; Boileau, N. T.; Bodnaryk, W. J.; Fong, D.; Adronov, A.; Lessard, B. H. *ACS Nano* **2021**, *15* (5), 8252.
(116) Nougaret, L.; Happy, H.; Dambrine, G.; Derycke, V.; Bourgoin, J. P.; Green, A. A.; Hersam, M. C. *Appl. Phys. Lett.* **2009**, *94* (24).
(117) *Fundamentals and Applications of Nano Silicon in Plasmonics and Fullerines: Current and Future Trends*; Nayfeh, M. H., Ed.; Micro and Nano Technologies; Elsevier: Amsterdam, 2018.
(118) Maheswaran, R.; Shanmugavel, B. P. *J. Electron. Mater.* **2022**, *51* (6), 2786.

(119) Zhang, W.; Ragab, T.; Basaran, C. *Int. J. Damage Mech.* **2017**, *26* (3), 447.
(120) Nanot, S.; Hároz, E. H.; Kim, J.-H.; Hauge, R. H.; Kono, J. *Adv. Mater.* **2012**, *24* (36), 4977.
(121) Odom, T. W.; Huang, J.-L.; Kim, P.; Lieber, C. M. *J. Phys. Chem. B* **2000**, *104* (13), 2794.
(122) Hofferber, E. M.; Stapleton, J. A.; Iverson, N. M. *J. Electrochem. Soc.* **2020**, *167* (3), 037530.
(123) Rice, N. A. Separation of Single-Walled Carbon Nanotubes by Electronic Type Using Conjugated Polymers, McMaster University: Hamilton, 2015.
(124) Tasis, D.; Tagmatarchis, N.; Bianco, A.; Prato, M. *Chem. Rev.* **2006**, *106* (3), 1105.
(125) Dyke, C. A.; Tour, J. M. *J. Phys. Chem. A* **2004**, *108* (51), 11151.
(126) Syrgiannis, Z.; Melchionna, M.; Prato, M. In *Encyclopedia of Polymeric Nanomaterials*; Kobayashi, S., Müllen, K., Eds.; Springer Berlin Heidelberg: Berlin, 2014; pp 1–8.
(127) Zhao, Y.-L.; Stoddart, J. F. *Acc. Chem. Res.* **2009**, *42* (8), 1161.
(128) Hirsch, A. *Angew. Chem. Int. Ed.* **2002**, *41* (11), 1853.
(129) Kharlamova, M. V.; Paukov, M.; Burdanova, M. G. *Materials* **2022**, *15* (15), 5386.
(130) Ramanathan, T.; Fisher, F. T.; Ruoff, R. S.; Brinson, L. C. *Chem. Mater.* **2005**, *17* (6), 1290.
(131) Basiuk, E. V.; Basiuk, V. A.; Bañuelos, J.-G.; Saniger-Blesa, J.-M.; Pokrovskiy, V. A.; Gromovoy, Taras. Yu.; Mischanchuk, A. V.; Mischanchuk, B. G. *J. Phys. Chem. B* **2002**, *106* (7), 1588.
(132) Yaghoubi, A.; Alavi Nikje, M. M. *Compos. Part Appl. Sci. Manuf.* **2018**, *109*, 338.
(133) Avilés, F.; Sierra-Chi, C. A.; Nistal, A.; May-Pat, A.; Rubio, F.; Rubio, J. *Carbon* **2013**, *57*, 520.
(134) Mao, J.; Wang, Y.; Zhu, J.; Yu, J.; Hu, Z. *Appl. Surf. Sci.* **2018**, *447*, 235.
(135) Khabashesku, V. N.; Billups, W. E.; Margrave, J. L. *Acc. Chem. Res.* **2002**, *35* (12), 1087.
(136) Kumar, I.; Rana, S.; Cho, J. W. *Chem. - Eur. J.* **2011**, *17* (40), 11092.
(137) Khabashesku, V. N. *Russ. Chem. Rev.* **2011**, *80* (8), 705.
(138) Setaro, A.; Adeli, M.; Glaeske, M.; Przyrembel, D.; Bisswanger, T.; Gordeev, G.; Maschietto, F.; Faghani, A.; Paulus, B.; Weinelt, M.; Arenal, R.; Haag, R.; Reich, S. *Nat. Commun.* **2017**, *8* (1), 14281.
(139) Britz, D. A.; Khlobystov, A. N. *Chem. Soc. Rev.* **2006**, *35* (7), 637.
(140) Kharissova, O. V.; Kharisov, B. I.; De Casas Ortiz, E. G. *RSC Adv.* **2013**, *3* (47), 24812.
(141) Audette, G. F.; Yaseen, A.; Bragagnolo, N.; Bawa, R. *Biomedicines* **2019**, *7* (2), 46.
(142) Chaudhary, H.; Fernandes, R. M. F.; Gowda, V.; Claessens, M. M. A. E.; Furó, I.; Lendel, C. *J. Colloid Interface Sci.* **2019**, *556*, 172.
(143) Karajanagi, S. S.; Vertegel, A. A.; Kane, R. S.; Dordick, J. S. *Langmuir* **2004**, *20* (26), 11594.
(144) Barone, P. W.; Strano, M. S. *Angew. Chem. Int. Ed.* **2006**, *45* (48), 8138.
(145) Angelikopoulos, P.; Bock, H. *Phys. Chem. Chem. Phys.* **2012**, *14* (27), 9546.
(146) Hirano, A.; Kameda, T.; Yomogida, Y.; Wada, M.; Tanaka, T.; Kataura, H. *ChemNanoMat* **2016**, *2* (9), 911.
(147) Ma, J.; Tang, J.; Cheng, Q.; Zhang, H.; Shinya, N.; Qin, L.-C. *Sci. Technol. Adv. Mater.* **2010**, *11* (6), 065005.
(148) Tkalya, E. E.; Ghislandi, M.; De With, G.; Koning, C. E. *Curr. Opin. Colloid Interface Sci.* **2012**, *17* (4), 225.
(149) Vaisman, L.; Wagner, H. D.; Marom, G. *Adv. Colloid Interface Sci.* **2006**, *128–130*, 37.

(150) Zhang, C.; Wang, P.; Barnes, B.; Fortner, J.; Wang, Y. *Chem. Mater.* **2021**, *33* (12), 4551.
(151) Ehli, C.; Rahman, G. M. A.; Jux, N.; Balbinot, D.; Guldi, D. M.; Paolucci, F.; Marcaccio, M.; Paolucci, D.; Melle-Franco, M.; Zerbetto, F.; Campidelli, S.; Prato, M. *J. Am. Chem. Soc.* **2006**, *128* (34), 11222.
(152) Shirsat, M. D.; Sarkar, T.; Kakoullis, J.; Myung, N. V.; Konnanath, B.; Spanias, A.; Mulchandani, A. *J. Phys. Chem. C* **2012**, *116* (5), 3845.
(153) López-Moreno, A.; Pérez, E. M. *Chem. Commun.* **2015**, *51* (25), 5421.
(154) Bodnaryk, W. J.; Li, K.; Adronov, A. *J. Polym. Sci.* **2020**, *58* (14), 1965.
(155) Fong, D.; Yeung, J.; Lang, A.; Adronov, A. *J. Polym. Sci. Part Polym. Chem.* **2019**, *57* (19), 2015.
(156) Aumaitre, C.; Fong, D.; Adronov, A.; Morin, J. F. *Polym. Chem.* **2019**, *10* (47), 6440.
(157) Lei, T.; Chen, X.; Pitner, G.; Wong, H.-S. P.; Bao, Z. *J. Am. Chem. Soc.* **2016**, *138* (3), 802.
(158) Chang, H.-C.; Wang, J.-T.; Li, D.-H.; Lu, C.; Hsu, H.-W.; Wu, H.-C.; Liu, C.-L.; Chen, W.-C. *Polym. J.* **2016**, *48* (4), 421.
(159) Duan, W. H.; Wang, Q.; Collins, F. *Chem. Sci.* **2011**, *2* (7), 1407.
(160) Yurekli, K.; Mitchell, C. A.; Krishnamoorti, R. *J. Am. Chem. Soc.* **2004**, *126* (32), 9902.
(161) Islam, M. F.; Rojas, E.; Bergey, D. M.; Johnson, A. T.; Yodh, A. G. *Nano Lett.* **2003**, *3* (2), 269.
(162) Li, H.; Zhou, L.; Wu, T. *Diam. Relat. Mater.* **2018**, *88*, 189.
(163) Goh, S. X. L.; Goh, E. X. Y.; Lee, H. K. *Talanta* **2021**, *221*.
(164) Rojas, J. A.; Ardila-Rodríguez, L. A.; Diniz, M. F.; Gonçalves, M.; Ribeiro, B.; Rezende, M. C. *Mater. Des.* **2019**, *166*, 107612.
(165) Yang, H.; Neal, L.; Flores, E. E.; Adronov, A.; Kim, N. Y. *J. Surfactants Deterg.* **2023**, jsde.12702.
(166) Fatemi, S. M.; Foroutan, M. *J. Iran. Chem. Soc.* **2015**, *12* (11), 1905.
(167) Zhang, Y.; Li, D.; Zhao, H.; Yin, C.; Wang, M.; Li, Y. *Mater. Chem. Phys.* **2019**, *231*, 60.
(168) Zeng, X.; Yang, D.; Liu, H.; Zhou, N.; Wang, Y.; Zhou, W.; Xie, S.; Kataura, H. *Adv. Mater. Interfaces* **2018**, *5* (2), 1700727.
(169) Bonaccorso, F.; Hasan, T.; Tan, P. H.; Sciascia, C.; Privitera, G.; Di Marco, G.; Gucciardi, P. G.; Ferrari, A. C. *J. Phys. Chem. C* **2010**, *114* (41), 17267.
(170) Arnold, M. S.; Stupp, S. I.; Hersam, M. C. *Nano Lett.* **2005**, *5* (4), 713.
(171) Arnold, M. S.; Green, A. A.; Hulvat, J. F.; Stupp, S. I.; Hersam, M. C. *Nat. Nanotechnol.* **2006**, *1* (1), 60.
(172) Ghosh, S.; Bachilo, S. M.; Weisman, R. B. *Nat. Nanotechnol.* **2010**, *5* (6), 443.
(173) Kim, S.; Kim, W.-J. *Gels* **2022**, *8* (2), 76.
(174) Yahya, I.; Bonaccorso, F.; Clowes, S. K.; Ferrari, A. C.; Silva, S. R. P. *Carbon* **2015**, *93*, 574.
(175) Fagan, J. A.; Khripin, C. Y.; Silvera Batista, C. A.; Simpson, J. R.; Hároz, E. H.; Hight Walker, A. R.; Zheng, M. *Adv. Mater.* **2014**, *26* (18), 2800.
(176) Khripin, C. Y.; Fagan, J. A.; Zheng, M. *J. Am. Chem. Soc.* **2013**, *135* (18), 6822.
(177) Zheng, Q.; Jung, B. J.; Sun, J.; Katz, H. E. *J. Am. Chem. Soc.* **2010**, *132* (15), 5394.
(178) Yang, F.; Wang, M.; Zhang, D.; Yang, J.; Zheng, M.; Li, Y. *Chem. Rev.* **2020**, *120* (5), 2693.
(179) Nish, A.; Hwang, J.-Y.; Doig, J.; Nicholas, R. J. *Nat. Nanotechnol.* **2007**, *2* (10), 640.

(180) Brady, G. J.; Joo, Y.; Wu, M.-Y.; Shea, M. J.; Gopalan, P.; Arnold, M. S. *ACS Nano* **2014**, *8* (11), 11614.
(181) Min, S. H.; Kim, H.-I.; Kim, K.; Cha, I.; Ha, S.; Yun, W. S.; Kwak, S. K.; Kim, J.-H.; Kim, B.-S.; Song, C. *Polymer* **2016**, *96*, 63.
(182) Ritaine, D.; Adronov, A. *Molecules* **2023**, *28* (3), 1471.
(183) Karim, M. R.; Lee, C. J.; Lee, M. S. *J. Polym. Sci. Part Polym. Chem.* **2006**, *44* (18), 5283.
(184) Rice, N. A.; Bodnaryk, W. J.; Mirka, B.; Melville, O. A.; Adronov, A.; Lessard, B. H. *Adv. Electron. Mater.* **2019**, *5* (1), 1800539.
(185) Jung, J.; Suh, E. H.; Jeong, Y. J.; Yang, H. S.; Lee, T.; Jang, J. *ACS Appl. Mater. Interfaces* **2019**, *11* (50), 47330.
(186) Samanta, S. K.; Fritsch, M.; Scherf, U.; Gomulya, W.; Bisri, S. Z.; Loi, M. A. *Acc. Chem. Res.* **2014**, *47* (8), 2446.
(187) Lee, H. W.; Yoon, Y.; Park, S.; Oh, J. H.; Hong, S.; Liyanage, L. S.; Wang, H.; Morishita, S.; Patil, N.; Park, Y. J.; Park, J. J.; Spakowitz, A.; Galli, G.; Gygi, F.; Wong, P. H.-S.; Tok, J. B.-H.; Kim, J. M.; Bao, Z. *Nat. Commun.* **2011**, *2* (1), 541.
(188) Barman, S. N.; LeMieux, M. C.; Baek, J.; Rivera, R.; Bao, Z. *ACS Appl. Mater. Interfaces* **2010**, *2* (9), 2672.
(189) Ding, J.; Li, Z.; Lefebvre, J.; Cheng, F.; Dubey, G.; Zou, S.; Finnie, P.; Hrdina, A.; Scoles, L.; Lopinski, G. P.; Kingston, C. T.; Simard, B.; Malenfant, P. R. L. *Nanoscale* **2014**, *6* (4), 2328.
(190) Qian, L.; Xu, W.; Fan, X.; Wang, C.; Zhang, J.; Zhao, J.; Cui, Z. *J. Phys. Chem. C* **2013**, *117* (35), 18243.
(191) Fong, D.; Adronov, A. *Chem. Sci.* **2017**, *8* (11), 7292.
(192) In *Biosurfaces: A Materials Science and Engineering Perspective*; John Wiley & Sons, Inc: Hoboken, 2015; pp 329–344.
(193) Gentekos, D. T.; Sifri, R. J.; Fors, B. P. *Nat. Rev. Mater.* **2019**, *4* (12), 761.
(194) Xu, C.; Dong, J.; He, C.; Yun, J.; Pan, X. *Giant* **2023**, *14*, 100154.
(195) McCullough, R. D.; Ewbank, P. C.; Loewe, R. S. *J. Am. Chem. Soc.* **1997**, *119* (3), 633.
(196) Arslan, H.; Saathoff, J. D.; Bunck, D. N.; Clancy, P.; Dichtel, W. R. *Angew. Chem. Int. Ed.* **2012**, *51* (48), 12051.
(197) Casey, A.; Ashraf, R. S.; Fei, Z.; Heeney, M. *Macromolecules* **2014**, *47* (7), 2279.
(198) Lancaster, J. R. A "Toolkit" of Small Molecules for Polymer Assembly and Post-Synthetic Modification Using "Click" and Photoactive Chemistries, Columbia University: New York, 2011.
(199) Jewett, J. C.; Sletten, E. M.; Bertozzi, C. R. *J. Am. Chem. Soc.* **2010**, *132* (11), 3688.
(200) Meier, H.; Petersen, H.; Kolshorn, H. *Chem. Ber.* **1980**, *113* (7), 2398.
(201) Turner, R. B.; Jarrett, A. D.; Goebel, P.; Mallon, B. J. *J. Am. Chem. Soc.* **1973**, *95* (3), 790.
(202) Dommerholt, J.; Rutjes, F. P. J. T.; Van Delft, F. L. *Top. Curr. Chem.* **2016**, *374* (2), 16.
(203) Li, K.; Fong, D.; Meichsner, E.; Adronov, A. *Chem. - Eur. J.* **2021**, *27* (16), 5057.
(204) Kim, E.; Koo, H. *Chem. Sci.* **2019**, *10* (34), 7835.
(205) Kardelis, V.; Chadwick, R. C.; Adronov, A. *Angew. Chem. Int. Ed.* **2016**, *128* (3), 957.
(206) Li, K.; Kardelis, V.; Adronov, A. *J. Polym. Sci. Part Polym. Chem.* **2018**, *56* (18), 2053.
(207) Stefan, M. C.; Javier, A. E.; Osaka, I.; McCullough, R. D. *Macromolecules* **2009**, *42* (1), 30.
(208) Sonogashira, K. *J. Organomet. Chem.* **2002**, *653* (1–2), 46.
(209) Suzuki, A. *J. Organomet. Chem.* **1999**, *576* (1–2), 147.

(210) Darko, A.; Wallace, S.; Dmitrenko, O.; Machovina, M. M.; Mehl, R. A.; Chin, J. W.; Fox, J. M. *Chem. Sci.* **2014**, *5* (10), 3770.
(211) Oliveira, B. L.; Guo, Z.; Bernardes, G. J. L. *Chem. Soc. Rev.* **2017**, *46* (16), 4895.
(212) Karver, M. R.; Weissleder, R.; Hilderbrand, S. A. *Bioconjug. Chem.* **2011**, *22* (11), 2263.
(213) Audebert, P.; Sadki, S.; Miomandre, F.; Clavier, G.; Vernières, M. C.; Saoud, M.; Hapiot, P. *New J. Chem.* **2004**, *28* (3), 387.
(214) Chen, W.; Wang, D.; Dai, C.; Hamelberg, D.; Wang, B. *Chem. Commun.* **2012**, *48* (12), 1736.
(215) Blackman, M. L.; Royzen, M.; Fox, J. M. *J. Am. Chem. Soc.* **2008**, *130* (41), 13518.
(216) Kardelis, V.; Denk, M. M.; Adronov, A. *Angew. Chem. - Int. Ed.* **2021**, *60* (6), 2980.
(217) Strano, M. S.; Dyke, C. A.; Usrey, M. L.; Barone, P. W.; Allen, M. J.; Shan, H.; Kittrell, C.; Hauge, R. H.; Tour, J. M.; Smalley, R. E. *Science* **2003**, *301* (5639), 1519.
(218) Weisman, R. B.; Bachilo, S. M. *Nano Lett.* **2003**, *3* (9), 1235.
(219) O'Connel, M. J.; Bachilo, S. M.; Huffman, C. B.; Moore, V. C.; Strano, M. S.; Haroz, E. H.; Rialon, K. L.; Boul, P. J.; Noon, W. H.; Kittrell, C.; Ma, J.; Hauge, R. H.; Weisman, R. B.; Smalley, R. E. *Science* **2002**, *297* (5581), 593.
(220) Dresselhaus, M. S.; Dresselhaus, G.; Saito, R.; Jorio, A. *Phys. Rep.* **2005**, *409* (2), 47.
(221) Fantini, C.; Jorio, A.; Santos, A. P.; Peressinotto, V. S. T.; Pimenta, M. A. *Chem. Phys. Lett.* **2007**, *439* (1–3), 138.
(222) Shah, K. C.; Shah, M. B.; Solanki, S. J.; Makwana, V. D.; Sureja, D. K.; Gajjar, A. K.; Bodiwala, K. B.; Dhameliya, T. M. *J. Mol. Struct.* **2023**, *1278*, 134914.
(223) Dresselhaus, M. S.; Dresselhaus, G.; Jorio, A.; Souza Filho, A. G.; Pimenta, M. A.; Saito, R. *Acc. Chem. Res.* **2002**, *35* (12), 1070.
(224) Jorio, A.; Pimenta, M. A.; Filho, A. G. S.; Saito, R.; Dresselhaus, G.; Dresselhaus, M. S. *New J. Phys.* **2003**, *5*, 139.
(225) Doorn, S. K. *J. Nanosci. Nanotechnol.* **2005**, *5* (7), 1023.
(226) Brown, S. D. M.; Jorio, A.; Dresselhaus, M. S.; Dresselhaus, G. *Phys. Rev. B* **2001**, *64* (7), 073403.
(227) Luo, Z.; Li, R.; Kim, S. N.; Papadimitrakopoulos, F. *Phys. Rev. B* **2004**, *70* (24), 245429.
(228) Strano, M. S.; Doorn, S. K.; Haroz, E. H.; Kittrell, C.; Hauge, R. H.; Smalley, R. E. *Nano Lett.* **2003**, *3* (8), 1091.
(229) Li, Z.; Deng, L.; Kinloch, I. A.; Young, R. J. *Prog. Mater. Sci.* **2023**, *135*, 101089.
(230) Brown, S. D. M.; Jorio, A.; Corio, P.; Dresselhaus, M. S.; Dresselhaus, G.; Saito, R.; Kneipp, K. *Phys. Rev. B* **2001**, *63* (15), 155414.
(231) Kupka, T.; Stachów, M.; Stobiński, L.; Kaminský, J. *Phys. Chem. Chem. Phys.* **2016**, *18* (36), 25058.
(232) Doorn, S. K.; Heller, D. A.; Barone, P. W.; Usrey, M. L.; Strano, M. S. *Appl. Phys. A* **2004**, *78* (8), 1147.
(233) Liu, C.-H.; Liu, Y.-Y.; Zhang, Y.-H.; Wei, R.-R.; Zhang, H.-L. *Phys. Chem. Chem. Phys.* **2009**, *11* (33), 7257.
(234) Bachilo, S. M.; Strano, M. S.; Kittrell, C.; Hauge, R. H.; Smalley, R. E.; Weisman, R. B. *Science* **2002**, *298* (5602), 2361.
(235) Lefebvre, J.; Fraser, J. M.; Finnie, P.; Homma, Y. *Phys. Rev. B* **2004**, *69* (7), 075403.
(236) Fong, D.; Bodnaryk, W. J.; Rice, N. A.; Saem, S.; Moran-Mirabal, J. M.; Adronov, A. *Chem. - Eur. J.* **2016**, *22* (41), 14560.
(237) Bodnaryk, W. J.; Fong, D.; Adronov, A. *ACS Omega* **2018**, *3* (11), 16238.

(238) Movia, D.; Del Canto, E.; Giordani, S. *Phys. Status Solidi B* **2009**, *246* (11–12), 2704.
(239) Lebedkin, S.; Hennrich, F.; Skipa, T.; Kappes, M. M. *J. Phys. Chem. B* **2003**, *107* (9), 1949.
(240) Wang, J.; Shea, M. J.; Flach, J. T.; McDonough, T. J.; Way, A. J.; Zanni, M. T.; Arnold, M. S. *J. Phys. Chem. C* **2017**, *121* (15), 8310.
(241) Cherukuri, T. K.; Tsyboulski, D. A.; Weisman, R. B. *ACS Nano* **2012**, *6* (1), 843.
(242) Fagan, J. A.; Simpson, J. R.; Bauer, B. J.; De Paoli Lacerda, S. H.; Becker, M. L.; Chun, J.; Migler, K. B.; Hight Walker, A. R.; Hobbie, E. K. *J. Am. Chem. Soc.* **2007**, *129* (34), 10607.
(243) Imin, P.; Cheng, F.; Adronov, A. *Polym. Chem.* **2011**, *2* (6), 1404.
(244) Swager, T. M. *Macromolecules* **2017**, *50* (13), 4867.
(245) Blouin, N.; Leclerc, M. *Acc. Chem. Res.* **2008**, *41* (9), 1110.
(246) Guo, X.; Baumgarten, M.; Müllen, K. *Prog. Polym. Sci.* **2013**, *38* (12), 1832.
(247) Li, K.; McNelles, S.; Adronov, A. *Synlett* **2018**, *29* (19), 2535.
(248) Koizumi, T.; Kameda, T.; Saito, H.; Sato, A.; Hayashi, S. *J. Polym. Sci. Part Polym. Chem.* **2019**, *57* (7), 827.
(249) Yuan, Y.; Michinobu, T.; Ashizawa, M.; Mori, T. *J. Polym. Sci. Part Polym. Chem.* **2011**, *49* (4), 1013.
(250) Ye, Q.; Neo, W. T.; Cho, C. M.; Yang, S. W.; Lin, T.; Zhou, H.; Yan, H.; Lu, X.; Chi, C.; Xu, J. *Org. Lett.* **2014**, *16* (24), 6386.
(251) Royzen, M.; Yap, G. P. A.; Fox, J. M. *J. Am. Chem. Soc.* **2008**, *130* (12), 3760.
(252) Zimmermann, F.; Lippert, Th.; Beyer, Ch.; Stebani, J.; Nuyken, O.; Wokaun, A. *Appl. Spectrosc.* **1993**, *47* (7), 986.
(253) Fong, D.; Adronov, A. *Macromolecules* **2017**, *50* (20), 8002.
(254) Bhatthula, B. K. G.; Kanchani, J. R.; Arava, V. R.; Subha, M. C. S. *Tetrahedron* **2019**, *75* (7), 874.
(255) Arrington, K. J.; Murray, C. B.; Smith, E. C.; Marand, H.; Matson, J. B. *Macromolecules* **2016**, *49* (10), 3655.
(256) Liu, D. S.; Tangpeerachaikul, A.; Selvaraj, R.; Taylor, M. T.; Fox, J. M.; Ting, A. Y. *J. Am. Chem. Soc.* **2012**, *134* (2), 792.
(257) Fong, D.; Andrews, G. M.; Adronov, A. *Polym. Chem.* **2018**, *9* (21), 2873.

Appendix I: Supporting Information for: Exploring the Reactivity and Interactions of a Poly(Fluorene-co-Tetrazine)-Conjugated Polymer with SWNTs

General Experimental

Unless otherwise specified, all reagents were purchased from commercial suppliers and used as received. 2-(2-(2-Methoxyethoxy)ethoxy)ethanamine was purchased was purchased from AK Scientific. Raw HiPco SWNTs were purchased from NanoIntegris (batch #HR37-087B, 10 wt % in anhydrous EtOH). Flash chromatography was performed using an IntelliFlash 280 and 310 systems from AnaLogix. Unless otherwise noted, compounds were monitored using a variable wavelength detector at 254 nm and 220 nm. Solvent amounts used for gradient or isocratic elution were reported in column volumes (CV). Columns were prepared in Teflon cartridges using 40 – 63 μm silica or 25 – 40 μm silica purchased from Silicycle.

^{1}H–NMR and ^{13}C-NMR spectra were recorded on Bruker Avance 600 MHz and shift-referenced to the residual solvent resonance. Polymer molecular weights and polydispersity indices (Đ) were analyzed (relative to polystyrene standards) *via* gel permeation chromatography (GPC) using a Waters 2695 Separations Module, equipped with a Waters 2414 refractive index detector a Jordi Fluorinated DVB mixed bed column in series with a Jordi Fluorinated DVB 10^5 Å pore size column. THF with 2% acetonitrile was used as the eluent at a flow rate of 2.0 mL/min and calibrated with polystyrene standards. Fourier-transform infrared (FTIR) spectra were recorded using a Thermo Scientific Nicolet 6700 FTIR spectrometer equipped with a Smart iTX attenuated total reflectance (ATR) sample analyzer. Polymer solutions in THF were drop-casted onto the ATR crystal and allowed to dry before collecting the data. UV-Vis and UV-Vis-NIR absorption spectra were recorded on a Cary 5000 spectrometer in dual beam mode, using matched

10 mm quartz cuvettes. High concentration polymer-SWNTs samples were diluted by a factor of 3 or 4 to reduce absorption oversaturation.

Sonication was performed using a QSonica Q700 Sonicator equipped with a 13 mm probe. Centrifugation of the polymer-SWNT samples was performed using a Beckman Coulter Allegra X-22 centrifuge. Raman spectra were collected with a Renishaw InVia Laser Raman spectrometer, using three different lasers: a 500 mW HeNe Renishaw laser (633 nm, 1800 L/mm grating), a 300 mW Renishaw laser (785 nm, 1200 L/mm grating), and a 50 mW Renishaw laser (532 nm, 1800 L/mm grating). Raman samples were drop-cast onto freshly cleaned silicon wafers and allowed to air-dry at room temperature. Unpurified SWNTs samples were prepared by wetting a small amount of the raw sample with THF and similarly drop-casted onto a clean silicon wafer. Extended scans (100 – 3000 cm^{-1}) were collected at each wavelength with a laser intensity of 0.1 – 5% for all polymer-SWNT samples. Fluorescence spectra were measured on a Jobin-Yvon SPEX Fluorolog 3.22 equipped with a 450 W Xe arc lamp, digital photon counting photomultiplier, and an InGaAs detector using a 10 mm quartz cuvette. Slit widths for both excitation and emission were set to 10 nm band-pass, and correction factor files were applied to account for instrument variations. Photoluminescence (PL) maps were obtained at 25 °C with 5 nm intervals for both the excitation and emission. Atomic force microscopy (AFM) images were obtained using a Bruker Dimension Icon AFM, with ScanAsyst-Air tips in ScanAysyst in Air mode. Basic image processing (flattening, removal of errant scan lines, adjusting height scale) was performed using NanoScope Analysis v.2.0. Height profile measurements were analyzed using Gwyddion v.2.63. Samples were prepared by spin-coating diluted dispersion samples onto mica substrate.

Experimental Procedures

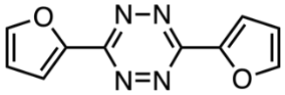

3,6-di(furan-2-yl)-1,2,4,5-tetrazine (1)[250]

To a 100 mL round bottom flask under inert conditions equipped with a magnetic stir a bar, 2-furonitrile (3.00 g, 32.2 mmol) and anhydrous ethanol (20 mL) were added. Then sulfur (4.13 g, 128.9 mmol) and hydrazine hydrate (6.27 mL, 128.9 mmol) were sequentially added to the stirring solution. A reflux condenser was attached, and the reaction was heated to reflux, stirred for 3 h before slowly cooling to room temperature, chilled to 0 °C, then filtered to isolate the precipitate. The yellow-orange solid was rinsed with cold ethanol (10 mL), then redissolved in ethanol:chloroform (20:40 mL). Isoamyl nitrite (15 mL) was added to the solution and the reaction mixture was refluxed overnight before evaporating the solvents under a flow of N_2. Silica gel column chromatography (40% CH_2Cl_2 in Hx) yielded tetrazine **1** as a bright red amorphous solid (1.89 g, 55%), M.W.: 214.18 g/mol; ^{1}H-NMR (600 MHz; $CDCl_3$): δ 7.81 (dd, *J* = 2.3, 0.9 Hz, 1H), 7.67 (dd, *J* = 3.5, 0.6 Hz, 1H), 6.71 (dd, *J* = 3.5, 1.7 Hz, 1H).

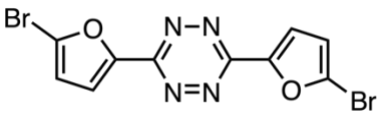

3,6-bis(5-dibromofuran-2-yl)-1,2,4,5-tetrazine (2)[250]

Compound **1** (700 mg, 3.26 mmol), *N*-bromosuccinimide (1.22 g, 6.86 mmol), silica gel (175 mg), and dichloromethane (20 mL) were added to a 50 mL round bottom flask and stirred at rt overnight. The reaction was then heated to reflux for an additional 6 h. The reaction mixture was cooled to 0 °C, then filtered. The precipitate was rinsed with excess isopropanol, dried, and redissolved in dichloromethane. The solution was passed through a silica plug, concentrated, and recrystallized

from toluene to yield **2** (717 mg, 59%) as a deep red crystalline solid. M.W.: 371.97 g/mol; ^{1}H-NMR (600 MHz; $CDCl_3$): δ 7.61 (d, *J* = 3.6 Hz, 2H), 6.66 (d, *J* = 3.6 Hz, 2H).

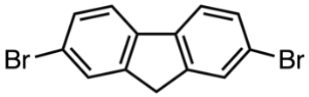

2,7-dibromo-9*H*-fluorene (3)[253]

A 1 L round bottom flask equipped with a stir bar was charged with fluorene (30.0 g, 180 mmol), *N*-bromosuccinimide (80.3 g, 451 mmol), and acetic acid (361 mL). Concentrated HBr (9 mL) was slowly added to the stirring mixture and was stirred at rt for 1.5 h. Water (200 mL) was added and the resulting suspension was filtered onto paper and rinsed with DI water. The solid was purified through recrystallization from 1.5:1 EtOH:Acetone (~1.9 L total volume), and the mother liquor was recrystallized again from the same solvent mixture (~1.4 L total volume). The crops were combined to afford compound **3** as a white solid (45.4 g, 78%). M.W.: 324.02 g/mol; ^{1}H-NMR (600 MHz; $CDCl_3$): δ 7.67 (d, *J* = 0.9 Hz, 2H), 7.61 (d, *J* = 8.1 Hz, 2H), 7.51 (dd, *J* = 8.1, 1.7 Hz, 2H), 3.88 (s, 2H).

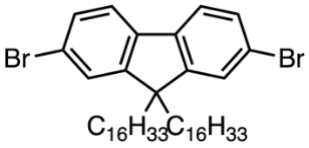

2,7-dibromo-9,9-dihexadecyl-9*H*-fluorene (4)[253]

Compound **3** (2.00 g, 6.17 mmol), 1-bromohexadecane (4.71 g, 15.4 mmol), and $^{n}Bu_4NBr$ (398 mg, 1.23 mmol) were added under N_2 to degassed toluene (33 mL) and saturated KOH (33 mL) in a 250 mL round bottom flask equipped with a magnetic stir bar. The reaction was heated to 60 °C and stirred vigorously for 1 h. The biphasic mixture was cooled to rt and then added to a separatory

funnel. The organic phase was isolated, and the aqueous phase was extracted twice with diethyl ether (20 mL). All organic phases were combined, dried with $MgSO_4$, and concentrated *in vacuo.* The crude material was purified first through column chromatography (100% Hx) to afford a clear colourless oil, and precipitated into a cold solution of 4:1 MeOH:Acetone (100 mL). The white solid was further purified *via* recrystallization from 1.5:1 EtOH:Acetone (~200 mL) to afford a solid fine white powder (3.83 g, 75%). M.W.: 772.88 g/mol; ^{1}H-NMR (600 MHz; $CDCl_3$): δ 7.51 (d, *J* = 7.9 Hz, 2H), 7.45 (dd, *J* = 7.7, 1.7 Hz, 1.7, 2H), 7.43 (d, *J* = 1.4 Hz, 2H), 1.91 (dt, *J* = 8.3, 4.5 Hz, 4H), 1.32-1.11 (m, 40H), 1.11-1.00 (m, 12H), 0.88 (dt, *J* = 7.2, 2.9 Hz, 12H), 0.58 (m, 4H).

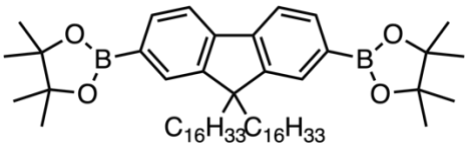

2,2'-(9,9-dihexadecyl-9*H*-fluorene-2,7-diyl)bis(4,4,5,5-tetramethyl-1,3,2-dioxaborolane) (5)[253]

Compound **4** (3.75 g, 4.85 mmol), bis(pinacolato)diboron (2.71 g, 10.7 mmol), and potassium acetate (1.43 g, 14.6 mmol) were added to degassed dioxane (10.5 mL) in a 25 mL round bottom flask equipped with a magnetic stir bar under N_2. $Pd(dppf)_2Cl_2$ (119 mg, 163 μmol) was then added to the flask under positive pressure of N_2 and the mixture was stirred at 80 °C overnight. The reaction was cooled to rt before partitioning the reaction mixture with water (15 mL). The aqueous phase was extracted thrice with dichloromethane (15 mL) and the combined organic phase was washed twice with water (15 mL) and once with brine (15 mL). The organic phase was dried with $MgSO_4$, concentrated *in vacuo,* and passed through a silica gel plug with 1:1 Hx:CH_2Cl_2 (100 mL). The solution was concentrated *in vacuo,* precipitated into a cold solution of 4:1 MeOH:Acetone

(100 mL). Recrystallization of the off-white powder from 1.5:1 EtOH:Acetone (~200 mL) yielded compound **5** as a beige crystalline solid (2.63 g, 62%). M.W.: 867.01 g/mol; ^{1}H-NMR (600 MHz; $CDCl_3$): δ 7.80 (d, *J* = 7.6 Hz, 2H), 7.73 (s, 2H), 7.71 (d, *J* = 7.5 Hz, 2H), 1.99 (dt, *J* = 8.2, 4.6 Hz, 4H), 1.38 (s, 24H), 1.32-1.08 (m, 40H), 1.07-0.96 (m, 12H), 0.87 (t, *J* = 7.0 Hz, 6H), 0.54 (m, 4H).

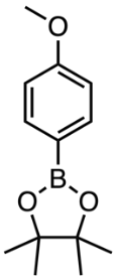

2-(4-methoxyphenyl)-4,4,5,5-tetramethyl-1,3,2-dioxaborolane (6)[254]

A Schlenk tube equipped with a magnetic stir bar was charged with 4-bromoanisole (1.00 g, 5.35 mmol), bis(pinacolato)diboron (1.49 g, 5.88 mmol), and potassium acetate (787 mg, 8.02 mmol), and DMSO (10 mL). The reaction mixture was degassed in a 25 mL Schlenk tube *via* three freeze-pump-thaw cycles. The biphasic mixture was frozen under liquid N_2, then [1,1'-Bis(diphenylphosphino)ferrocene] dichloropalladium(II) (130 mg, 0.160 mmol) was added under a positive pressure of N_2 gas. The head space was evacuated and the Schlenk tube was purged thrice with N_2, then reaction mixture was stirred for at 70 °C for 6 h. The resultant mixture was cooled to rt, then partitioned between water (40 mL) and diethyl ether (40 mL). The organic phase was washed with water (2 x 20 mL), dried with magnesium sulfate, filtered, and concentrated *in vacuo*. The crude product was purified *via* column chromatography run with 30% CH_2Cl_2 in Hx for 10 CVs, then a 3 CV ramp to 35% CH_2Cl_2, followed by 5 CVs at 35% and flushed with 5 CVs at 50% CH_2Cl_2. Purification yielded **6** (718 mg, 86%) as a crystalline white solid. M.W.: 234.10

g/mol; ^{1}H-NMR (600 MHz; $CDCl_3$): δ 7.75 (d, *J* = 8.7 Hz, 2H), 6.89 (d, *J* = 7.6 Hz, 2H), 3.82 (s, 3H), 1.33 (s, 12H).

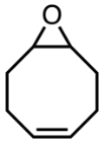

5,6-epoxycyclooctene[255]

A solution of 3-chloroperbenzoic acid (20.71 g, 92.4 mmol) in chloroform (130 mL) was chilled to -78 °C in a 150 mL round bottom equipped with a magnetic stir bar and stirred vigorously. A solution of 1,5-cyclooctadiene (10.00 g, 92.4 mmol) in chloroform (20 mL) was added dropwise to the solution *via* addition funnel, resulting in the formation of a white precipitate. The reaction mixture was warmed to rt and stirred overnight. The reaction mixture was filtered onto paper, then the filtrate was transferred to a separatory funnel and washed with sodium bicarbonate. The organic phase was dried with $MgSO_4$ and concentrated *in vacuo* to yield a mixture of the mono- and di-epoxidated products. The mixture was transferred into a 100 mL round bottom flask on a distillation apparatus equipped with a 15 cm vigreux column. Distillation (60 °C, 10 mbar) afforded compound **7** (4.06 g, 35%) as a clear colourless oil. M.W.: 124.18 g/mol; ^{1}H-NMR (600 MHz; $CDCl_3$): δ 5.57 (m, 2H), 3.03 (m, 2H), 2.44 (m, 2H), 2.13 (m, 2H), 2.03 (m, 4H).

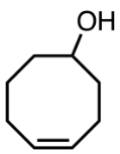

(*Z*)-Cyclooct-4-enol[255]

Crushed lithium aluminum hydride pellets (2.27 g, 59.9 mmol) were added under positive pressure of N_2 gas into a flame dried 250 mL three-neck round bottom flask equipped with an addition funnel and magnetic stir bar. Dry diethyl ether (80 mL) was dropwise at 0 °C while vigorously stirring. A solution of 5,6-epoxycyclocetene (6.77 g, 54.5 mmol) in dry diethyl ether (80 mL) was added dropwise to the mixture and allowed to stir at 0 °C for 30 min before warming to rt and left overnight. The reaction mixture was quenched using the Fieser method by sequentially adding water (3 mL), 15% (w/v) potassium hydroxide solution (3 mL), and water (9 mL) at 0 °C. The precipitated alumina was filtered over celite and washed with excess diethyl ether (200 mL). The filtrate was dried with $MgSO_4$, filtered, and then concentrated *in vacuo* to yield compound **8** (5.20 g, 75%) as a clear colourless oil. Synthesized according to literature procedure. M.W.: 126.20 g/mol; ^{1}H-NMR (600 MHz; $CDCl_3$): δ 5.70 (m, 1H), 5.59 (m, 1H), 3.82 (m, 1H), 2.30 (m, 1H), 2.14 (m, 1H), 1.93 (m, 1H), 1.86 (m, 1H), 1.73 (m, 1H), 1.64 (m, 1H), 1.54 (m, 2H), 1.29 (s, 1H).

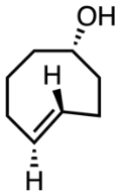

***rel*-(1*R*, 4*E*, p*R*)-Cyclooct-4-enol (7)**[251]

The bottom of a 25 g Biotage® cartridge was packed with silica gel (13 g) then layered with $AgNO_3$-impregnated silica gel (12 g), then wrapped in tinfoil. The column was fully wetted by passing through 9:1 ether:hexanes (200 mL) with a peristaltic pump at a flow rate of 25 mL/min. The column and pump were then connected through PTFE tubing to a stirring solution of previously prepared **(*Z*)-Cyclooct-4-enol** (1.00 g, 7.92 mmol) and methyl benzoate (2.00 mL, 15.8 mmol) dissolved in 9:1 ether:hexanes (100 mL) in a 500 mL quartz flask. The flask was placed in

a home-built UV reactor equipped with a 25 W lamp exhibiting emission at 254 nm and irradiated for 16 h while continuously pumping the solution through the column. The column was flushed with additional of 9:1 ether:hexanes (400 mL) to wash any remaining cis-isomer and methyl benzoate, then dried by a flow of N_2. The contents of the column were emptied into an Erlenmeyer flask (250 mL) then partitioned with dichloromethane (100 mL) and $NH_4OH_{(aq)}$ (100 mL) and vigorously stirred for 30 min and filtered over Celite. The filtrate was transferred into a separatory funnel and the organic phase was isolated. The aqueous phase was further washed with dichloromethane (2 x 25 mL) and the organic phases were combined, washed with water (25 mL), dried with $MgSO_4$, filtered, and concentrated. The two diastereomers of (*E*)-Cyclooct-4-enol were separated *via* column chromatography (R_fs = 0.2 (major) and 0.4 (minor) in 1:4 EtOAc:Hexanes). The column was run with 5 CVs at 1:9 EtOAc:Hx, then a 10 CV ramp from 1:9 to 1:3 EtOAc:Hx, followed by 5 CVs at 1:3 EtOAc:Hx. Separation yielded **9** (270 mg, 27%) as a colourless clear oil. M.W.: 126.20 g/mol; ^{1}H-NMR (600 MHz; $CDCl_3$): δ 5.57 (m, 1H), 5.38 (m, 1H), 3.46 (m, 1H), 2.37-2.25 (m, 3H), 2.00-1.89 (m, 4H), 1.72-1.53 (m, 3H), 1.15 (s, 1H).

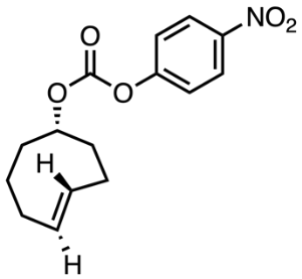

(1*R*, 4*E*)-cyclooct-4-en-1-yl (4-nitrophenyl) carbonate (8)[256]

Compound **7** (169 mg, 1.34 mmol) and pyridine (265 mg, 3.35 mmol) were dissolved in dried dichloromethane (23 mL) in a 50 mL Schlenk tube at room temperature under N_2. A solution of 4-nitrophenyl chloroformate in dried dichloromethane (5.5 mL) was added *via* syringe under N_2

and stirred at rt overnight. Another 0.2 eq of 4-nitrophenyl chloroformate (540 mg, 268 μmol) was added to the reaction mixture at 16 h and the reaction was stirred at rt for another 2 h. The reaction was partitioned with $NH_4OH_{(aq)}$ (20 mL), turning the biphasic mixture yellow (phenolate anion), then transferred to a separatory funnel. The organic phase washed with another 20 mL aliquot of ammonium hydroxide, followed by water (20 mL) and brine (20 mL). The organic phase was dried over $MgSO_4$, concentrated, then purified *via* column chromatography (1:19 to 1:9 EtOAc:Hx) to yield **10** (340 mg, 98%) as a white solid. M.W.: 291.30 g/mol; ^{1}H-NMR (600 MHz; $CDCl_3$): δ 8.27 (d, *J* = 9.2, 2H), 7.36 (d, *J* = 9.2, 2H), 5.65-5.58 (m, 1H), 5.54-5.45 (m, 1H), 4.48-4.43 (m, 1H), 2.47-2.34 (m, 3H), 2.21-2.08 (m, 2H), 2.04-1.93 (m, 2H), 1.89 (dd, *J* = 14.1, 5.7 Hz, 1H), 1.80-1.68 (m, 2H).

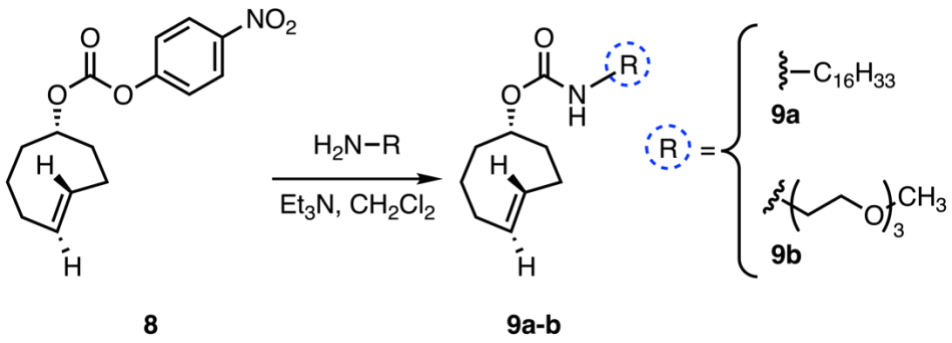

8 **9a-b**

General Procedure for Substitution of Compound 8 with Aliphatic Amines (9a-9b)[256]

The respective amine (264 μmol) and triethylamine (31.2 mg, 309 μmol) were dissolved in dichloromethane (0.2 mL) in a 4 mL small screw-cap vial equipped with a stir bar. A solution of compound **8** (51.3 mg, 176 μmol) in dichloromethane (0.2 mL) was added to the vial *via* syringe. The reaction mixture was covered in aluminum foil and stirred at rt overnight before evaporating under a flow of N_2. The yellow residue was purified *via* column chromatography. All substituted products were covered with aluminum foil and stored at -20 °C until ready for use.

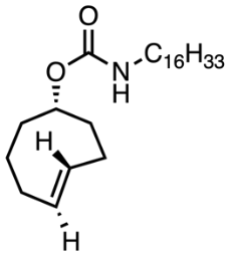

(1*R*, 4*E*)-cyclooct-4-en-1-yl hexadecylcarbamate (9a)

Purification *via* column chromatography (100% CH_2Cl_2) yielded **9a** (68 mg, 98%) as a white crystalline solid. M.W.: 393.65 g/mol; ^{1}H-NMR (600 MHz; $CDCl_3$): δ 5.61-5.45 (m, 2H), 4.51 (s, 1H), 4.34 (m, 1H), 3.13 (t, *J* = 6.0 Hz, 2H), 2.39-2.30 (m, 3H), 2.01 (d, *J* = 12.1 Hz, 1H), 1.97-1.86 (m, 3H), 1.82-1.67 (m, 2H), 1.49-1.41 (m, 2H), 1.30-1.22 (m, 27H), 0.88 (t, *J* = 6.9 Hz, 3H).

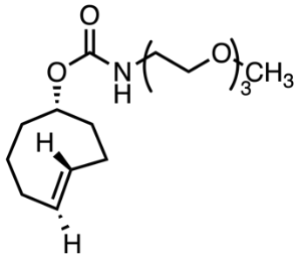

(1*R*, 4*E*)-cyclooct-4-en-1-yl (2-(2-(2-methoxyethoxy)ethoxy)ethyl)carbamate (9b)

Purification *via* column chromatography (100% CH_2Cl_2 for 15 CVs, ramp up to 2% MeOH: CH_2Cl_2 for 5 CVs, then hold at 2% MeOH: CH_2Cl_2 for 5 CVs) yielded **9b** (51 mg, 92%) as a clear colourless oil. M.W.: 315.14 g/mol; ^{1}H-NMR (600 MHz; $CDCl_3$): δ 5.61-5.46 (m, 2H), 5.11 (s, 1H), 5.34 (dd, *J* = 9.8, 5.7 Hz, 1H), 3.66-3.60 (m, 6H), 3.57-3.51 (m, 4H), 3.38 (s, 3H), 3.36-3.31 (m, 2H), 2.38-2.31 (m, 3H), 2.02 (d, *J* = 12.8 Hz, 1H), 1.97-1.88 (m, 3H), 1.80-1.69 (m, 2H), 1.57-1.49 (m, 1H). ^{13}C-NMR (151 MHz; $CDCl_3$): 156.4, 135.0, 133.1, 80.6, 72.0, 70.6, 70.3, 70.3, 59.2, 41.3, 40.8, 38.8, 34.4, 32.6, 31.1.

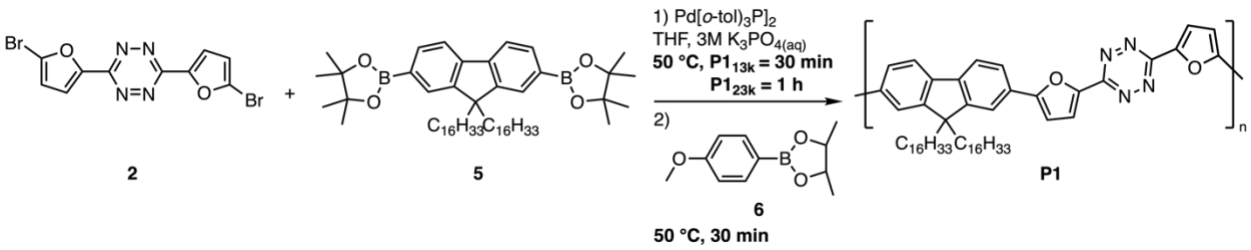

General Synthesis of *s*-tetrazine-containing Polymer - Poly[(9,9-dihexadecyl-9*H*-fluorenene)-*alt*-(3,6-bis(furan-2-yl)-*s*-tetrazine)] ($P1_{xxk}$)[216]

A mixture of compound **2** (250 mg, 672 μmol) and compound **5** (559 mg, 645 μmol) in tetrahydrofuran (6.25 mL) and 3M potassium phosphate (6.25 mL) was degassed in a 100 mL Schlenk tube equipped with a stir bar *via* three freeze-pump-thaw cycles. The biphasic mixture was frozen under liquid N_2, then bis[tris(2-methylphenyl)phosphine]palladium (24.0 mg, 33.6 μmol) was then added to the frozen mixture under argon. The head space was evacuated and the Schlenk tube was purged thrice with argon. The reaction mixture was vigorously stirred at 50 °C. After allowing to react for an allotted amount of time, a degassed solution of compound **6** (31.5 mg, 134 μmol) in tetrahydrofuran (1 mL) was added *via* syringe. The mixture was allowed to react for another 30 min, then cooled to rt, filtered through a neutral alumina plug, concentrated *in vacuo* and precipitated into cold 1:1 EtOH:THF (100 mL). The precipitate was filtered, yielding **P1** as a deep red-orange amorphous solid. The polymers were characterized by ^{1}H-NMR, GPC, UV-Vis, and FTIR spectroscopy.

13kDa Poly[(9,9-dihexadecyl-9*H*-fluorenene)-alt-(3,6-bis(furan-2-yl)-s-tetrazine)] ($P1_{13k}$)

Reaction was allowed to react for 30 min before adding solution of compound **6**. Yield: 485 mg, 87%. Repeat unit M.W.: 825.26 g/mol. M_n: 22.9 kDa (NMR), M_n: 13.0 kDa (GPC), M_w: 38.0 kDa (GPC); ^{1}H-NMR (600 MHz; $CDCl_3$): δ 7.96-7.71 (m, 8H), 7.08-6.99 (s, 2H), 3.87 (s,), 2.14 (s, 4H), 1.32-0.98 (m, 54H), 0.90-0.79 (t, *J* = 6.5 Hz, 6H), 0.67 (s, 4H).

24kDa Poly[(9,9-dihexadecyl-9*H*-fluorenene)-alt-(3,6-bis(furan-2-yl)-s-tetrazine)] ($P1_{24k}$)

Reaction was allowed to react for 1 h before adding solution of compound **6**. Yield: 457 mg, 82%. Repeat unit M.W.: 825.26 g/mol. M_n: 46.4 kDa (NMR), M_n: 23.7 kDa (GPC), M_w: 81.8 kDa (GPC); ^{1}H-NMR (600 MHz; $CDCl_3$): δ 8.05-7.63 (m, 8H), 7.04 (s, 2H), 3.88 (s,), 2.15 (s, 4H), 1.33-0.98 (m, 54H), 0.84 (t, *J* = 7.0 Hz, 6H), 0.68 (s, 4H).

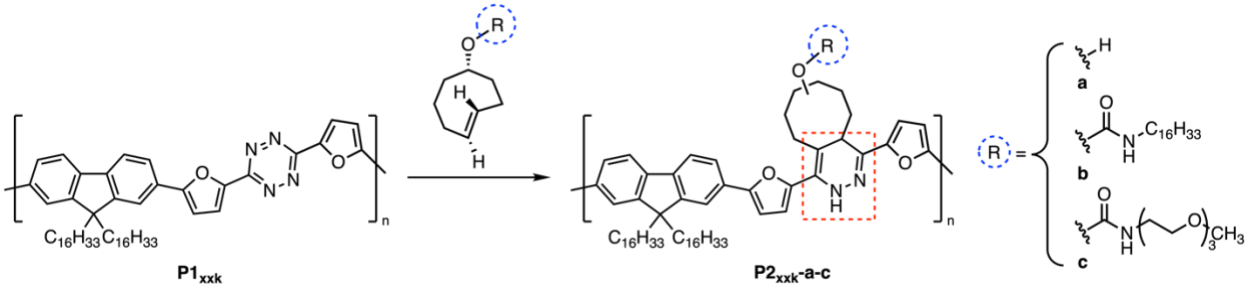

General Procedures for IEDDA Reactions on $P1_{xxk}$[216]

$P2_{xxk}$-a:

$P1_{xxk}$ (35 mg, 42.4 μmol) was dissolved in tetrahydrofuran (0.4 mL) in a 4 mL small screw-cap vial equipped with a stir bar. A solution of compound **7** (8.3 mg, 65.8 μmol) in tetrahydrofuran (0.2 mL) was added to the polymer, resulting in an effervescent reaction mixture. After stirring for 30 min, the mixture was precipitated into cold ethanol (20 mL). The precipitate was filtered and dried overnight under reduced pressure at 45 °C yielded **$P2_{xxk}$** as an orange amorphous solid. The polymers were characterized by ^{1}H-NMR, GPC, UV-Vis, and FTIR spectroscopy.

$P2_{xxk}$-b and $P2_{xxk}$-c:

$P1_{xxk}$ (35 mg, 42.4 μmol) was dissolved in tetrahydrofuran (0.4 mL) in a 4 mL small screw-cap vial equipped with a stir bar. A solution of compound the respective carbamate (63.6 μmol) in tetrahydrofuran (0.2 mL) was added to the polymer, resulting in an effervescent reaction mixture. After stirring for 30 min, the mixture was precipitated into cold ethanol (20 mL). The precipitate

was filtered and dried overnight under reduced pressure at 45 °C yielded dihydropyridazine polymer **P2$_{xxk}$-x** as an orange amorphous solid. The polymers were characterized by ^{1}H-NMR, GPC, UV-Vis, and FTIR spectroscopy.

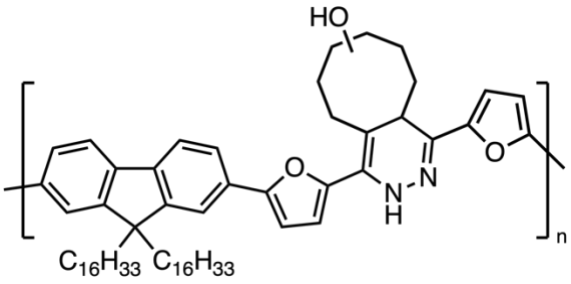

Poly[(9,9-dihexadecyl-9*H*-fluorenene)-*alt*-(3,6-bis(furan-2-yl)-cycloocta-1,4-dihydropyridazin-8-ol)] (P2$_{13k}$-a)

Yield: 33.5 mg, 86%. Repeat unit M.W.: 923.42 g/mol. M_n: 24.2 kDa (NMR), M_n: 6.6 kDa (GPC), M_w: 18.8 kDa (GPC); ^{1}H-NMR (600 MHz; $CDCl_3$): δ 8.16-8.02 (m, 1H), 7.85-7.50 (m, 6H), 7.03-6.56 (m, 4H), 4.19 (s, 1H), 3.87 (m,), 3.63 (s, 1H), 3.43-3.00 (m, 1H), 2.35-2.19 (m, 1H), 2.09 (s, 6H), 1.87 (s, 3H), 1.46 (s, 1H), 1.30-0.98 (m, 60H), 0.84 (t, *J* = 6.9 Hz, 7H), 0.65 (s, 4H).

Poly[(9,9-dihexadecyl-9*H*-fluorenene)-*alt*-(3,6-bis(furan-2-yl)-cycloocta-1,4-dihydropyridazin-8-ol)] (P2$_{24k}$-a)

Yield: 32.9 mg, 84%. Repeat unit M.W.: 923.42 g/mol. M_n: 54.1 kDa (NMR), M_n: 9.97 kDa (GPC), M_w: 30.8 kDa (GPC); ^{1}H-NMR (600 MHz; $CDCl_3$): δ 8.19-8.00 (m, 1H), 7.88-7.47 (m, 6H), 7.06-6.51 (m, 4H), 4.19 (s, 1H), 3.86 (m,), 3.63 (s, 1H), 3.45-2.99 (m, 1H), 2.23 (s, 1H), 2.09 (s, 6H), 1.88 (s, 4H), 1.29-0.97 (m, 64H), 0.84 (t, *J* = 6.6 Hz, 7H), 0.65 (s, 4H)

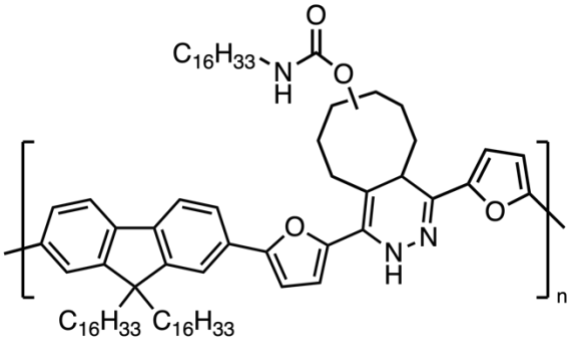

Poly[(9,9-dihexadecyl-9*H*-fluorenene)-*alt*-(3,6-bis(furan-2-yl)-1,4-dihydropyridazine)]-*graft*-hexadecyl carbamate ($P2_{13k}$-b)

Yield: 44.1 mg, 87%. Repeat unit M.W.: 1190.88 g/mol. M_n: 32.0 kDa (NMR), M_n: 13.1 kDa (GPC), M_w: 28.1 kDa (GPC); ^{1}H-NMR (600 MHz; $CDCl_3$): δ 8.10 (s, 1H), 7.86-7.56 (m, 6H), 7.04-6.59 (m, 4H), 5.09 (s, 1H), 4.63 (s, 1H), 3.87 (m,), 3.65 (s, 1H), 3.19 (s, 3H), 2.28 (s, 1H), 2.09 (s, 7H), 1.94-1.72 (m, 4H), 1.50 (s, 3H), 1.35-1.00 (m, 84H), 0.86 (dt, *J* = 13.7, 6.4 Hz, 11H), 0.65 (s, 4H).

Poly[(9,9-dihexadecyl-9*H*-fluorenene)-*alt*-(3,6-bis(furan-2-yl)-1,4-dihydropyridazine)]-*graft*-hexadecyl carbamate ($P2_{24k}$-b)

Yield: 42.0 mg, 83%. Repeat unit M.W.: 1190.88 g/mol. M_n: 73.8 kDa (NMR), M_n: 23.8 kDa (GPC), M_w: 68.4 kDa (GPC); ^{1}H-NMR (600 MHz; $CDCl_3$): δ 8.08 (s, 1H), 7.86-7.57 (m, 6H), 7.02-6.62 (m, 4H), 5.08 (s, 1H), 4.62 (s, 1H), 3.86 (m,), 3.77-3.54 (m, 1H), 3.30-2.99 (m, 3H), 2.27 (s, 1H), 2.08 (s, 7H), 1.95-1.70 (m, 4H), 1.49 (s, 3H), 1.39-0.95 (m, 90H), 0.85 (dt, 14.0, 6.5 Hz, 10H), 0.64 (s, 4H).

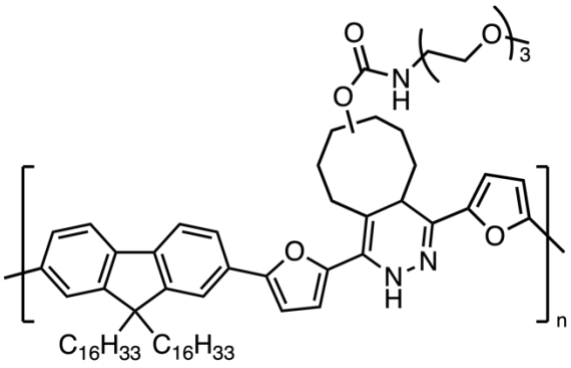

Poly[(9,9-dihexadecyl-9*H*-fluorenene)-*alt*-(3,6-bis(furan-2-yl)-1,4-dihydropyridazine)]-*graft*-(2-(2-(2-methoxyethoxy)ethoxy)ethyl)carbamate ($P2_{13k}$-c)

Yield: 37.7 mg, 80%. Repeat unit M.W.: 1112.64 g/mol. M_n: 35.7 kDa (NMR), M_n: 16.3 kDa (GPC), M_w: 36.6 kDa (GPC); ^{1}H-NMR (600 MHz; $CDCl_3$): δ 8.14 (m, 1H), 7.85-7.47 (m, 6H), 7.02-6.58 (m, 4H), 5.30-4.99 (m, 2H), 3.85 (m,), 3.72-3.51 (m, 11H), 3.47-3.31 (m, 5H), 3.29-2.97 (m, 1H), 2.27 (s, 1H), 2.08 (s, 6H), 1.94-1.68 (m, 4H), 1.31-0.95 (m, 62H), 0.84 (t, *J* = 7.0 Hz, 8H), 0.64 (s, 4H).

Poly[(9,9-dihexadecyl-9*H*-fluorenene)-*alt*-(3,6-bis(furan-2-yl)-1,4-dihydropyridazine)]-*graft*-(2-(2-(2-methoxyethoxy)ethoxy)ethyl)carbamate ($P2_{24k}$-c)

Yield: 39.2 mg, 83%. Repeat unit M.W.: 1112.64 g/mol. M_n: 62.3 kDa (NMR), M_n: 23.2 kDa (GPC), M_w: 61.7 kDa (GPC); ^{1}H-NMR (600 MHz; $CDCl_3$): δ 8.29-8.06 (m, 1H), 7.90-7.56 (m, 6H), 7.06-6.64 (m, 4H), 5.36-4.96 (m, 2H), 3.86 (m,), 3.75-3.50 (m, 11H), 3.49-3.32 (m, 5H), 3.27-2.97 (m, 1H), 2.28 (s, 1H), 2.09 (s, 6H), 1.95-1.70 (m, 4H), 1.33-1.00 (m, 62H), 0.84 (t, *J* = 7.1 Hz, 8H), 0.64 (s, 4H).

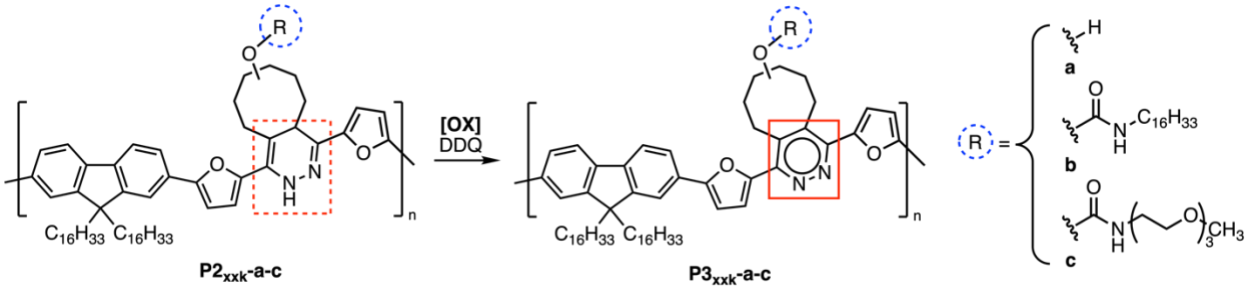

General Procedure for Oxidation of Polydihydropyridazines P2$_{xxk}$-x[216]

A solution of **P2$_{xxk}$-x** and 2,3-dichloro-5,6-dicyano-1,4-benzoquinone (1.5 eq – repeat unit basis) in tetrahydrofuran (0.7 mL) was stirred for 60 min at rt in a 4 mL small screw-cap vial equipped with a stir bar. The reaction mixture was concentrated under flow of N_2 and precipitated in cold ethanol (10 mL) and filtered onto paper. The precipitate was dried overnight under reduced pressure at 45 °C yielded pyridazine to yield polymer **P3$_{xxk}$-x** as an orange amorphous solid. The polymers were characterized by ^{1}H-NMR, GPC, UV-Vis, and FTIR spectroscopy.

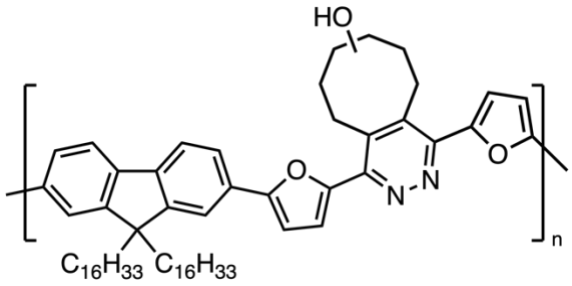

Poly[(9,9-dihexadecyl-9*H*-fluorenene)-*alt*-(3,6-bis(furan-2-yl)-cycloocta-pyridazin-8-ol)] (P3$_{13k}$-a)

Yield: 17.3 mg, 72%. Repeat unit M.W.: 921.41 g/mol. M_n: 30.0 kDa (NMR), M_n: 7.02 kDa (GPC), M_w: 20.0 kDa (GPC); ^{1}H-NMR (600 MHz; $CDCl_3$): δ 8.04-7.29 (m, 8H), 6.94 (s, 2H), 3.92 (m, 1H), 3.86 (m,), 3.60-2.97 (m, 3H), 2.57 (s, 1H), 2.48-1.68 (m, 11H), 1.29-0.96 (m, 57H), 0.83 (s, 7H), 0.71 (s, 4H).

Poly[(9,9-dihexadecyl-9*H*-fluorenene)-*alt*-(3,6-bis(furan-2-yl)-cycloocta-pyridazin-8-ol)] (P3$_{24k}$-a)

Yield: 17.3 mg, 72%. Repeat unit M.W.: 921.41 g/mol. M_n: 58.6 kDa (NMR), M_n: 15.6 kDa (GPC), M_w: 32.2 kDa (GPC); ^{1}H-NMR (600 MHz; $CDCl_3$): δ 8.21-7.34 (m, 8H), 6.96 (s, 2H), 4.02-3.89 (m, 1H), 3.86 (s,), 3.60-3.14 (m, 3H), 2.58 (s, 1H), 2.46-1.70 (m, 11H), 1.28-0.94 (m, 60H), 0.84 (s, 8H), 0.72 (s, 4H).

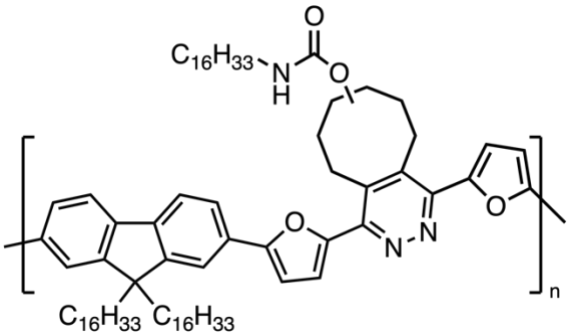

Poly[(9,9-dihexadecyl-9*H*-fluorenene)-*alt*-(3,6-bis(furan-2-yl)-pyridazine)]-*graft*-hexadecyl carbamate (P3$_{13k}$-b)

Yield: 27.2 mg, 91%. Repeat unit M.W.: 1188.87 g/mol. M_n: 31.9 kDa (NMR), M_n: 12.0 kDa (GPC), M_w: 22.9 kDa (GPC); ^{1}H-NMR (600 MHz; $CDCl_3$): δ 8.19-7.46 (m, 8H), 6.97 (s, 2H), 5.34-4.78 (m, 1H), 4.76-4.43 (m, 1H), 3.87 (m,), 3.59-3.24 (m, 2H), 3.18 (s, 2H), 2.57 (s, 1H), 2.30 (s, 2H), 2.07 (s, 4H), 1.88 (s, 2H), 1.50 (s, 3H), 1.39-0.93 (m, 87H), 0.92-0.80 (m, 10H), 0.71 (s, 4H).

Poly[(9,9-dihexadecyl-9*H*-fluorenene)-*alt*-(3,6-bis(furan-2-yl)-pyridazine)]-*graft*-hexadecyl carbamate (P3$_{24k}$-b)

Yield: 28.5 mg, 95%. Repeat unit M.W.: 1188.87 g/mol. M_n: 65.4 kDa (NMR), M_n: 23.3 kDa (GPC), M_w: 72.3 kDa (GPC); ^{1}H-NMR (600 MHz; $CDCl_3$): δ 8.18-7.48 (m, 9H), 6.96 (s, 2H), 5.45-4.78 (m, 1H), 4.78-4.44 (m, 1H), 3.87 (m,), 3.58-3.27 (m, 2H), 3.18 (s, 3H), 2.56 (s, 1H), 2.29 (s, 2H), 2.06 (s, 2H), 1.88 (s, 1H), 1.68 (s, 3H), 1.49 (s, 3H), 1.31-1.00 (m, 96H), 0.88-0.80 (m, 11H), 0.70 (s, 4H).

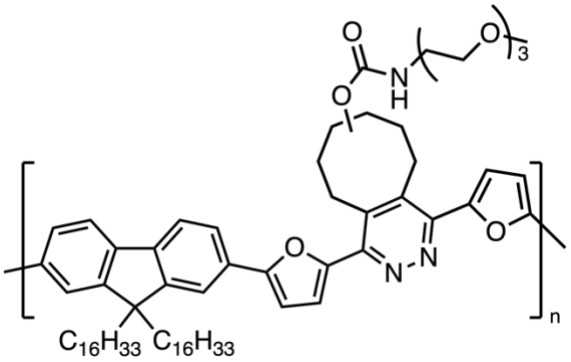

Poly[(9,9-dihexadecyl-9*H*-fluorenene)-*alt*-(3,6-bis(furan-2-yl)-pyridazine)]-*graft*-(2-(2-(2-methoxyethoxy)ethoxy)ethyl)carbamate ($P3_{13k}$-c)

Yield: 30.1 mg, 86%. Repeat unit M.W.: 1110.62 g/mol. M_n: 39.2 kDa (NMR), M_n: 7.19 kDa (GPC), M_w: 22.1 kDa (GPC); ^{1}H-NMR (600 MHz; $CDCl_3$): δ 8.16-7.46 (m, 8H), 6.97 (s, 2H), 5.22 (s, 1H), 4.88 (s, 1H), 3.87 (m,), 3.71-3.48 (m, 11H), 3.45-3.31 (m, 6H), 2.56 (s, 1H), 2.29 (s, 2H), 2.07 (s, 5H), 1.88 (s, 2H), 1.75-1.54 (m, 4H), 1.51-1.44 (m, 1H), 1.28-1.01 (m, 58H), 0.84 (t, *J* = 6.6 Hz, 7H), 0.70 (s, 3H).

Poly[(9,9-dihexadecyl-9*H*-fluorenene)-*alt*-(3,6-bis(furan-2-yl)-pyridazine)]-*graft*-(2-(2-(2-methoxyethoxy)ethoxy)ethyl)carbamate ($P3_{24k}$-c)

Yield: 31.2 mg, 89%. Repeat unit M.W.: 1110.62 g/mol. M_n: 63.2 kDa (NMR), M_n: 19.1 kDa (GPC), M_w: 45.1 kDa (GPC); ^{1}H-NMR (600 MHz; $CDCl_3$): δ 8.00-7.48 (m, 8H), 7.00 (s, 2H), 5.26

(s, 1H), 4.91 (s, 1H), 3.90 (m,), 3.75-3.51 (m, 10H), 3.48-3.33 (m, 6H), 2.59 (s, 1H), 2.33 (s, 3H), 2.10 (s, 5H), 1.90 (s, 2H), 1.67 (s, 3H), 1.33-1.02 (m, 59H), 0.87 (t, J = 6.8 Hz, 7H), 0.73 (s, 4H).

NMR Spectra

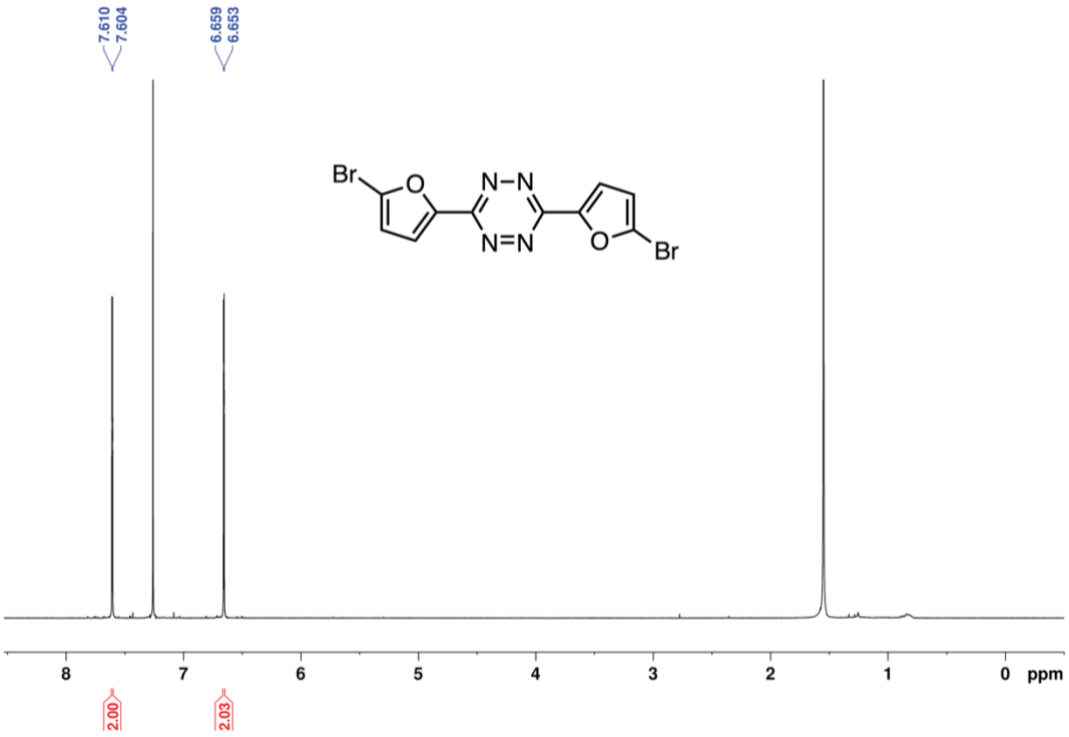

Figure S1. ^{1}H-NMR spectrum of **1** in $CDCl_3$.

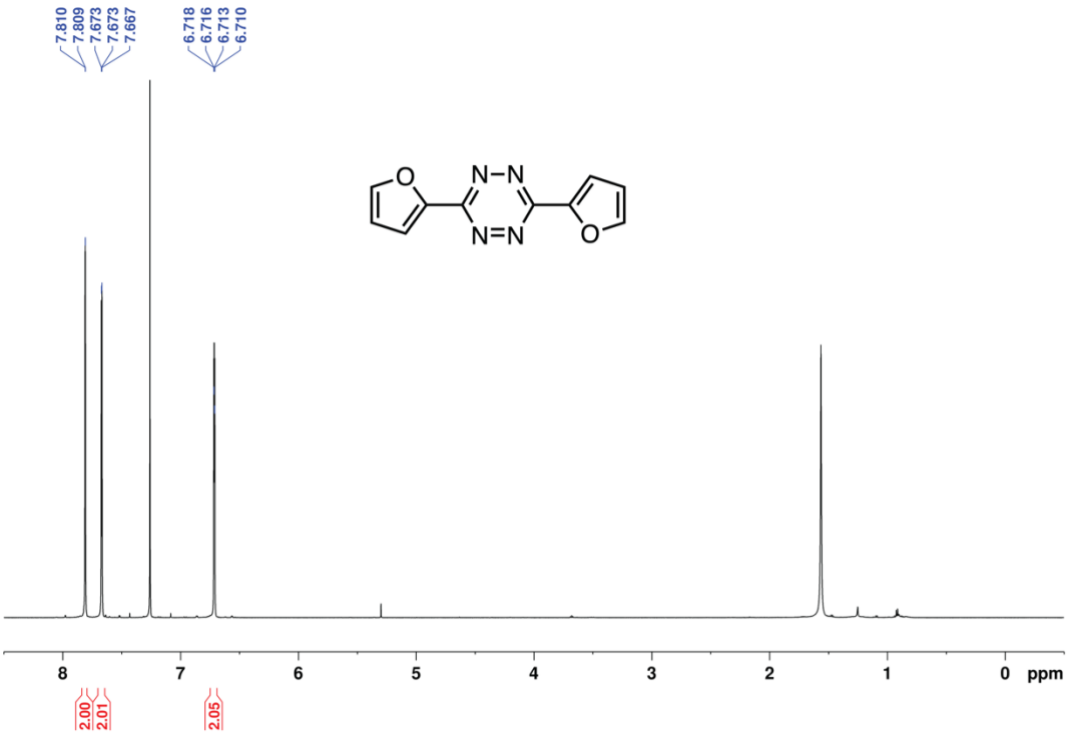

Figure S2. ^{1}H-NMR spectrum of **2** in $CDCl_3$.

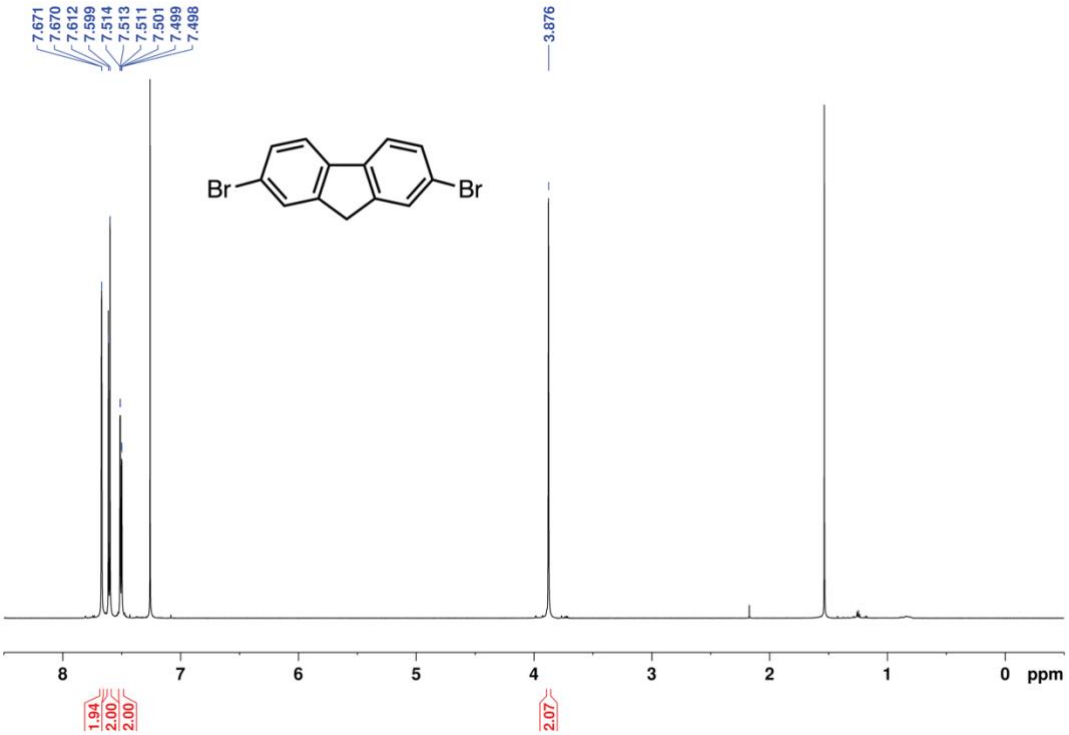

Figure S3. ^{1}H-NMR spectrum of **3** in $CDCl_3$.

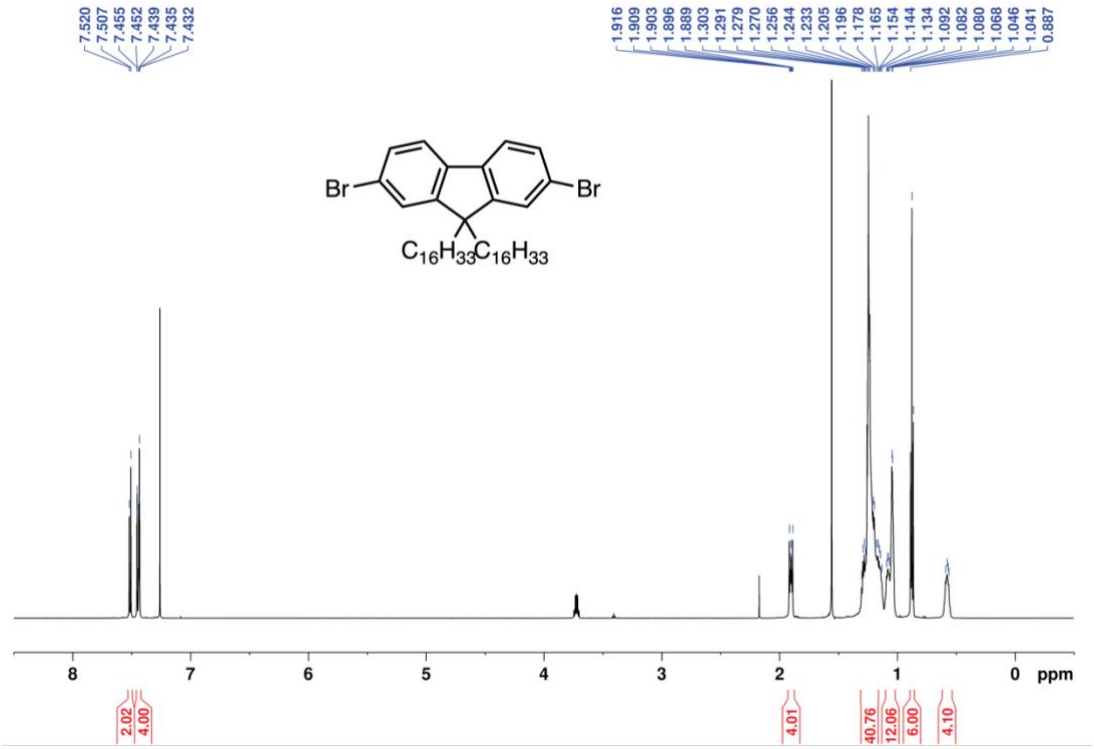

Figure S4. ^{1}H-NMR spectrum of **4** in $CDCl_3$.

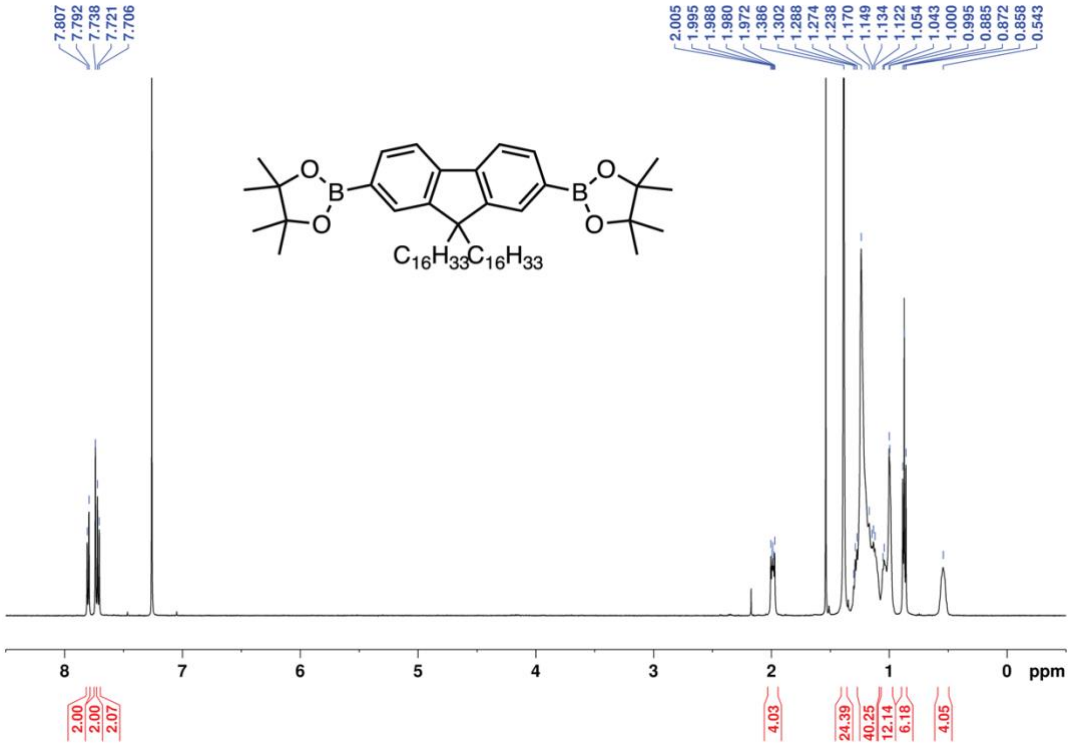

Figure S5. ^{1}H-NMR spectrum of **5** in $CDCl_3$.

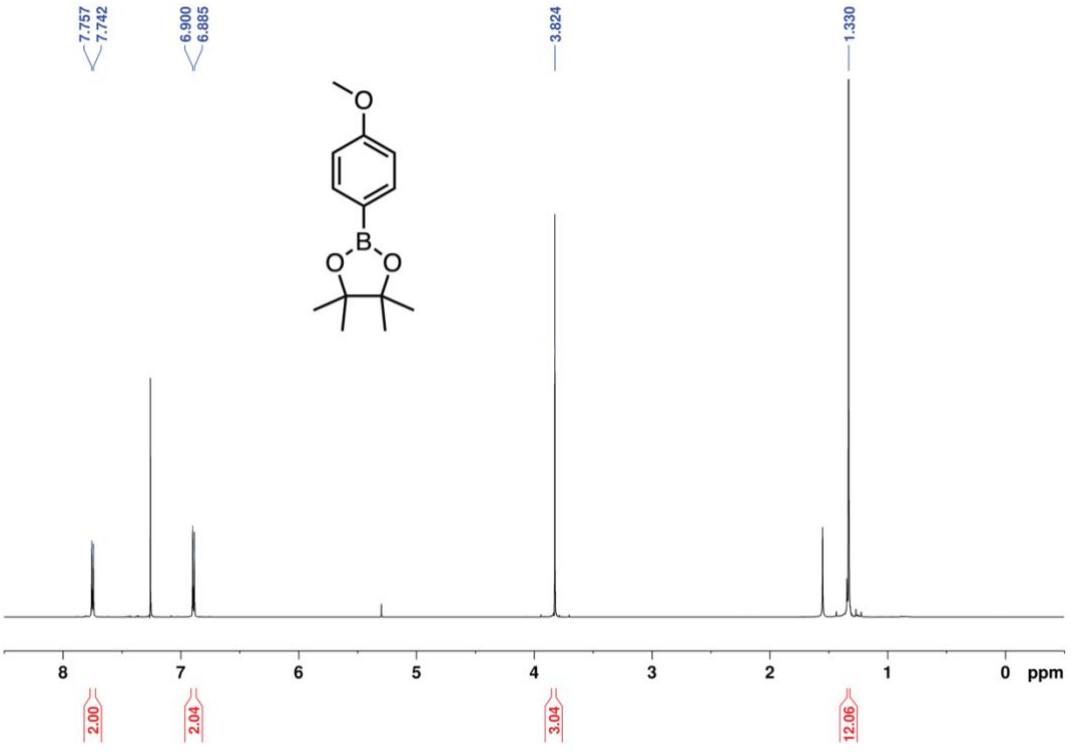

Figure S6. ^{1}H-NMR spectrum of **6** in $CDCl_3$.

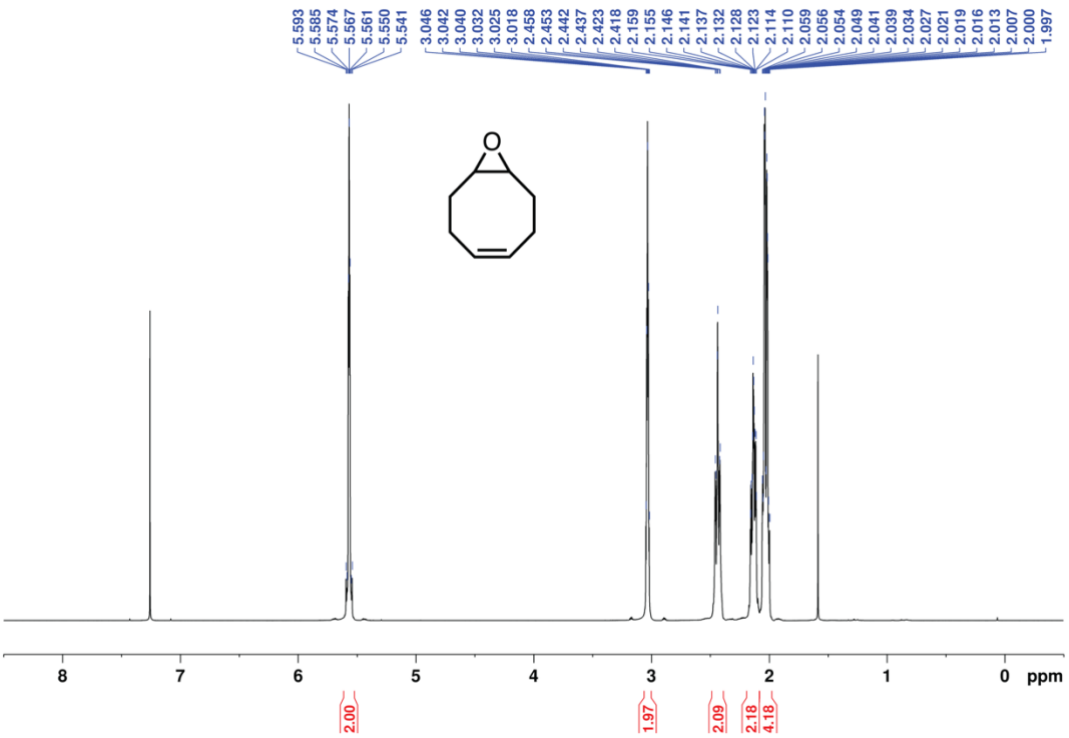

Figure S7. ^{1}H-NMR spectrum of 5,6-epoxycyclooctene in $CDCl_3$.

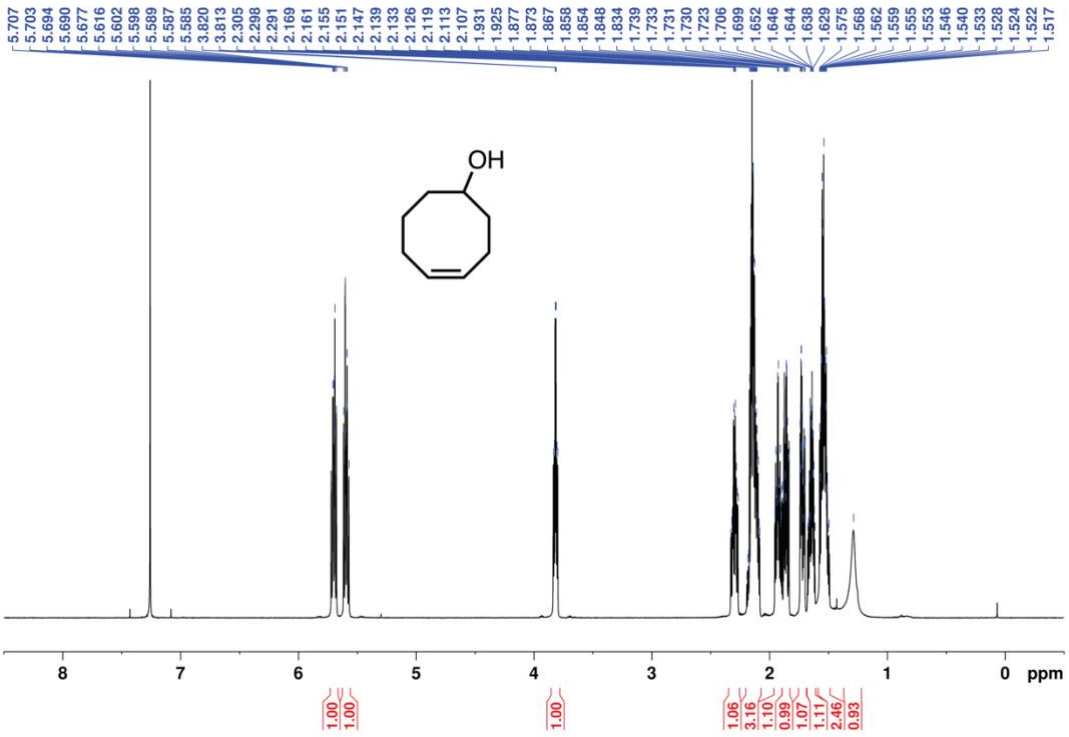

Figure S8. ^{1}H-NMR spectrum of (*Z*)-Cyclooct-4-enol in $CDCl_3$.

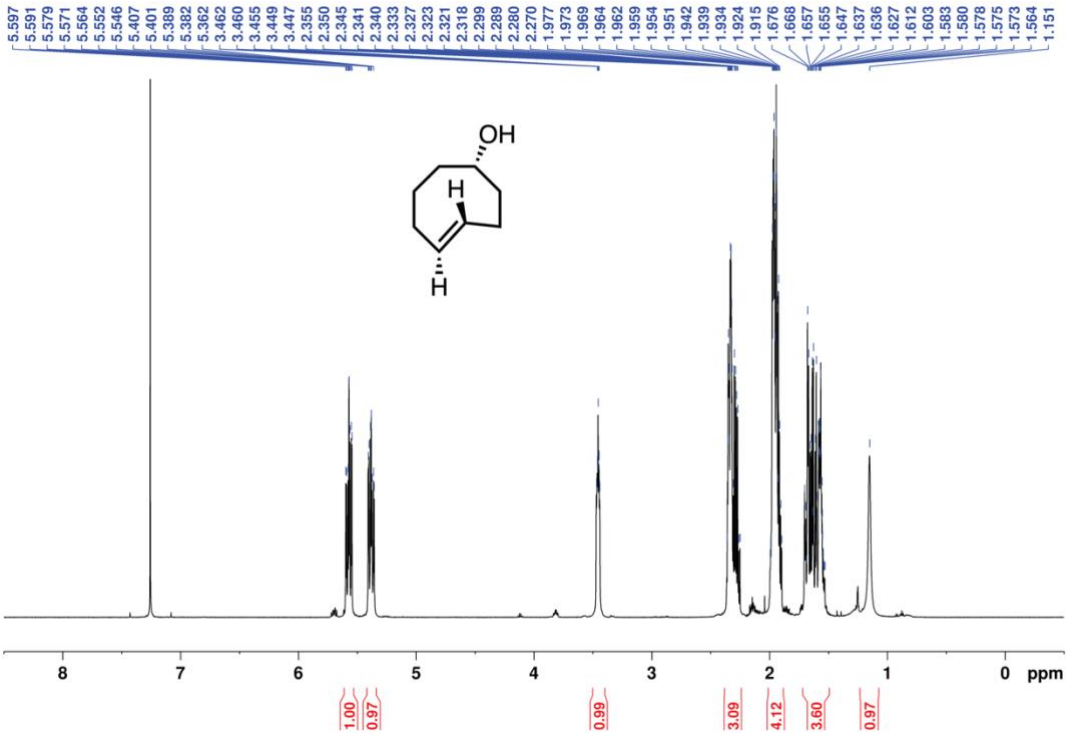

Figure S9. ^{1}H-NMR spectrum of **7** in $CDCl_3$.

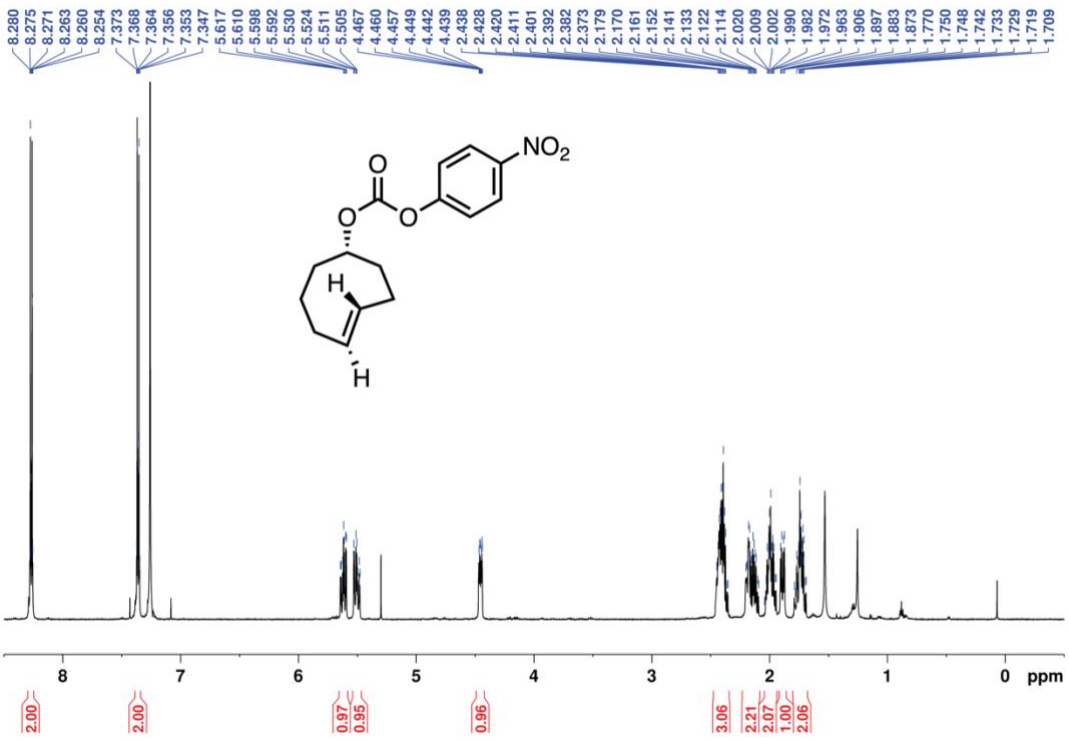

Figure S10. ^{1}H-NMR spectrum of **8** in $CDCl_3$.

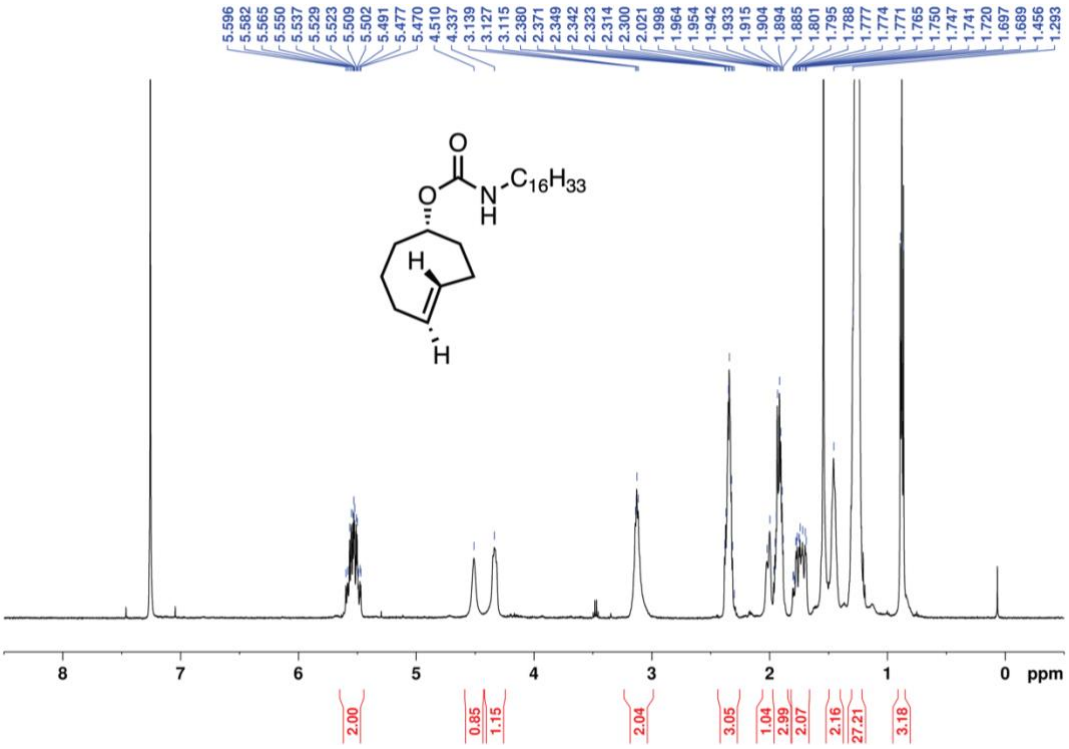

Figure S11. ^{1}H-NMR spectrum of **9a** in $CDCl_3$.

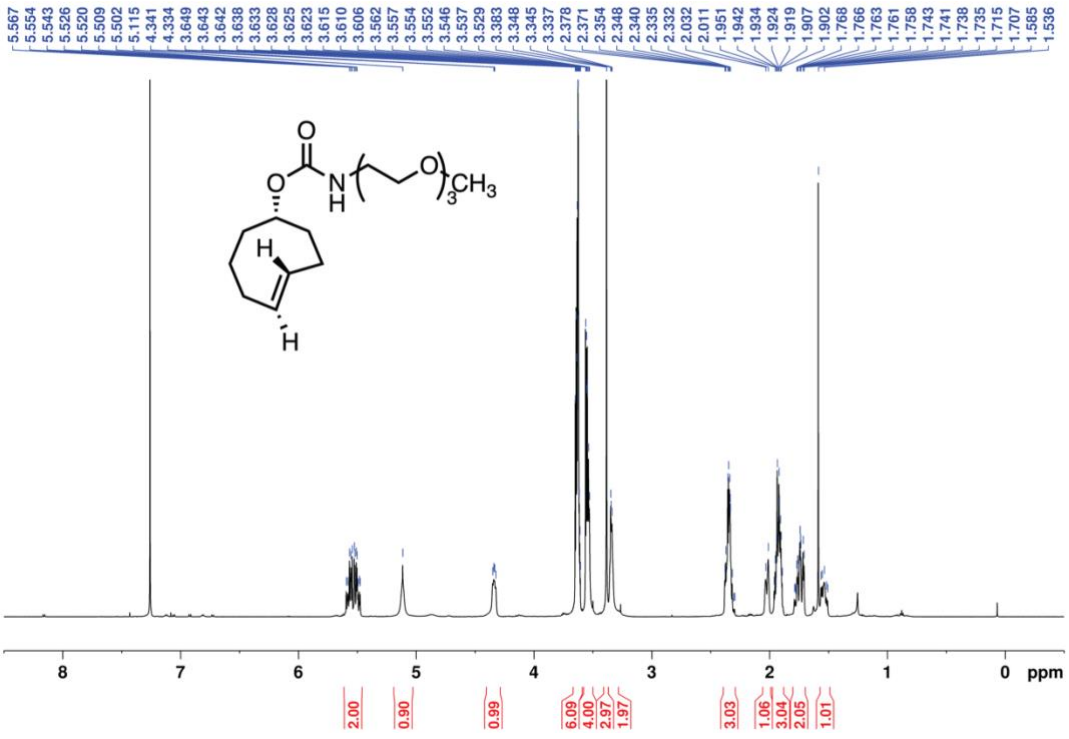

Figure S12. ^{1}H-NMR spectrum of **9b** in $CDCl_3$.

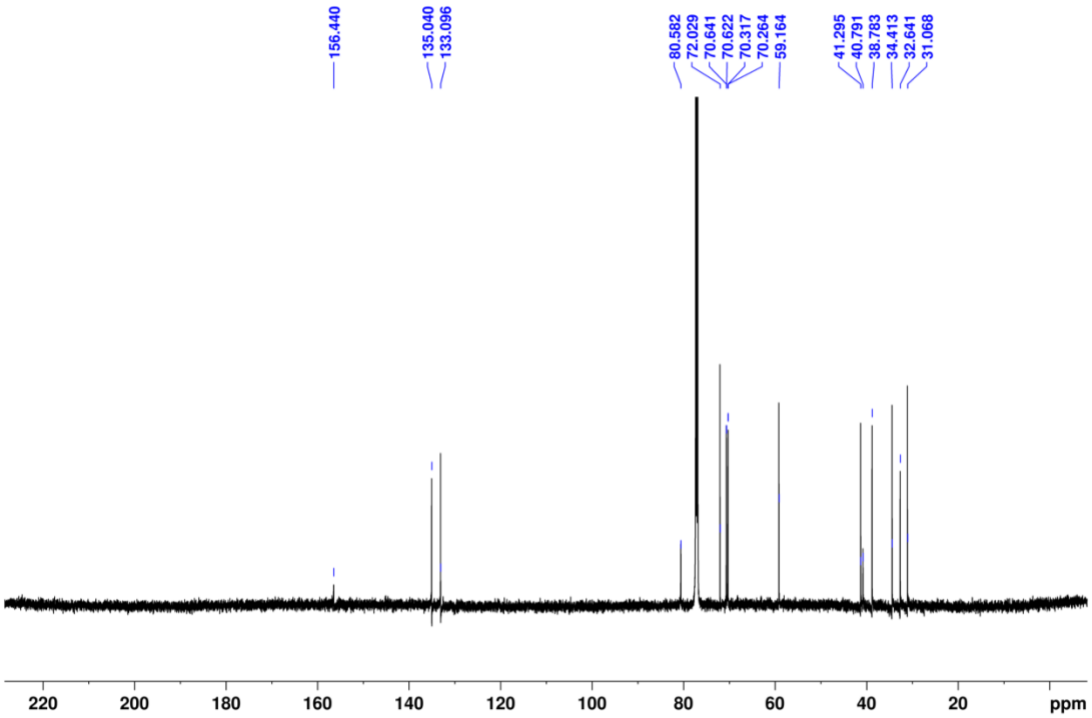

Figure S13. ^{13}C-NMR spectrum of **9b** in $CDCl_3$.

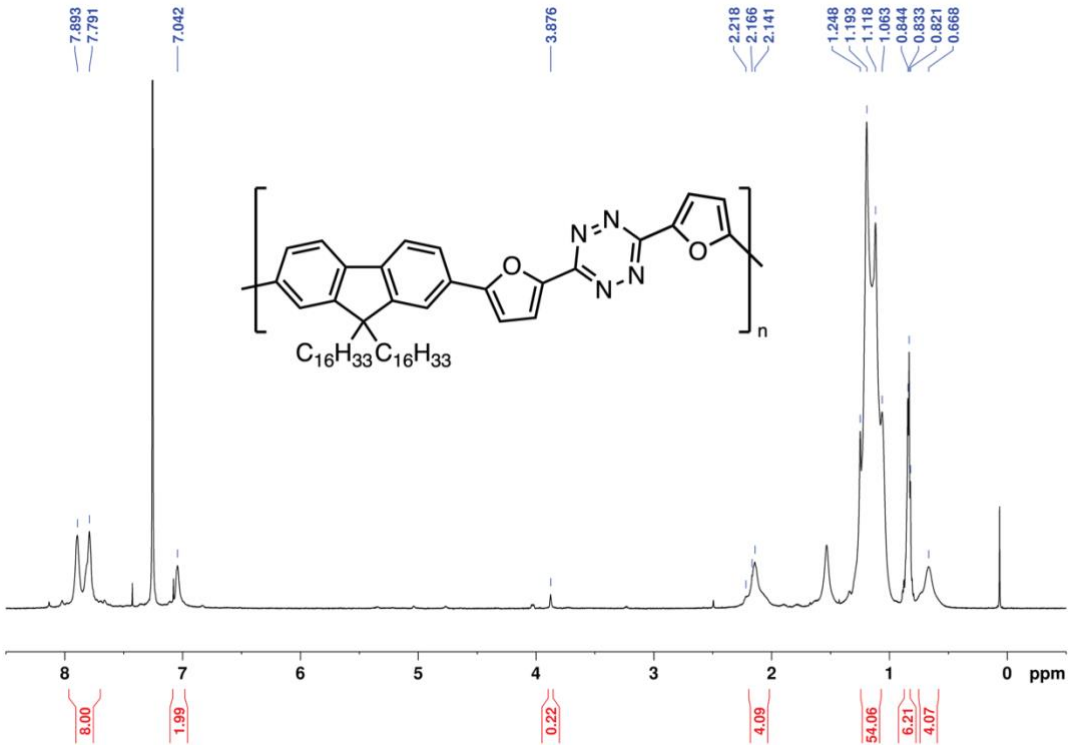

Figure S14. ^{1}H-NMR spectrum of **P1$_{13k}$** in $CDCl_3$.

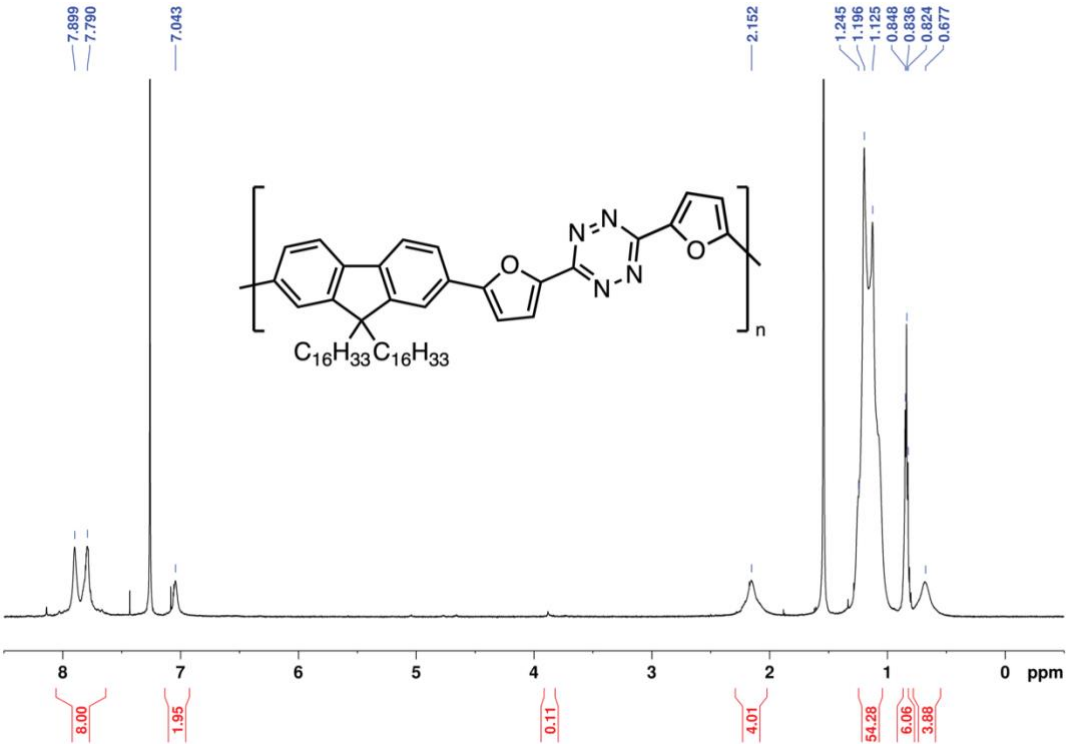

Figure S15. ^{1}H-NMR spectrum of **P1$_{24k}$** in $CDCl_3$.

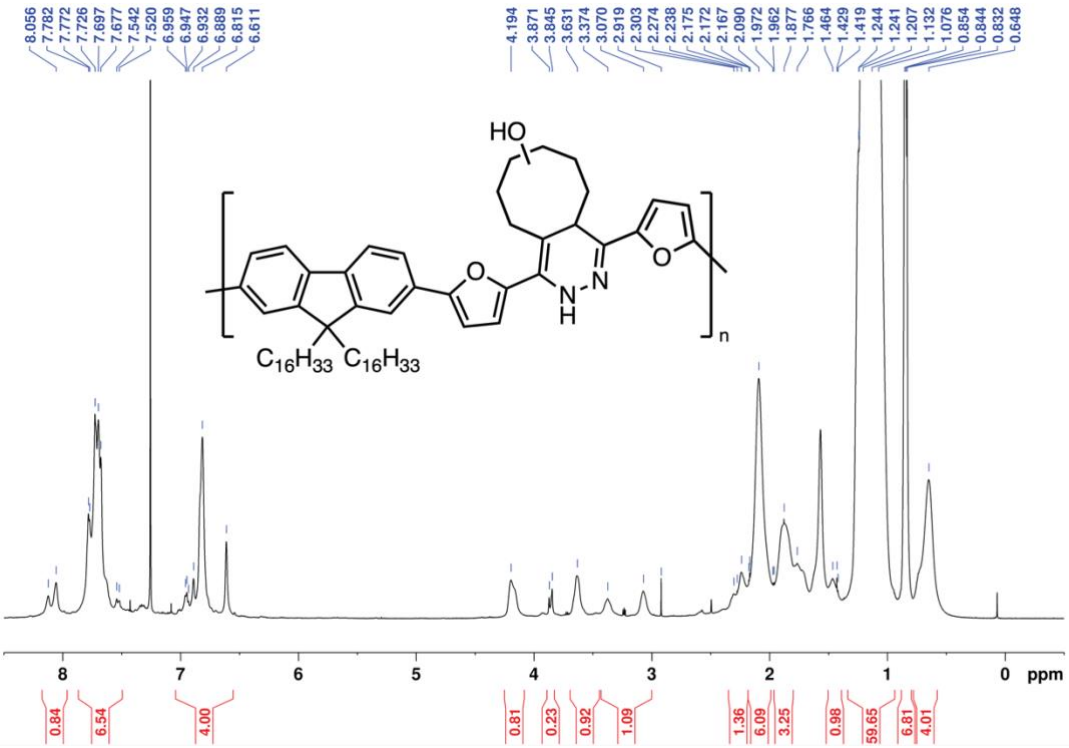

Figure S16. ^{1}H-NMR spectrum of **P2$_{13k}$-a** in $CDCl_3$.

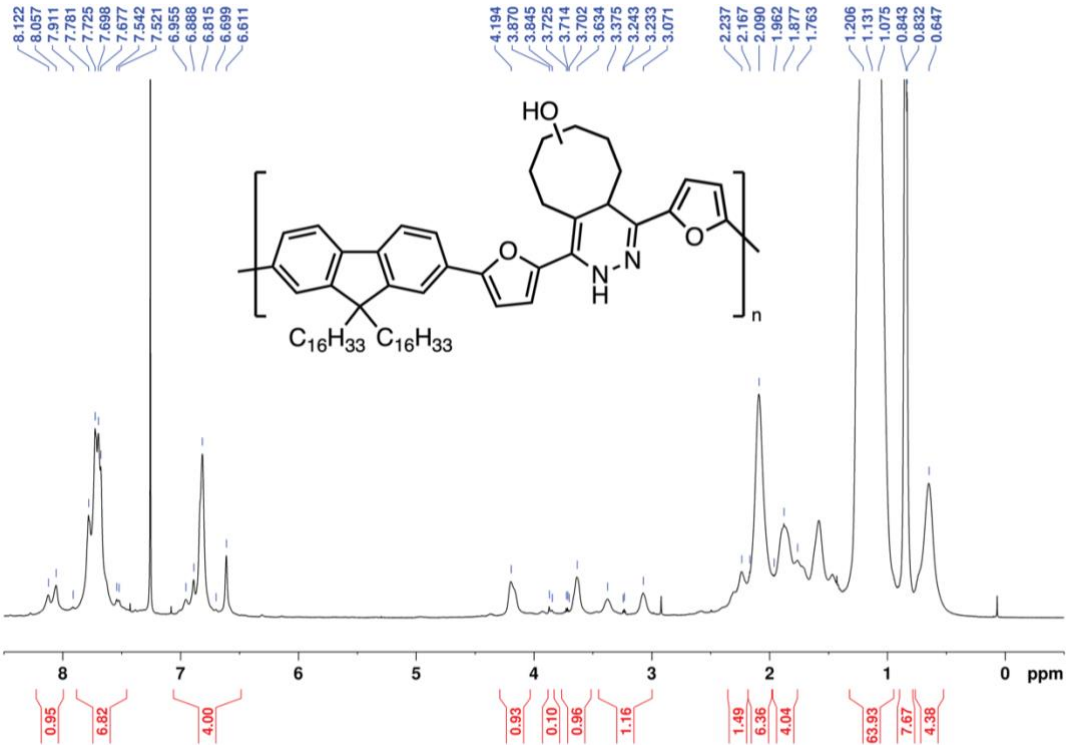

Figure S17. ^{1}H-NMR spectrum of **P2$_{24k}$-a** in $CDCl_3$.

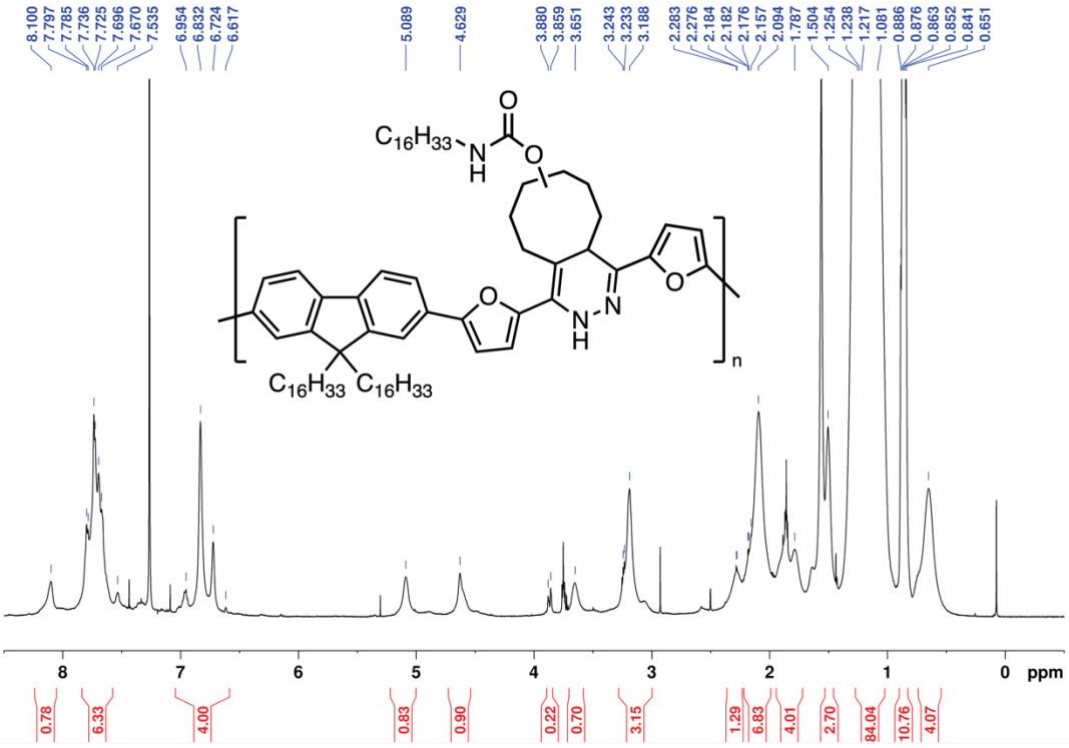

Figure S18. ^{1}H-NMR spectrum of **P2$_{13k}$-b** in $CDCl_3$.

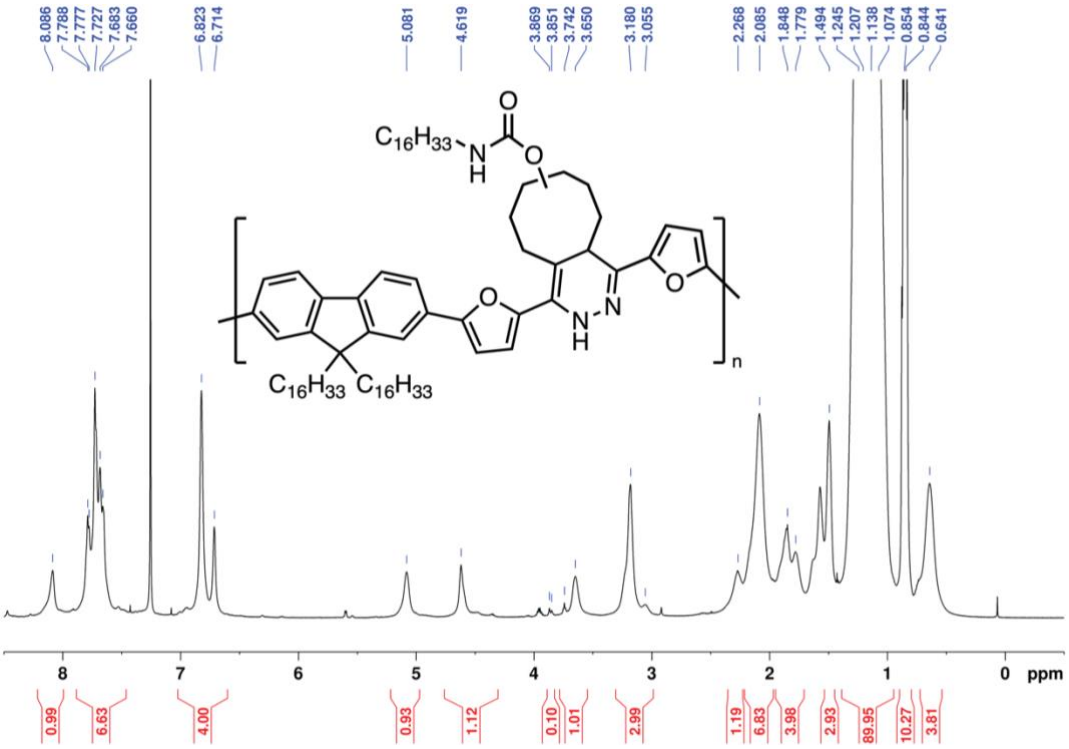

Figure S19. ^{1}H-NMR spectrum of **P2$_{24k}$-b** in $CDCl_3$.

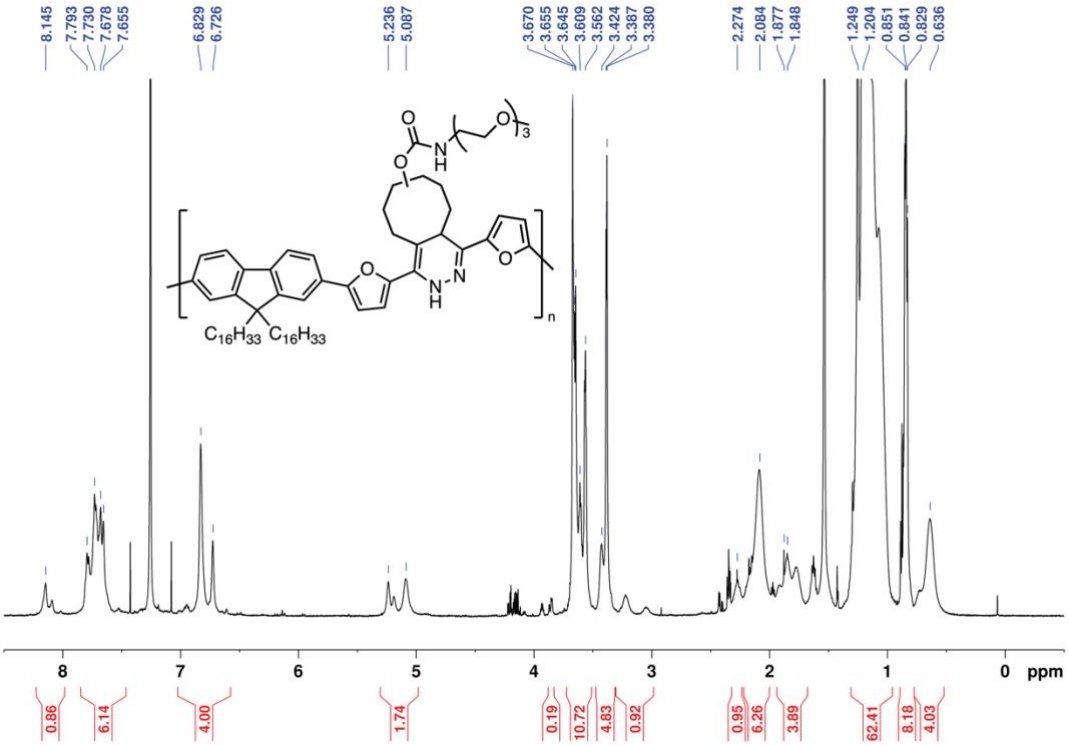

Figure S20. ^{1}H-NMR spectrum of **P2$_{13k}$-c** in $CDCl_3$.

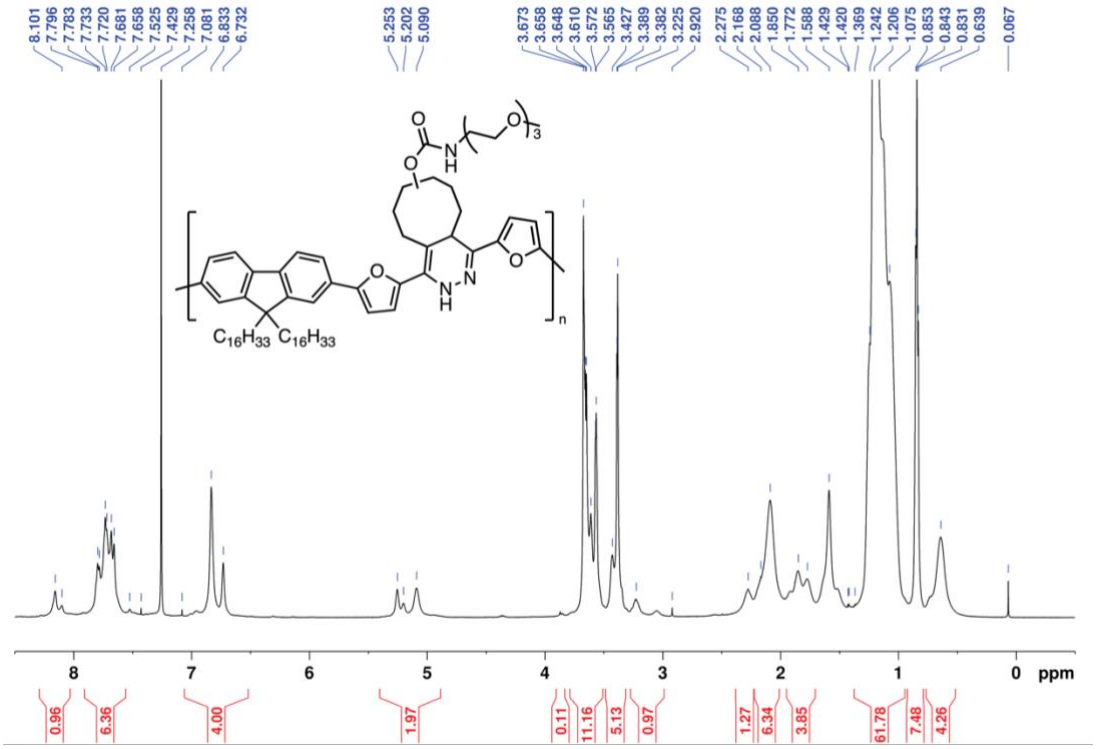

Figure S21. ^{1}H-NMR spectrum of **P2$_{24k}$-c** in $CDCl_3$.

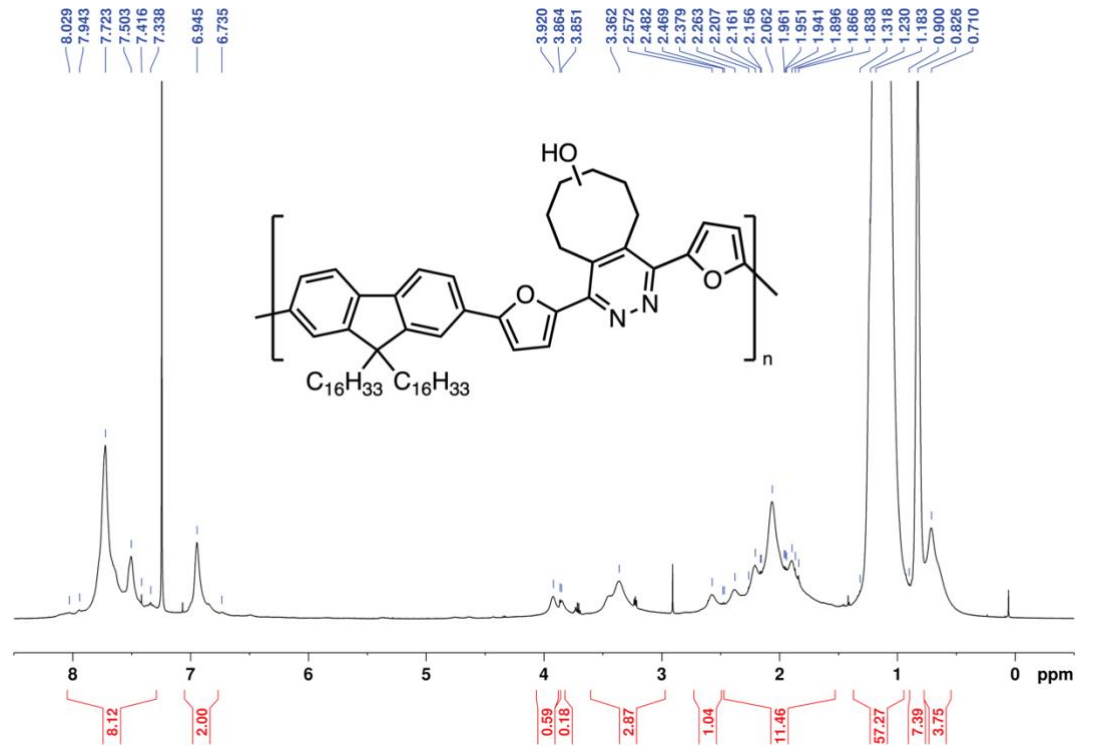

Figure S22. ^{1}H-NMR spectrum of **P3$_{13k}$-a** in $CDCl_3$.

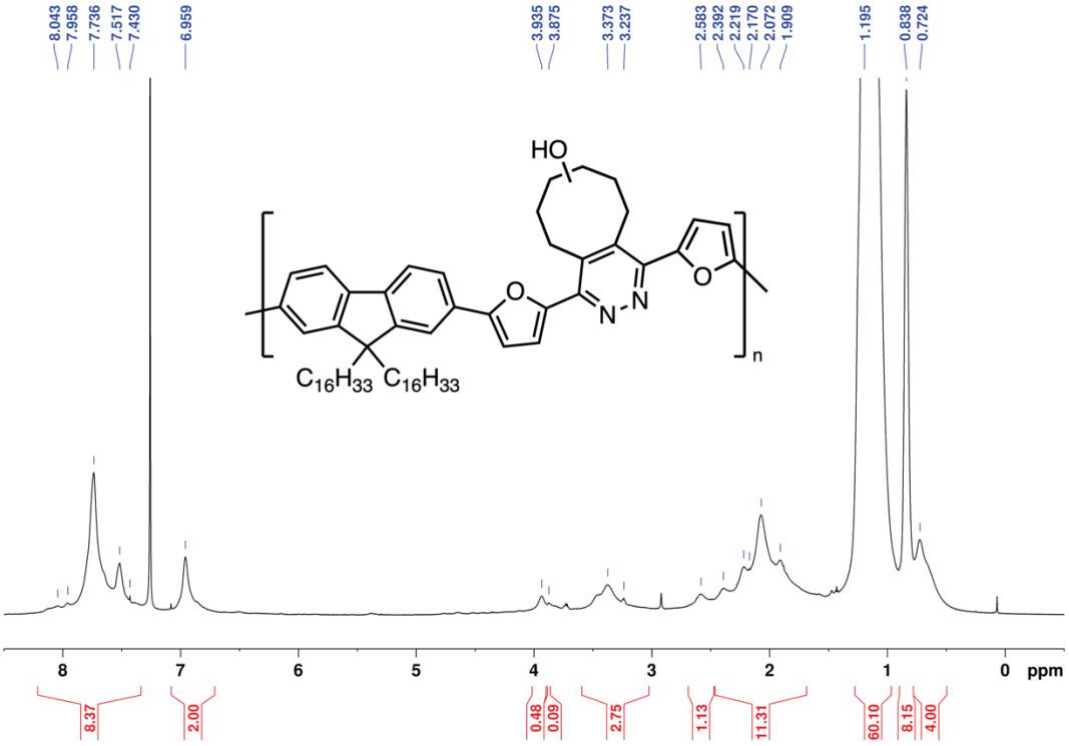

Figure S 23. ^{1}H-NMR spectrum of **P3$_{24k}$-a** in $CDCl_3$.

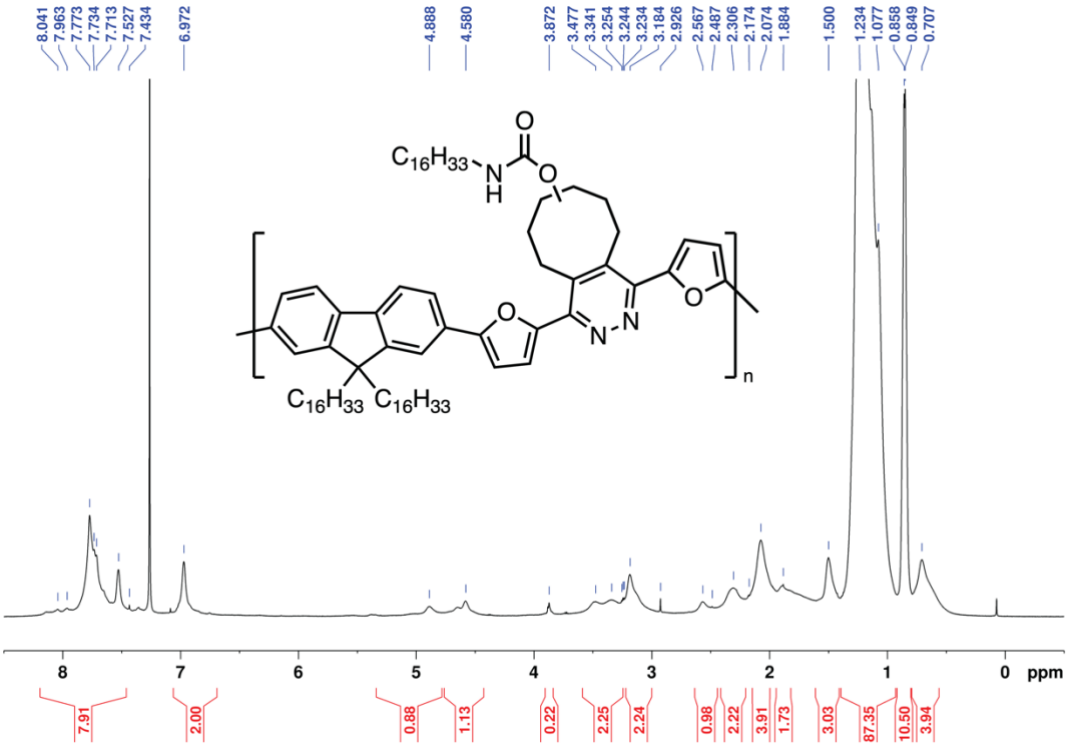

Figure S24. ^{1}H-NMR spectrum of **P3$_{13k}$-b** in $CDCl_3$.

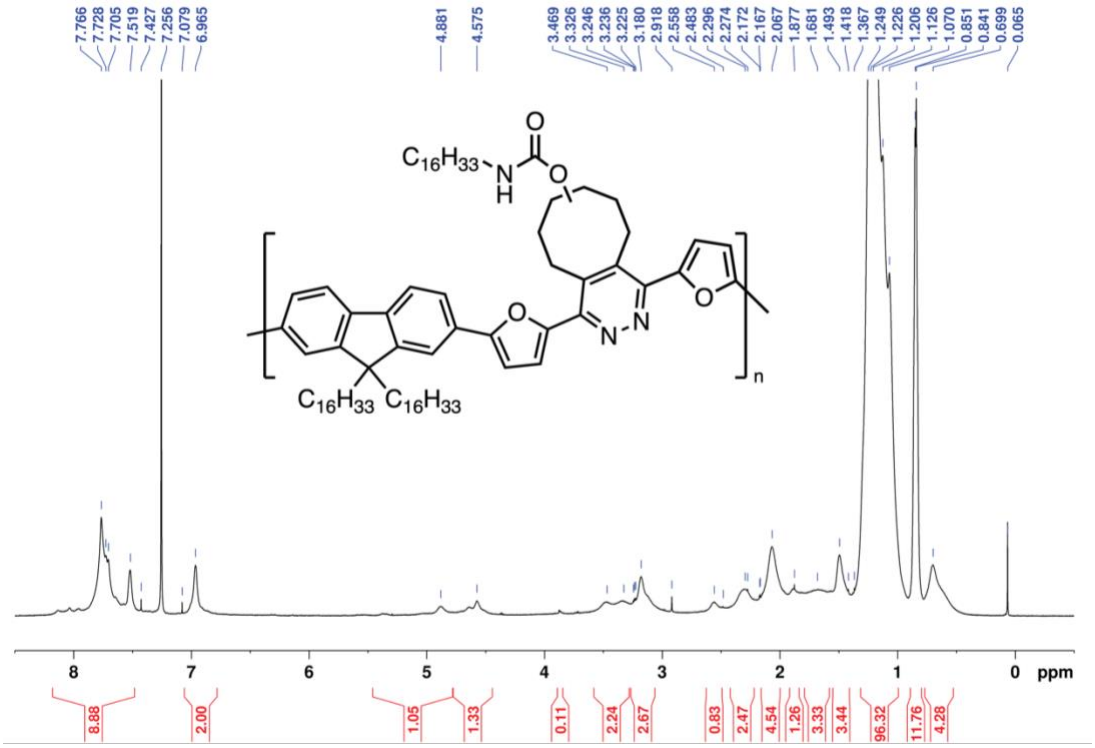

Figure S 25. ^{1}H-NMR spectrum of **P3$_{24k}$-b** in $CDCl_3$.

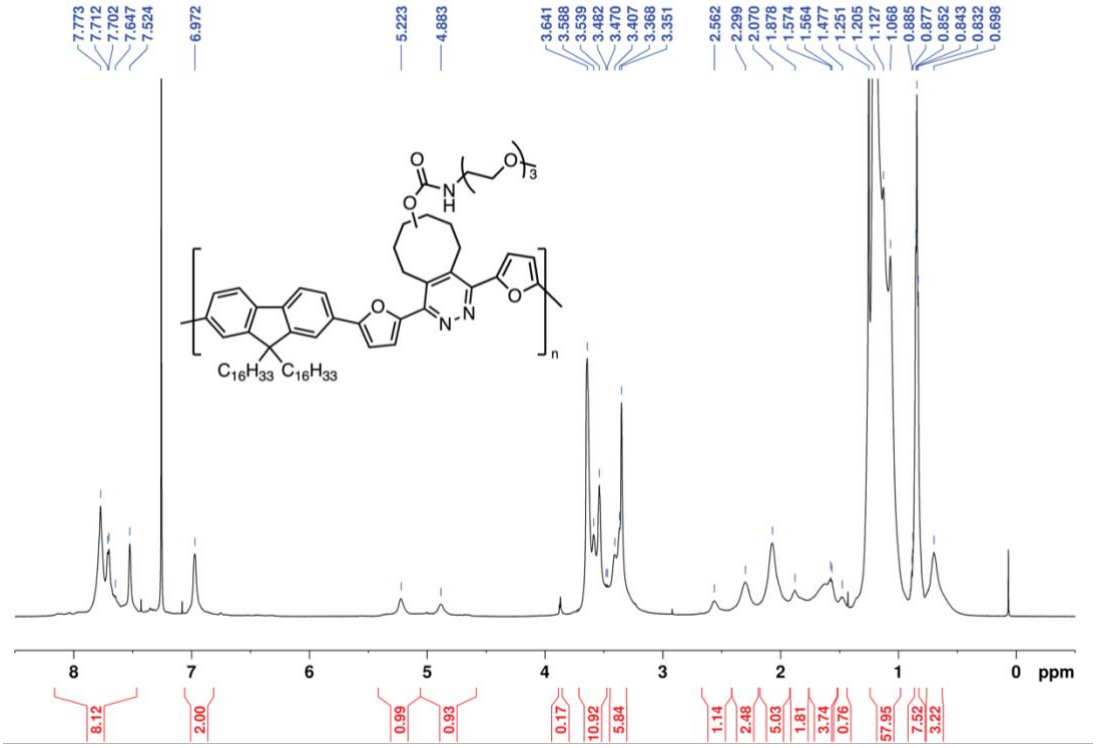

Figure S26. ^{1}H-NMR spectrum of **P3$_{13k}$-c** in $CDCl_3$.

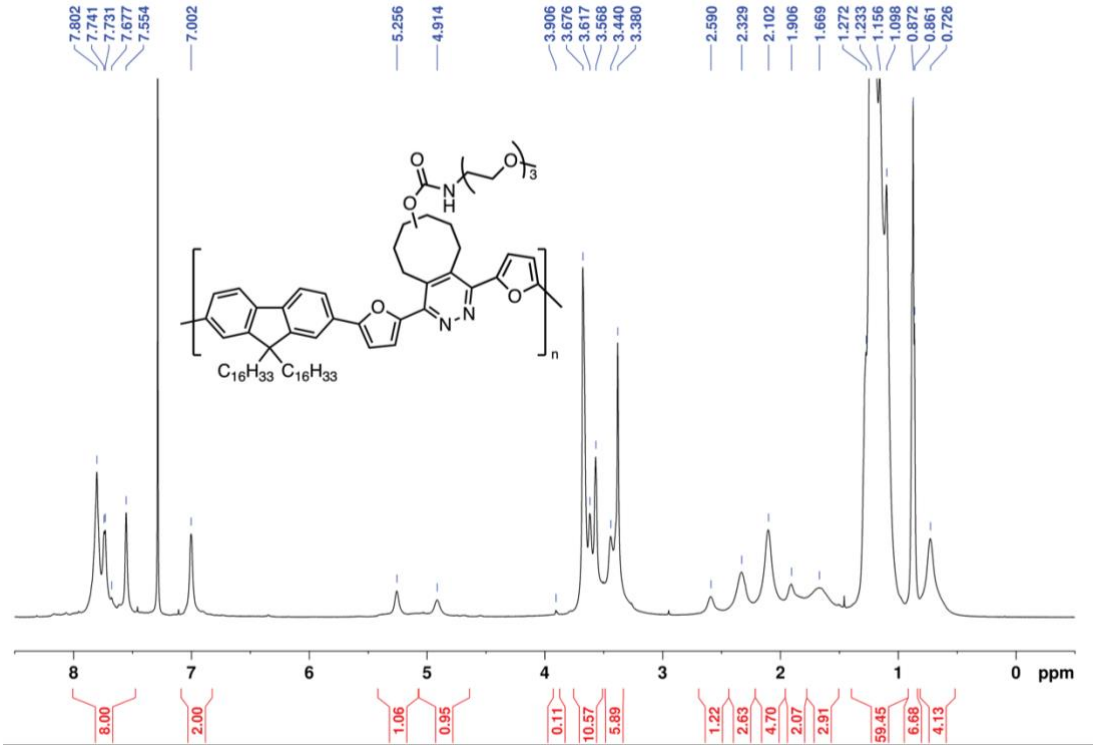

Figure S27. ^{1}H-NMR spectrum of **P3$_{24k}$-c** in $CDCl_3$.

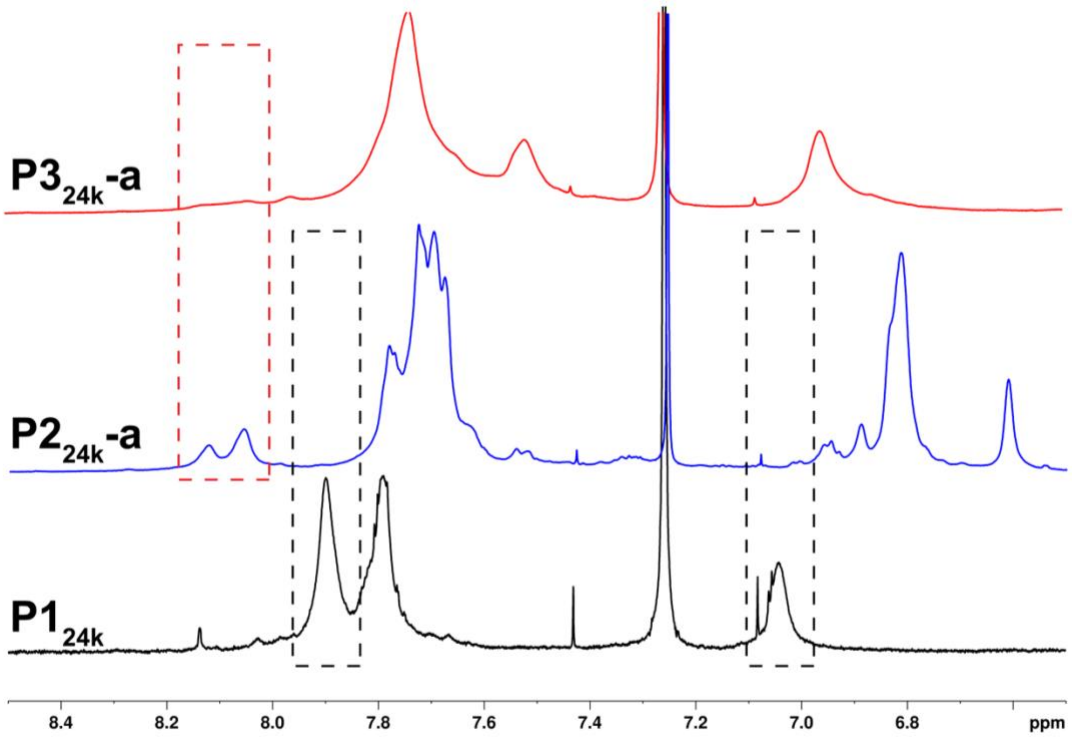

Figure S28. ^{1}H-NMR spectrum overlay of **P1$_{24k}$**, **P2$_{24k}$-a**, and **P3$_{24k}$-a** in $CDCl_3$.

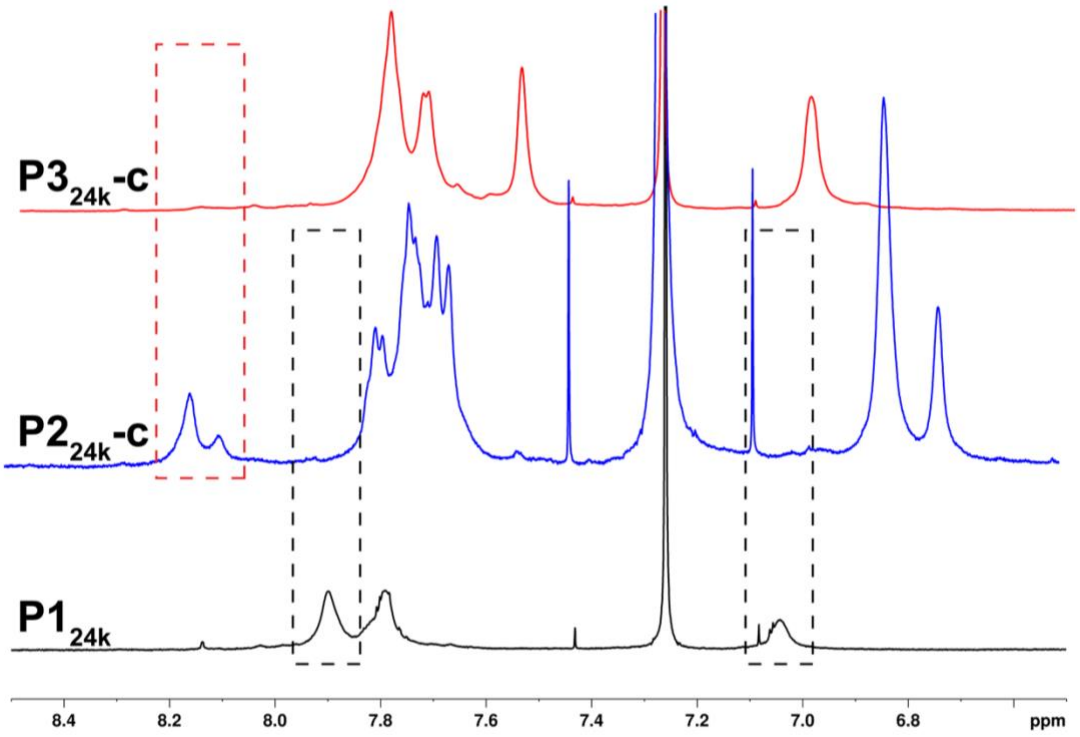

Figure S29. ^{1}H-NMR spectrum overlay of **P1$_{24k}$**, **P2$_{24k}$-c**, and **P3$_{24k}$-c** in $CDCl_3$.

UV-Vis Spectra

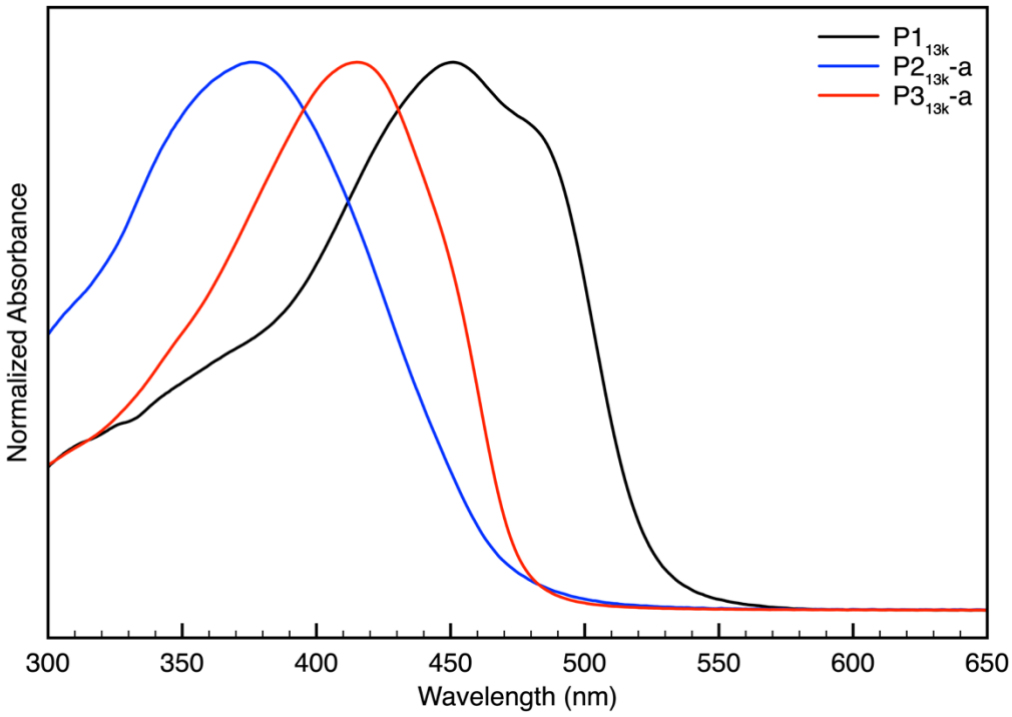

Figure S30. UV-Vis absorption spectrum overlay of **P1$_{13k}$**, **P2$_{13k}$-a**, and **P3$_{13k}$-a** in THF.

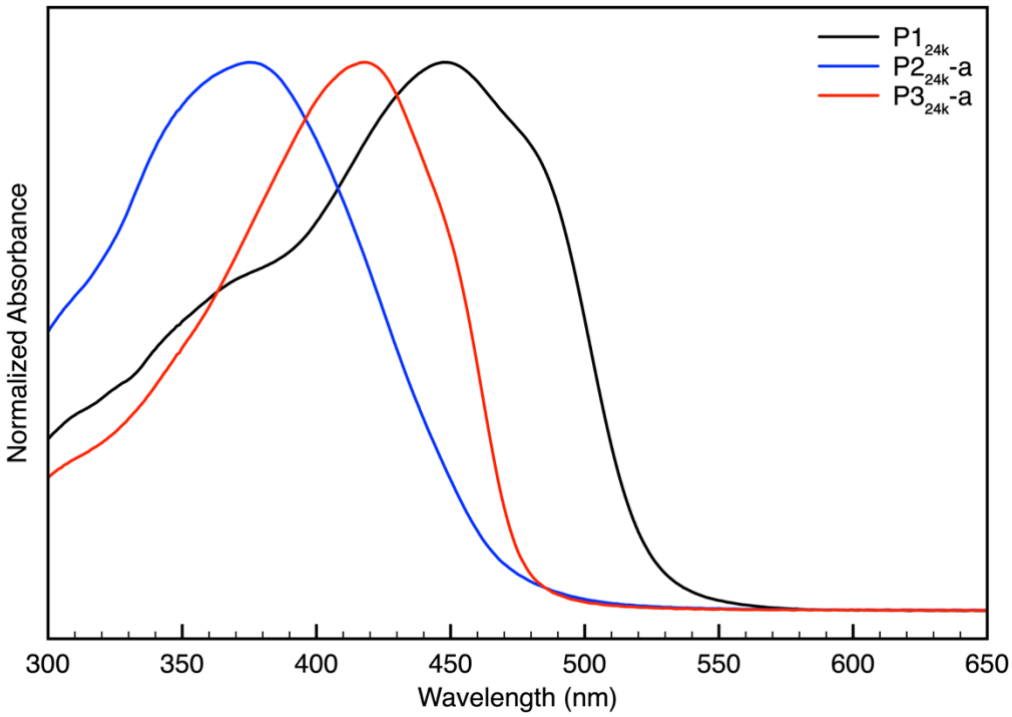

Figure S31. UV-Vis absorption spectrum overlay of **P1$_{24k}$**, **P2$_{24k}$-a**, and **P3$_{24k}$-a** in THF.

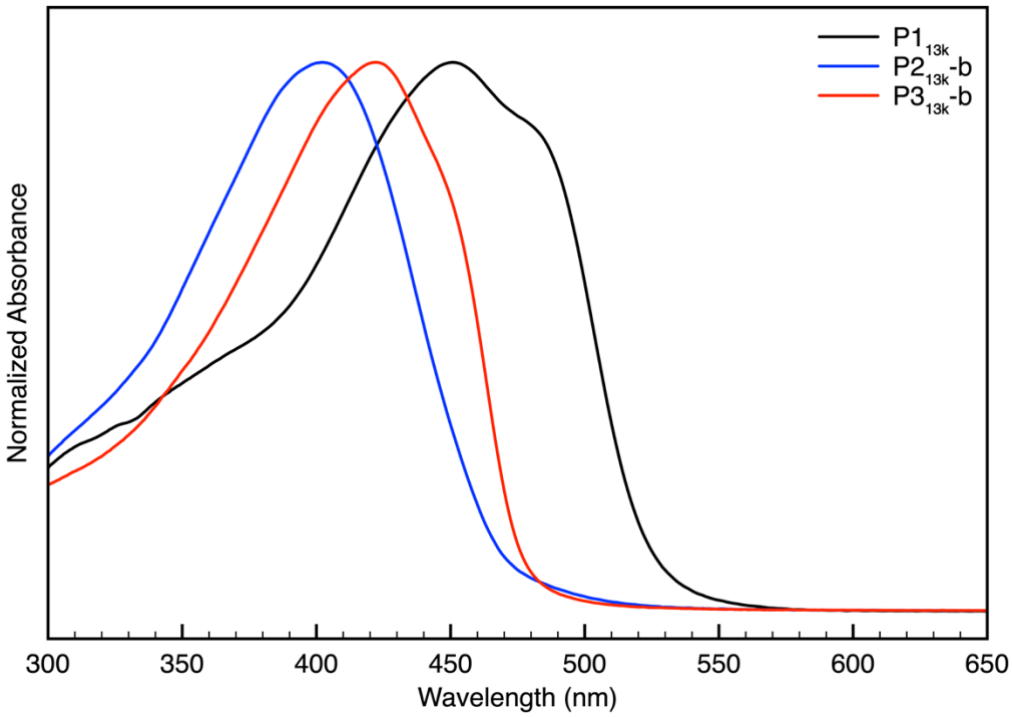

Figure S32. UV-Vis absorption spectrum overlay of **P1$_{13k}$**, **P2$_{13k}$-b**, and **P3$_{13k}$-b** in THF.

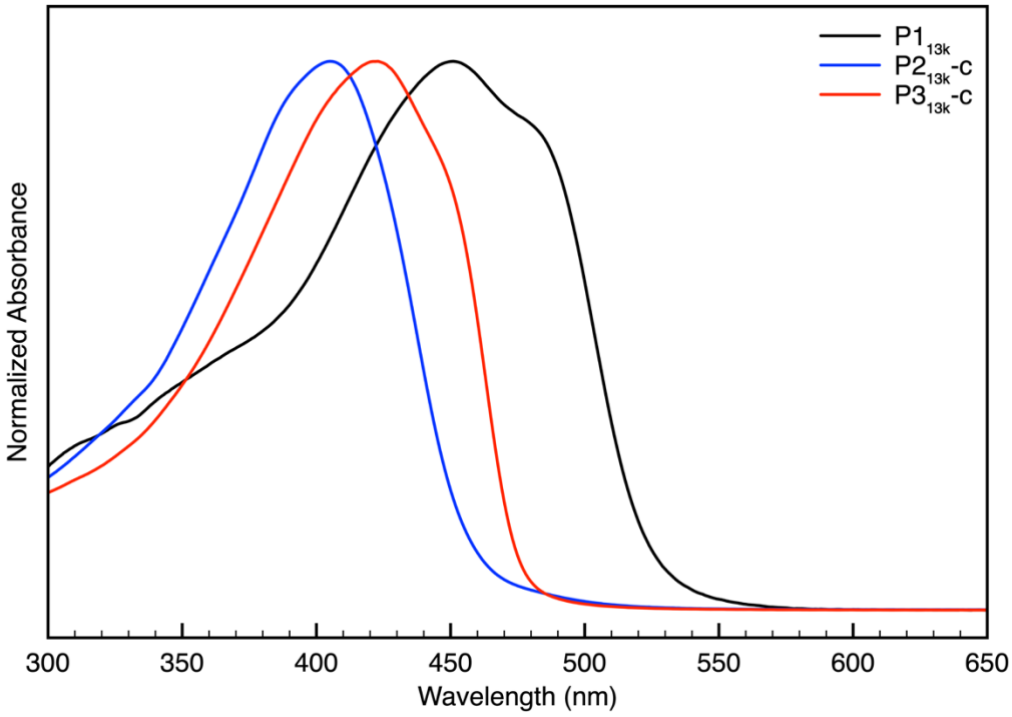

Figure S33. UV-Vis absorption spectrum overlay of **P1$_{13k}$**, **P2$_{13k}$-c**, and **P3$_{13k}$-c** in THF.

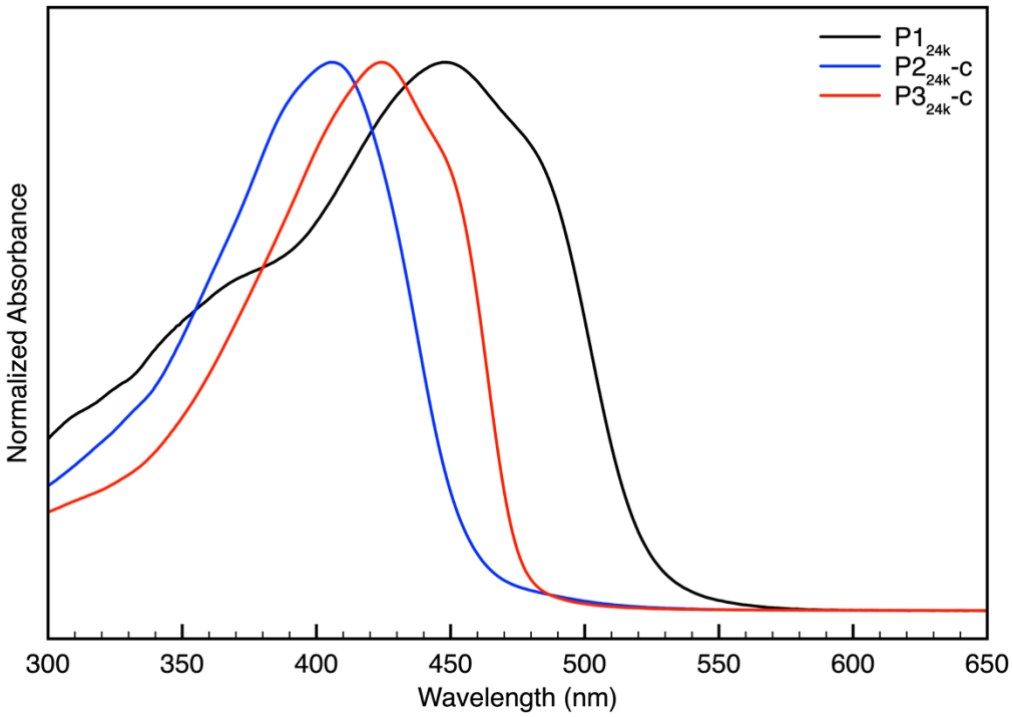

Figure S34. UV-Vis absorption spectrum overlay of **P1$_{24k}$**, **P2$_{24k}$-c**, and **P3$_{24k}$-c** in THF.

Table S1. Tabulated values of hypsochromic and bathochromic shifts of polymers after undergoing the IEDDA reaction and oxidation and the respective λ_{max} values.

Polymer	λ_{max} (nm)	Polymer	λ_{max} (nm)	Shift (nm)	Polymer	λ_{max} (nm)	Shift (nm)
P1$_{13k}$	451	**P2$_{13k}$-a**	376	− 75	**P3$_{13k}$-a**	415	+ 39
P1$_{24k}$	447	**P2$_{24k}$-a**	375	− 72	**P3$_{24k}$-a**	418	+ 43
		P2$_{13k}$-b	402	− 49	**P3$_{13k}$-b**	422	+ 20
		P2$_{24k}$-b	405	− 42	**P3$_{24k}$-b**	425	+ 20
		P2$_{13k}$-c	405	− 46	**P3$_{13k}$-c**	423	+ 18
		P2$_{24k}$-c	405	− 42	**P3$_{24k}$-c**	424	+ 19

Fluorescence Spectra

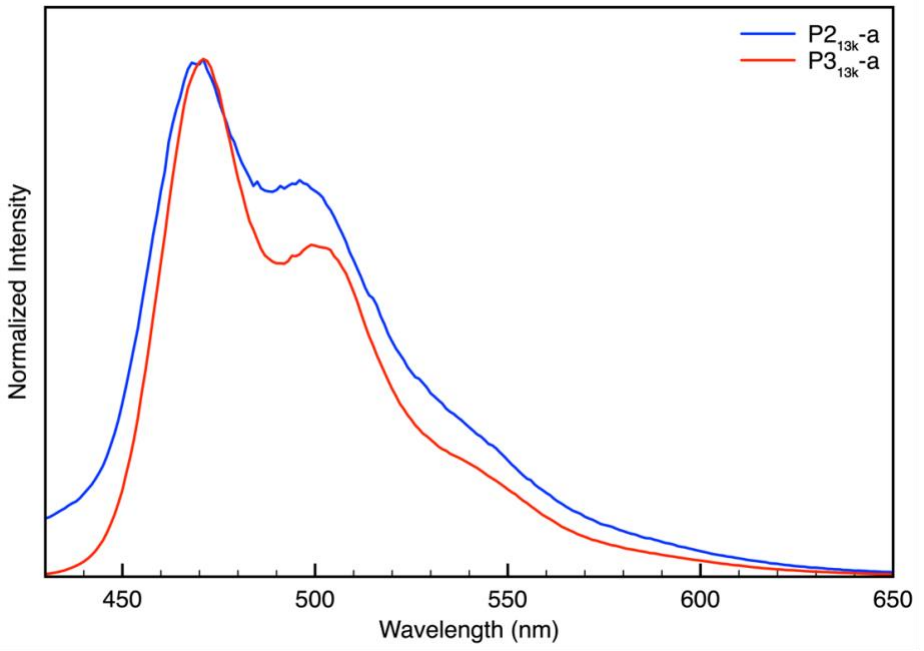

Figure S35. Fluorescence emission spectrum overlay of **P2$_{13k}$-a**, and **P3$_{13k}$-a** in THF excited at 400 and 420 nm, respectively.

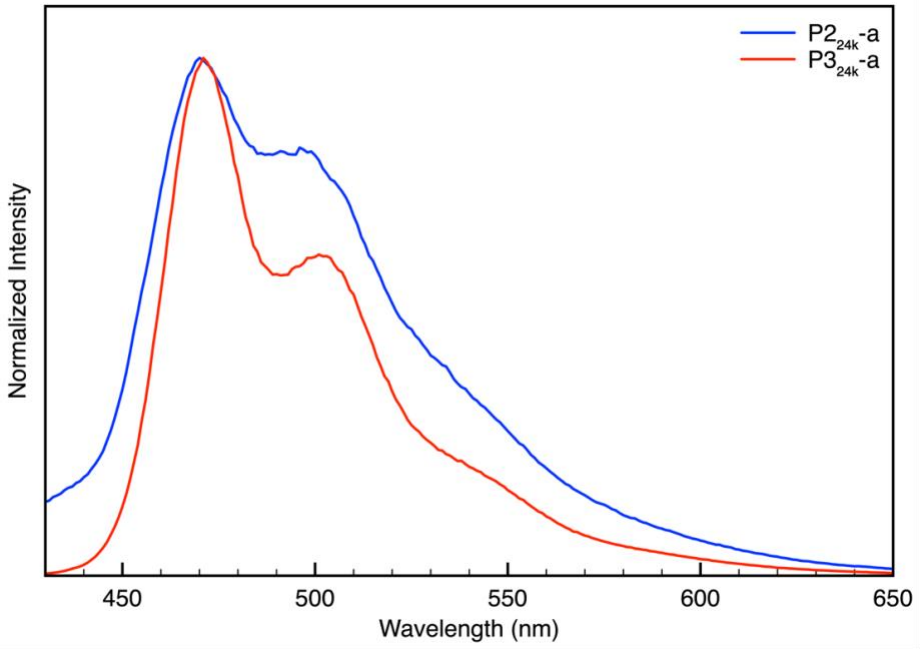

Figure S36. Fluorescence emission spectrum overlay of **P2$_{24k}$-a**, and **P3$_{24k}$-a** in THF excited at 400 and 420 nm, respectively.

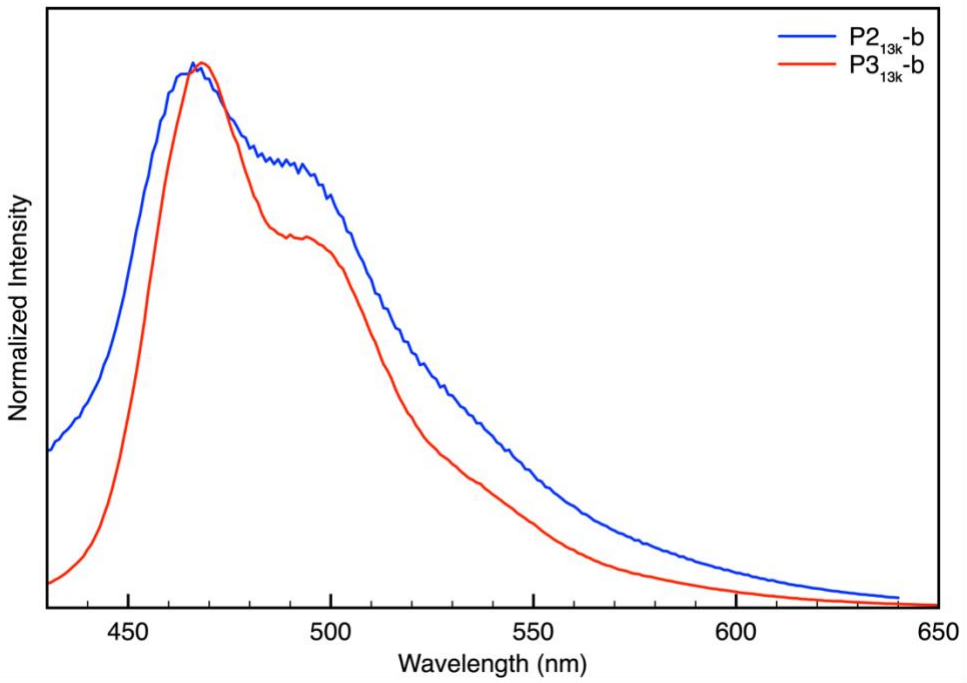

Figure S37. Fluorescence emission spectrum overlay of **P2$_{13k}$-b**, and **P3$_{13k}$-b** in THF excited at 400 and 420 nm, respectively.

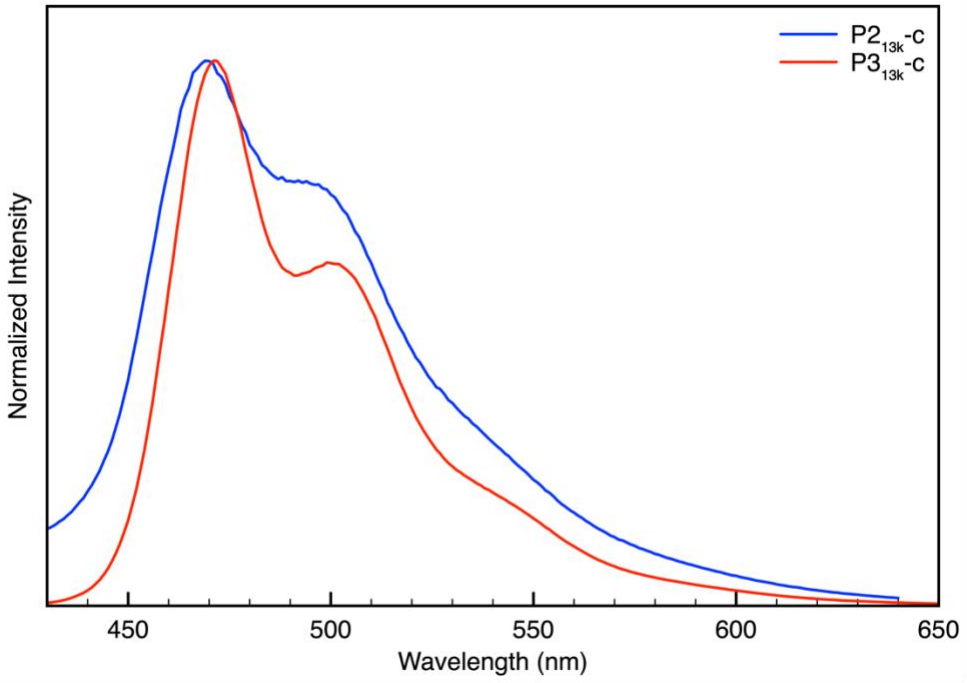

Figure S38. Fluorescence emission spectrum overlay of **P2$_{13k}$-c**, and **P3$_{13k}$-c** in THF excited at 400 and 420 nm, respectively.

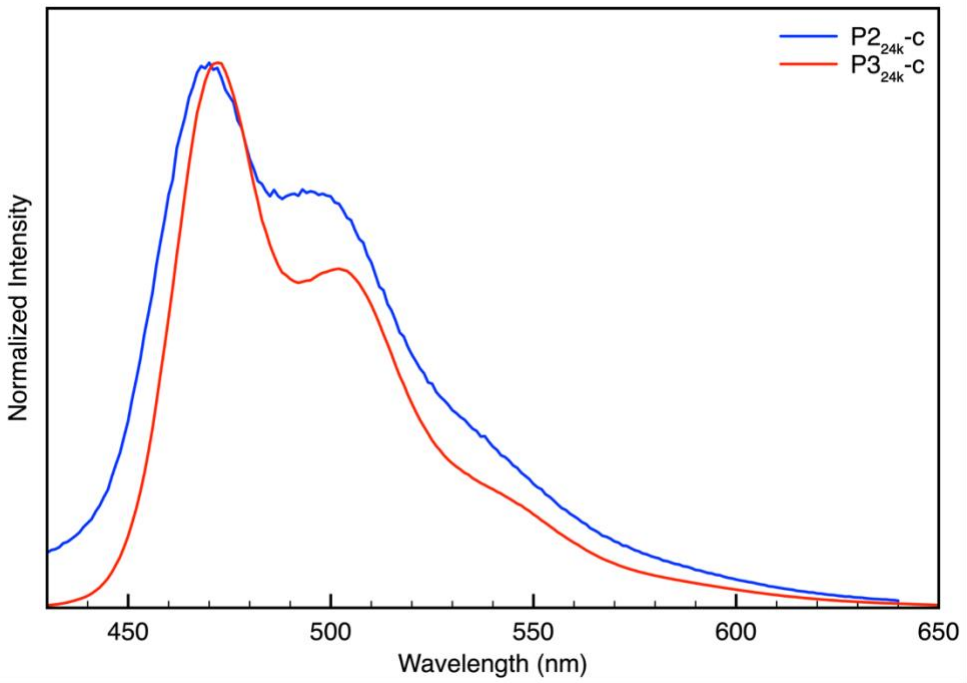

Figure S39. Fluorescence emission spectrum overlay of **P2$_{24k}$-c**, and **P3$_{24k}$-c** in THF excited at 400 and 420 nm, respectively.

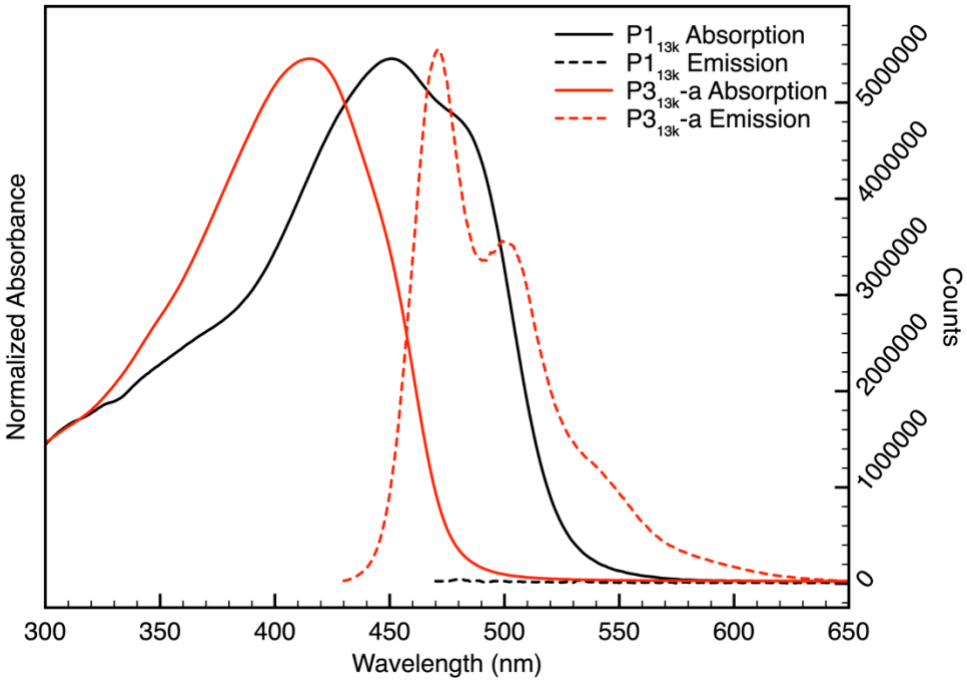

Figure S40. UV-Vis absorption and fluorescence emission spectra overlay of **P1$_{13k}$**, and **P3$_{13k}$-a** in THF excited at 450 and 420 nm, respectively.

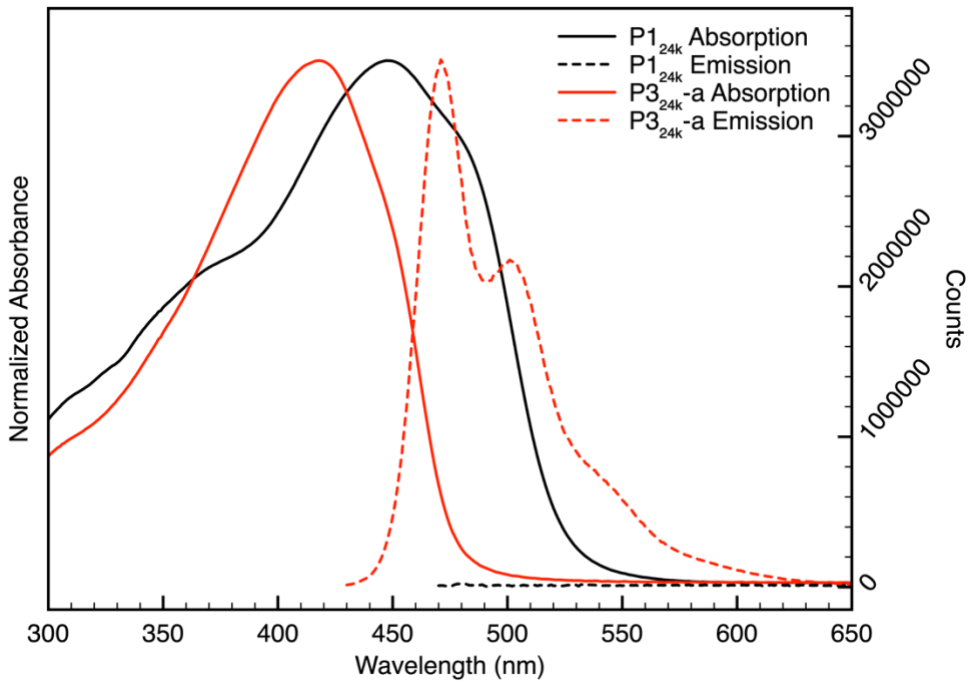

Figure S41. UV-Vis absorption and fluorescence emission spectra overlay of **P1$_{24k}$**, and **P3$_{24k}$-a** in THF excited at 450 and 420 nm, respectively.

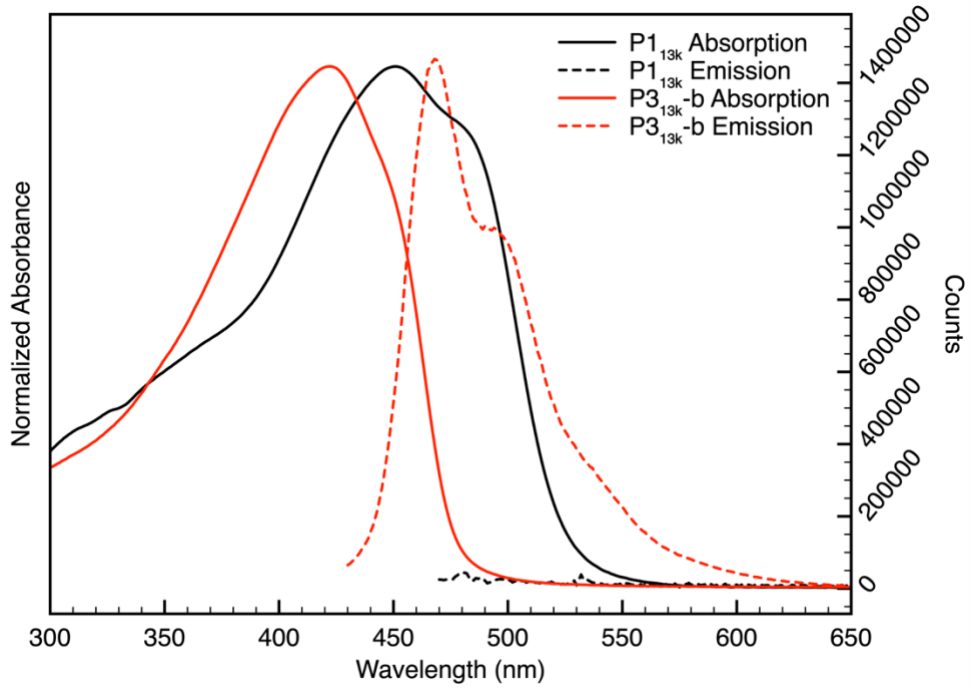

Figure S42. UV-Vis absorption and fluorescence emission spectra overlay of **P1$_{13k}$**, and **P3$_{13k}$-b** in THF excited at 450 and 420 nm, respectively.

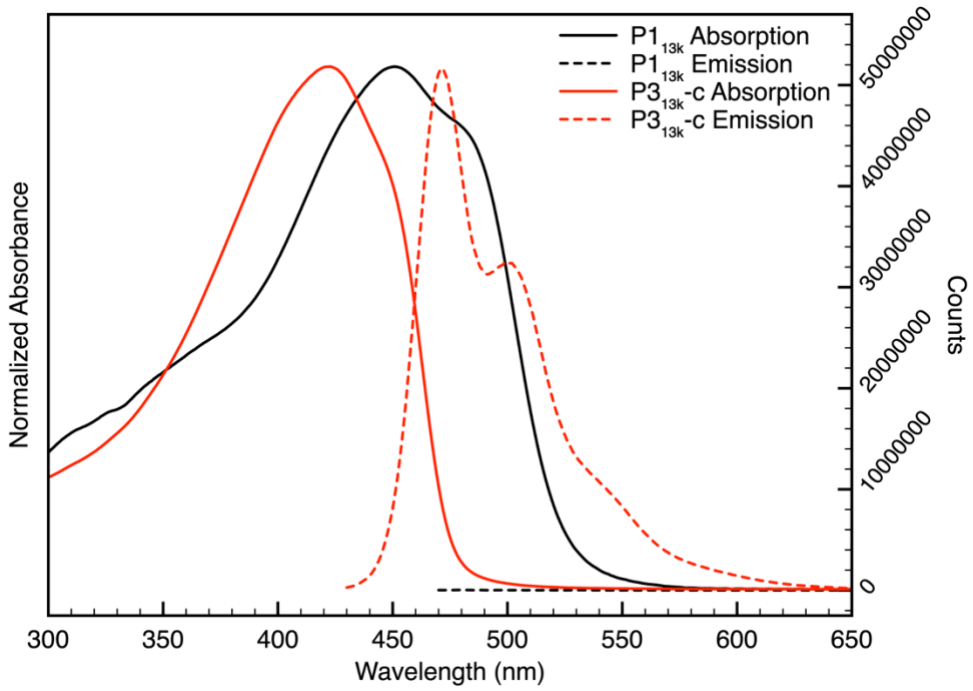

Figure S43. UV-Vis absorption and fluorescence emission spectra overlay of **P1$_{13k}$**, and **P3$_{13k}$-c** in THF excited at 450 and 420 nm, respectively.

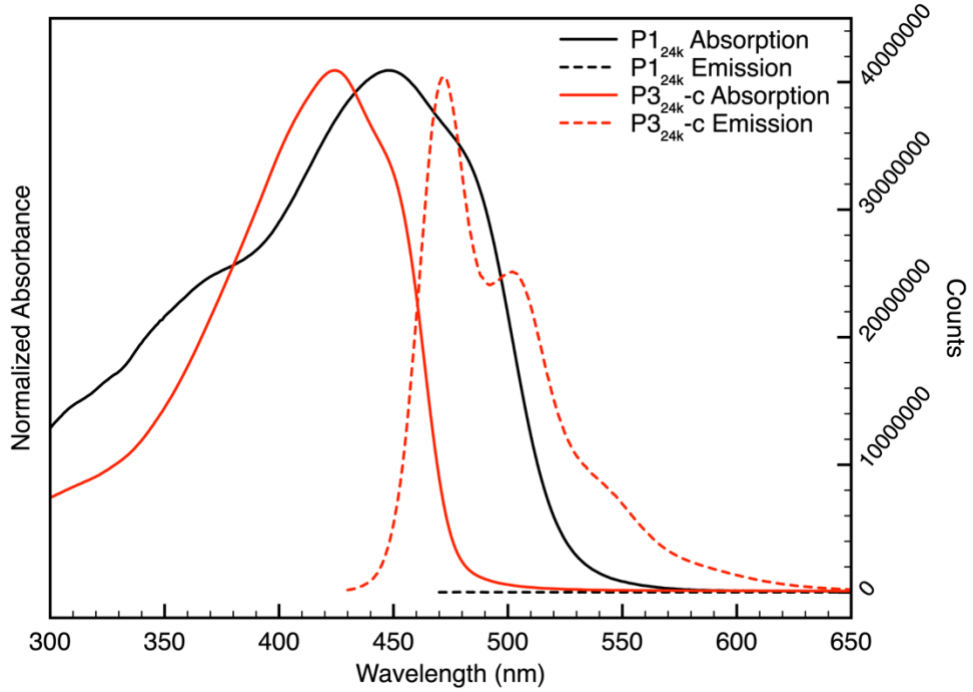

Figure S44. UV-Vis absorption and fluorescence emission spectra overlay of **P1$_{24k}$**, and **P3$_{24k}$-c** in THF excited at 450 and 420 nm, respectively.

GPC traces

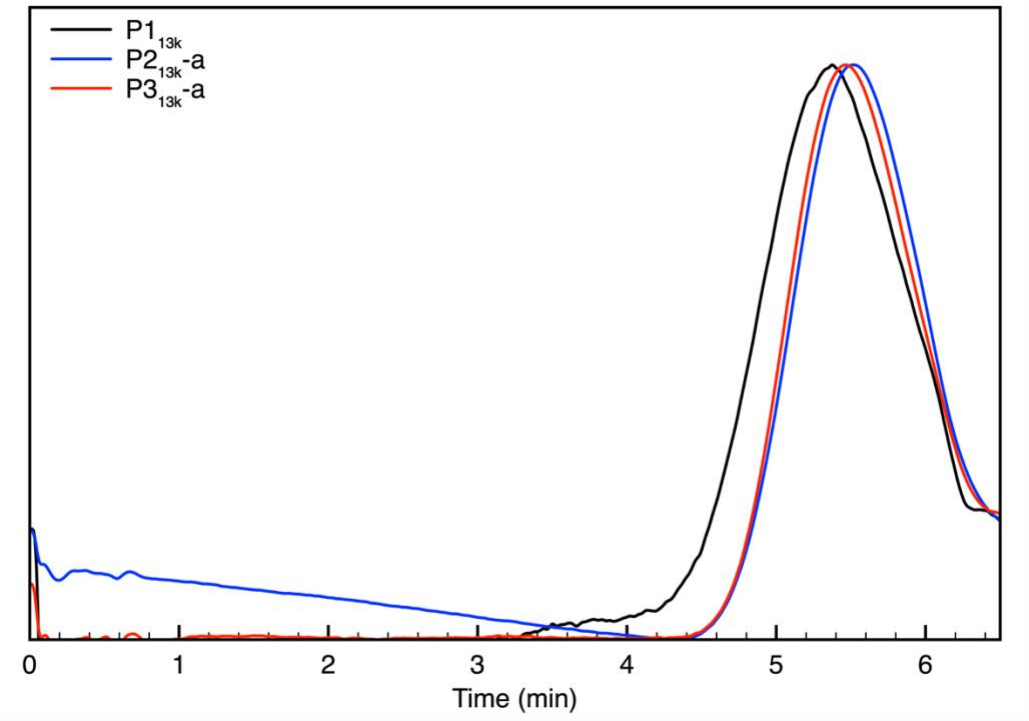

Figure S45. GPC trace overlay of **P1$_{13k}$, P2$_{13k}$-a**, and **P3$_{13k}$-a**.

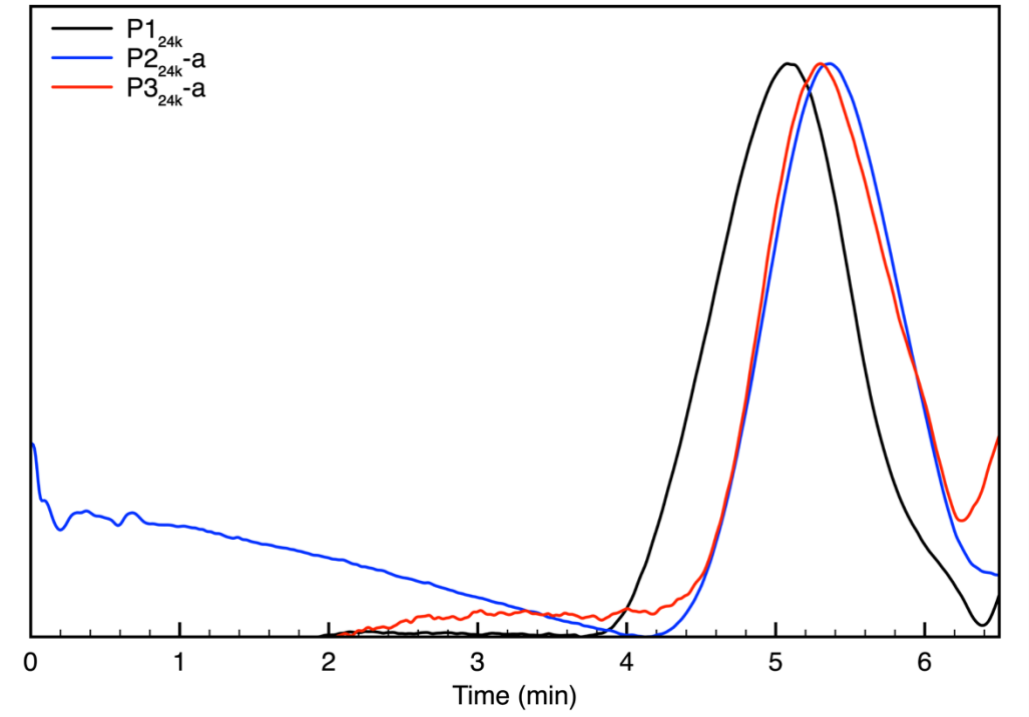

Figure S46. GPC trace overlay of **P1$_{24k}$, P2$_{24k}$-a**, and **P3$_{24k}$-a**.

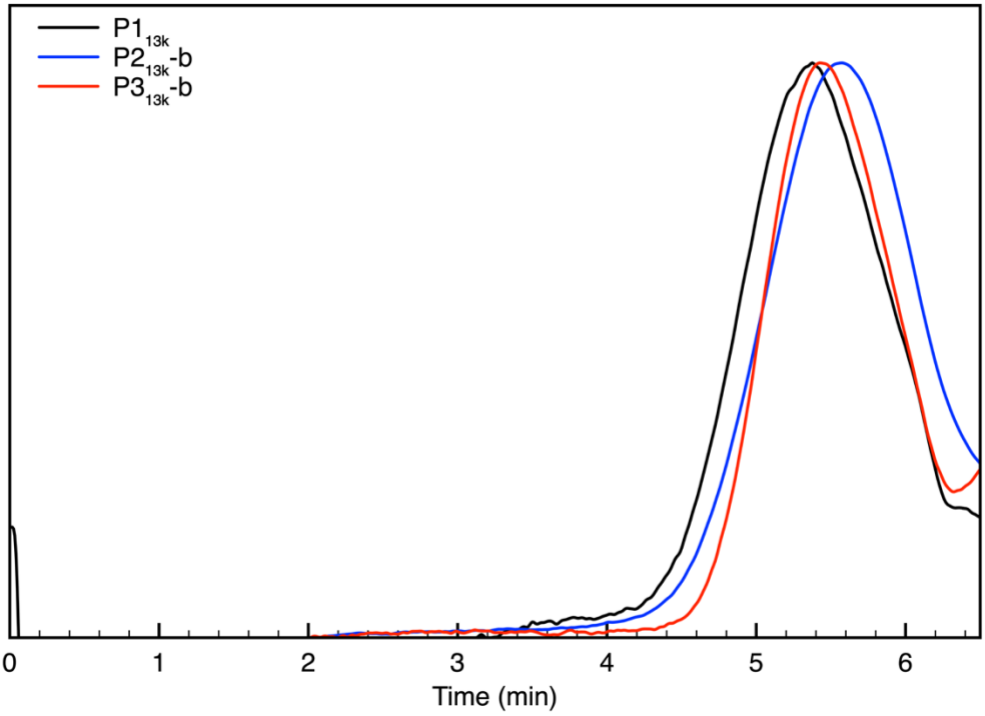

Figure S47. GPC trace overlay of **P1$_{13k}$, P2$_{13k}$-b**, and **P3$_{13k}$-b**.

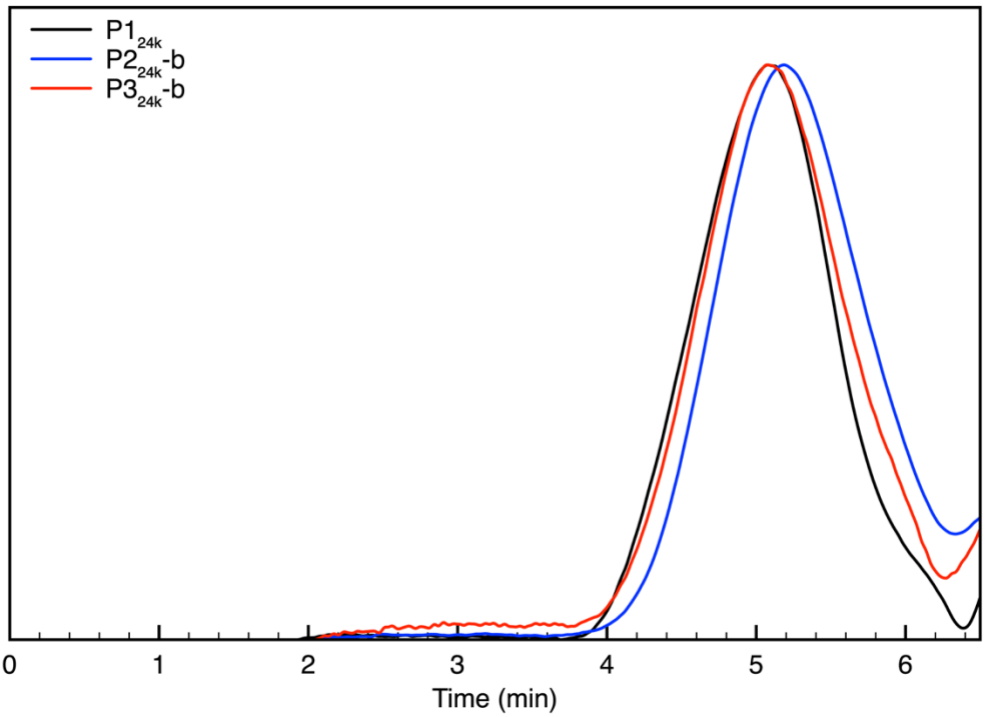

Figure S48. GPC trace overlay of **P1$_{24k}$, P2$_{24k}$-b**, and **P3$_{24k}$-b**.

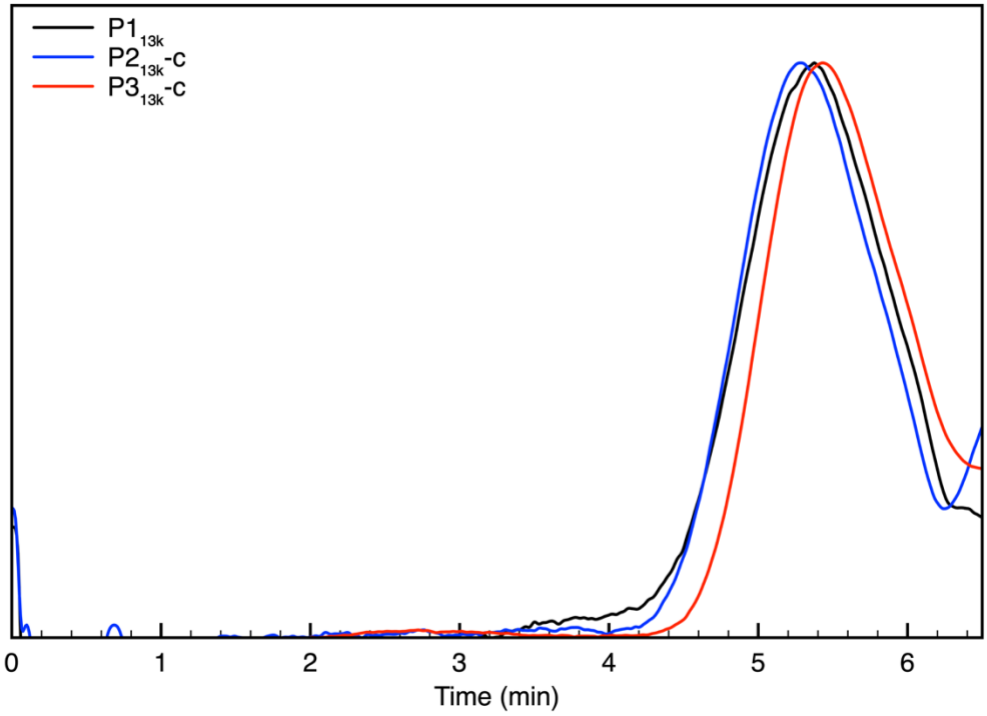

Figure S49. GPC trace overlay of **P1$_{13k}$, P2$_{13k}$-c**, and **P3$_{13k}$-c**.

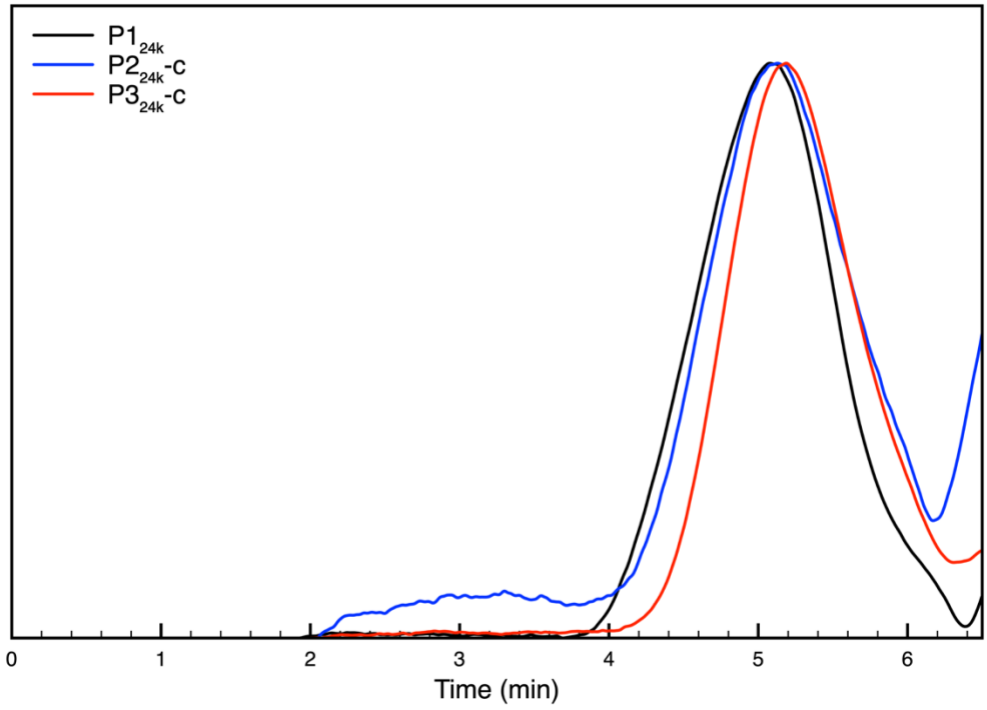

Figure S50. GPC trace overlay of **P1$_{24k}$, P2$_{24k}$-c**, and **P3$_{24k}$-c**.

Table S2. Tabulated values of polymer molecular weights calculated by NMR and analyzed by GPC.

	DP	NMR M_n (kDa)	GPC M_n (kDa)	GPC M_w (kDa)	$Đ$
$P1_{13k}$	28	22.9	13.0	38.0	2.5
$P2_{13k}$-a	26	24.2	6.6	18.8	2.8
$P3_{13k}$-a	33	30.0	7.0	20.0	2.9
$P2_{13k}$-b	27	32.0	13.1	28.1	2.8
$P3_{13k}$-b	27	31.9	12.0	22.9	1.9
$P2_{13k}$-c	32	35.8	16.3	36.6	2.2
$P3_{13k}$-c	35	39.2	7.2	22.1	3.1
$P1_{24k}$	56	46.4	23.7	81.8	3.4
$P2_{24k}$-a	59	54.2	10.0	30.8	3.1
$P3_{24k}$-a	64	58.6	15.6	32.2	2.1
$P2_{24k}$-b	62	73.8	23.8	68.4	2.7
$P3_{24k}$-b	55	65.4	23.3	72.3	3.1
$P2_{24k}$-c	56	62.3	23.2	61.7	2.7
$P3_{24k}$-c	57	63.2	19.1	45.1	2.4

FTIR Spectra

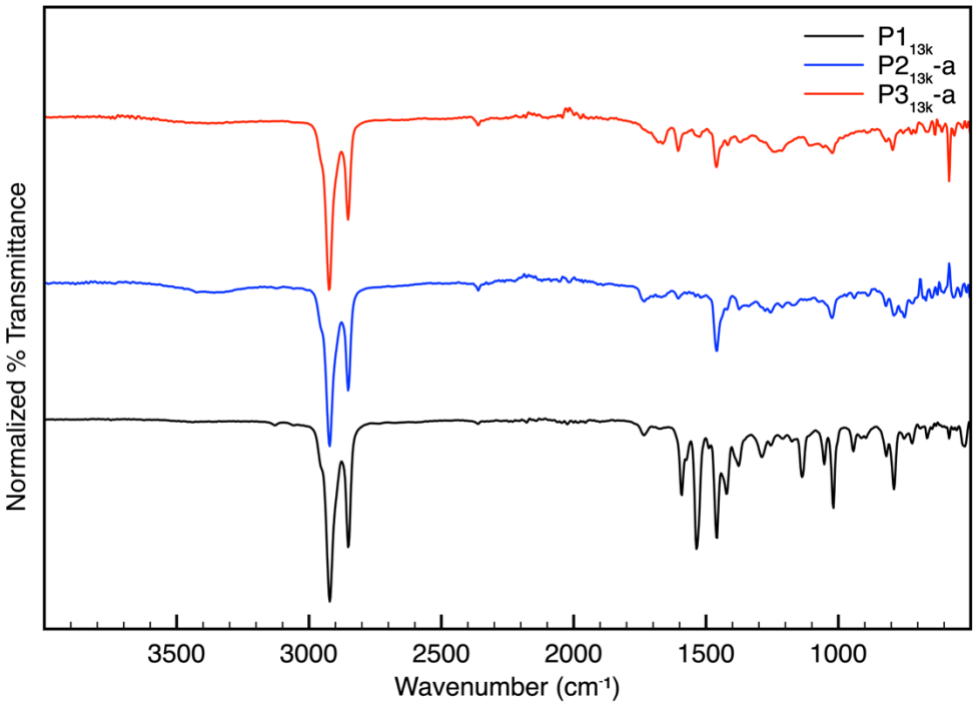

Figure S51. FTIR spectrum overlay of **P1$_{13k}$**, **P2$_{13k}$-a**, and **P3$_{13k}$-a**.

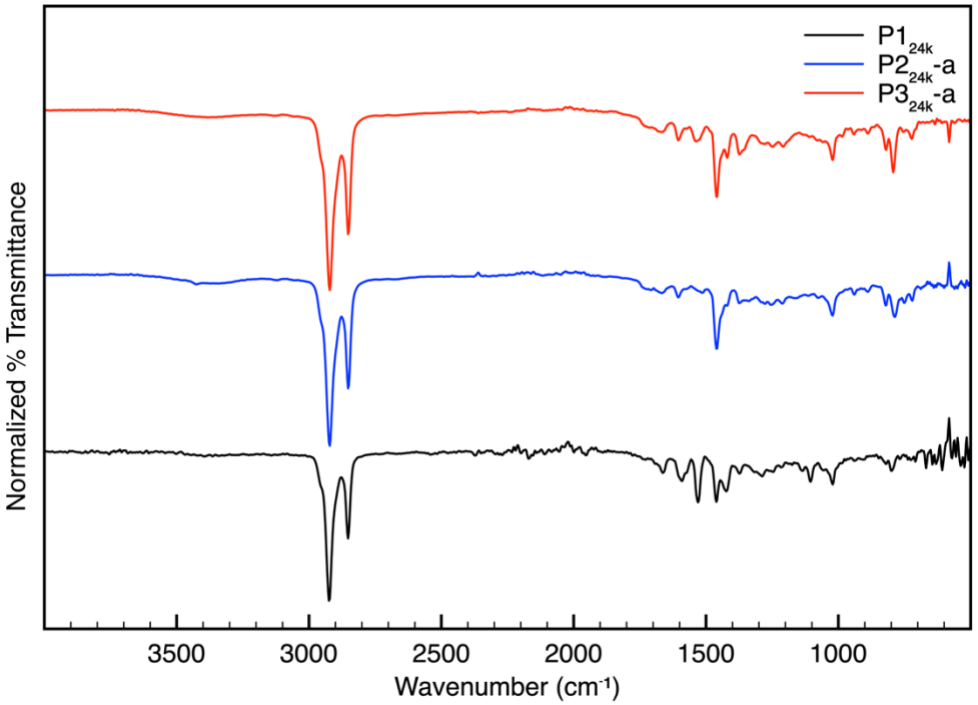

Figure S52. FTIR spectrum overlay of **P1$_{24k}$**, **P2$_{24k}$-a**, and **P3$_{24k}$-a**.

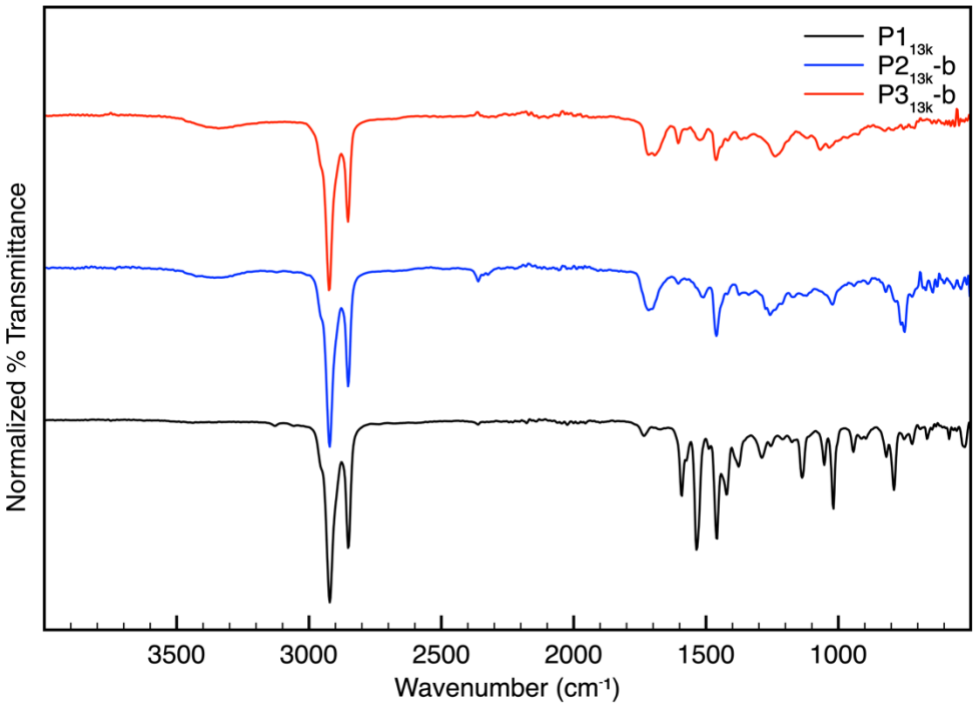

Figure S53. FTIR spectrum overlay of **P1$_{13k}$**, **P2$_{13k}$-b**, and **P3$_{13k}$-b**.

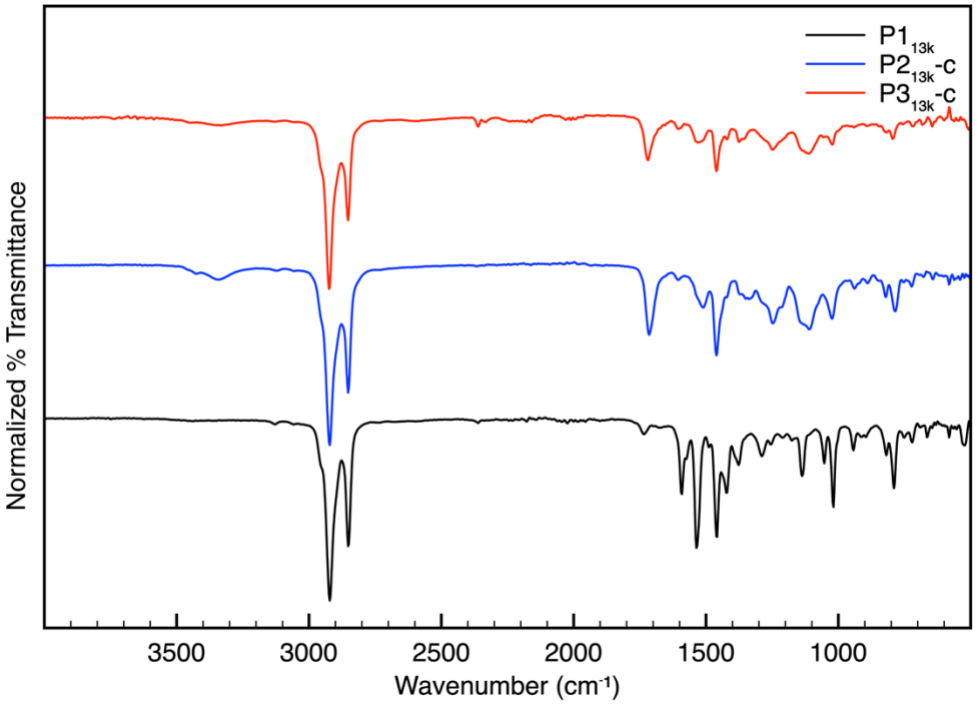

Figure S54. FTIR spectrum overlay of **P1$_{13k}$**, **P2$_{13k}$-c**, and **P3$_{13k}$-c**.

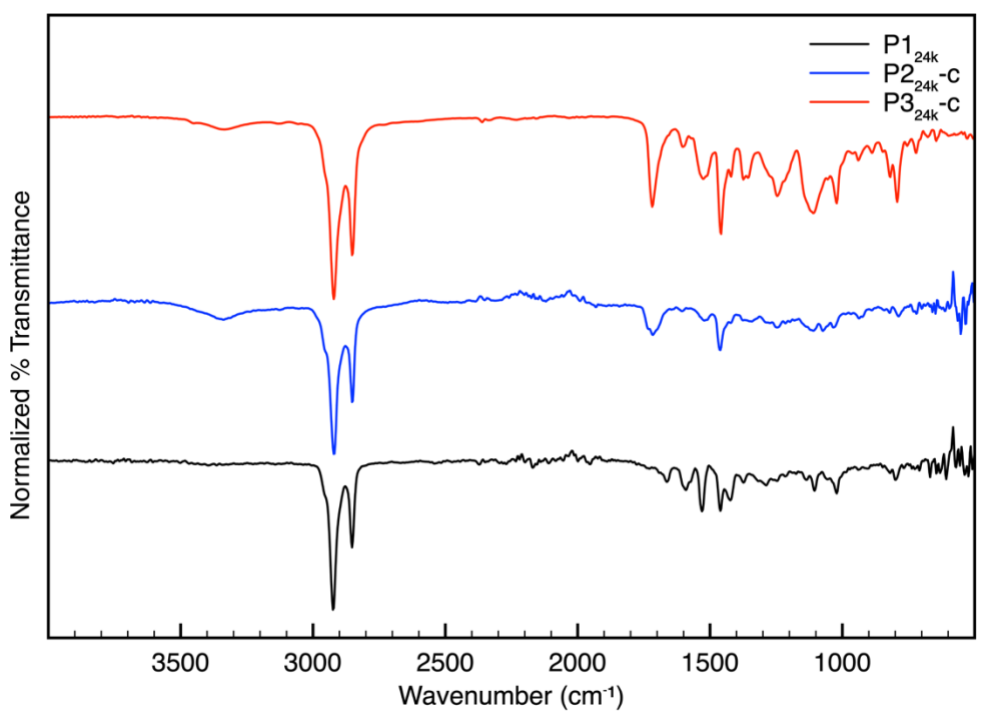

Figure S55. FTIR spectrum overlay of **P1$_{24k}$**, **P2$_{24k}$-c**, and **P3$_{24k}$-c**.

TGA Thermograms

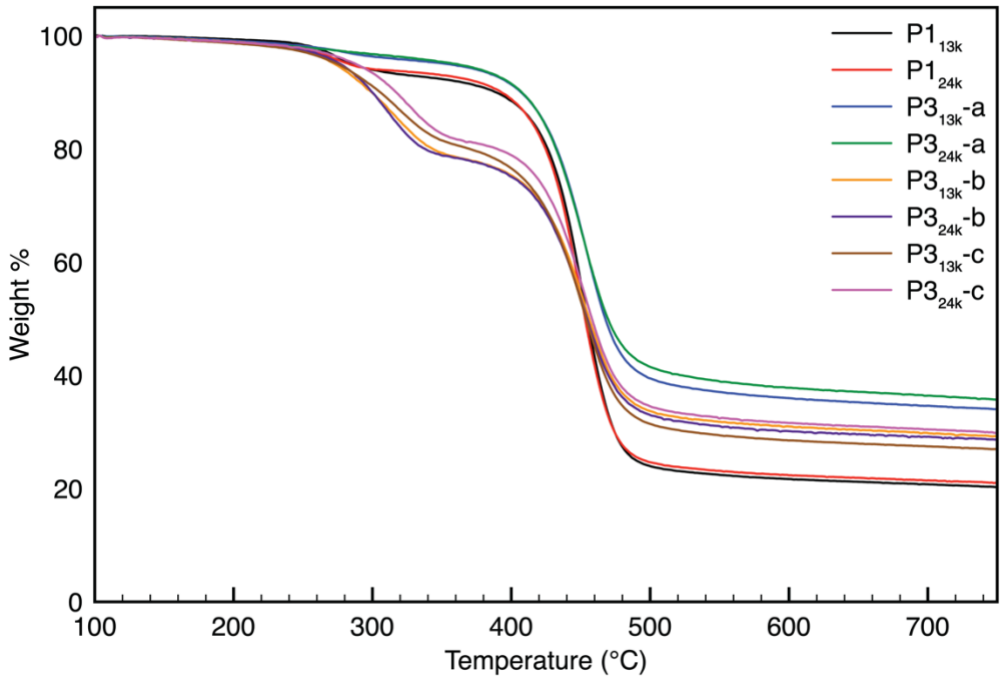

Figure S56. TGA thermogram overlay of **P1$_{13k}$**, **P1$_{24k}$**, **P3$_{13k}$-a**, **P3$_{24k}$-a**, **P3$_{13k}$-b**, **P3$_{24k}$-b**, **P3$_{13k}$-c**, and **P3$_{24k}$-c**.

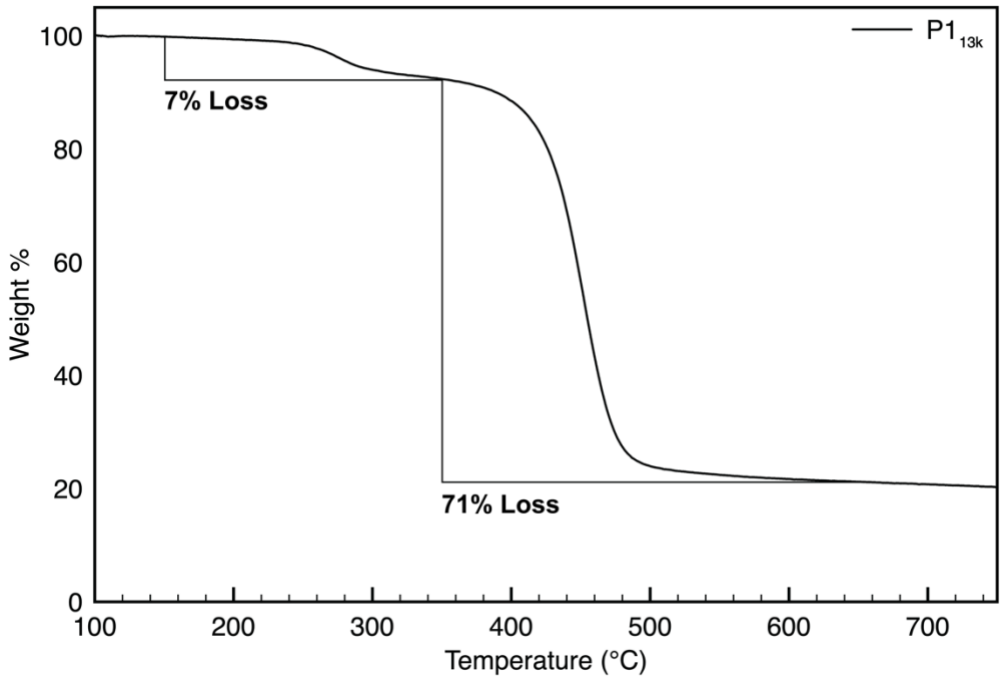

Figure S57. TGA thermogram of **P1$_{13k}$**.

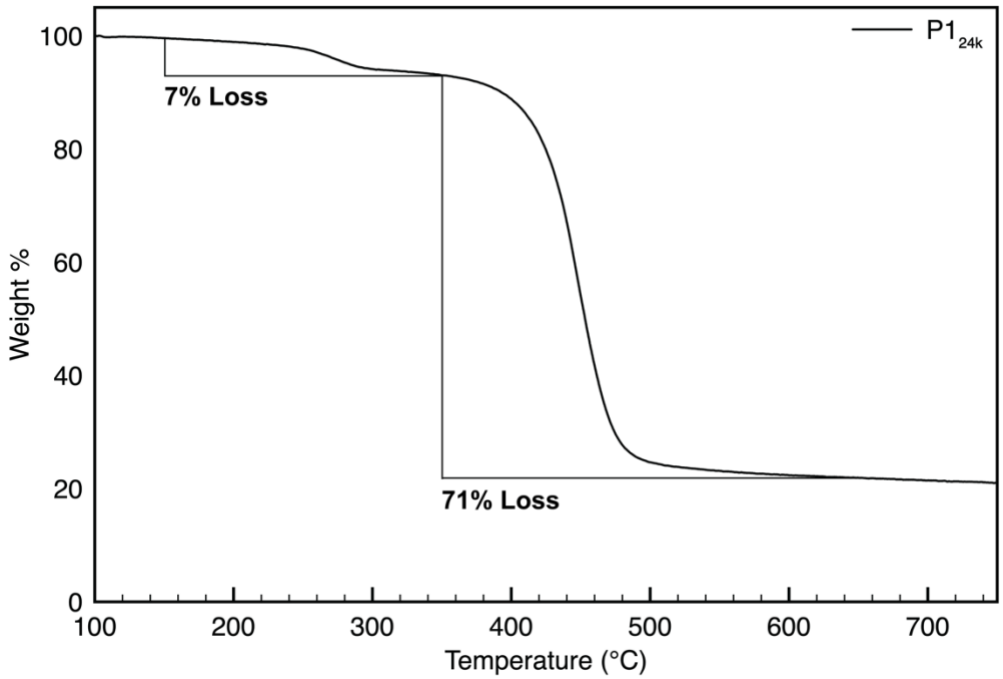

Figure S58. TGA thermogram of **P1$_{24k}$**.

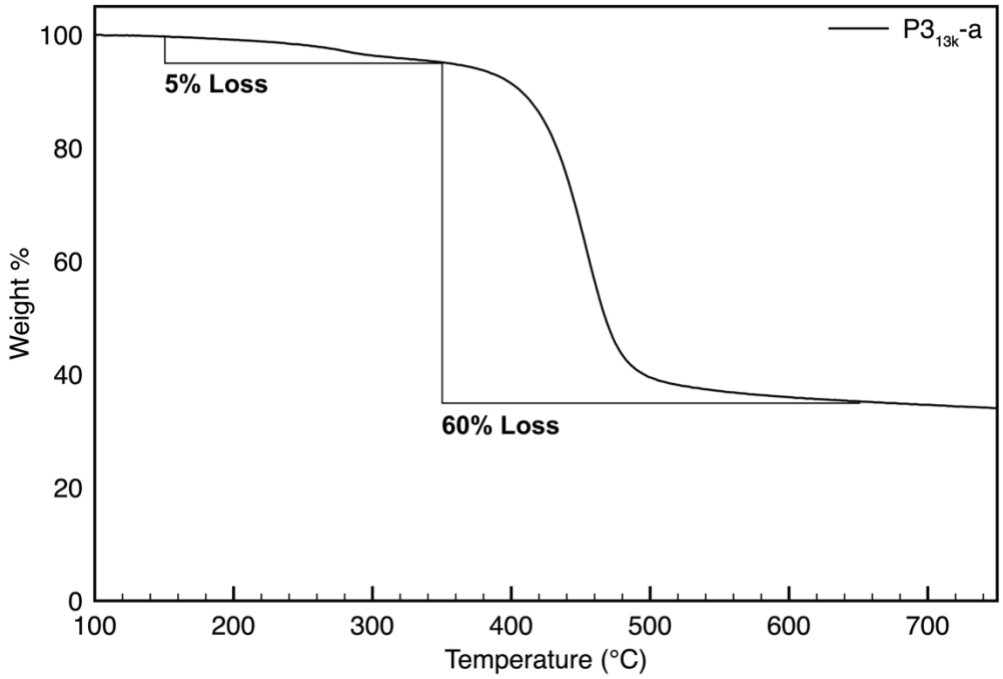

Figure S59. TGA thermogram of **P3$_{13k}$-a**.

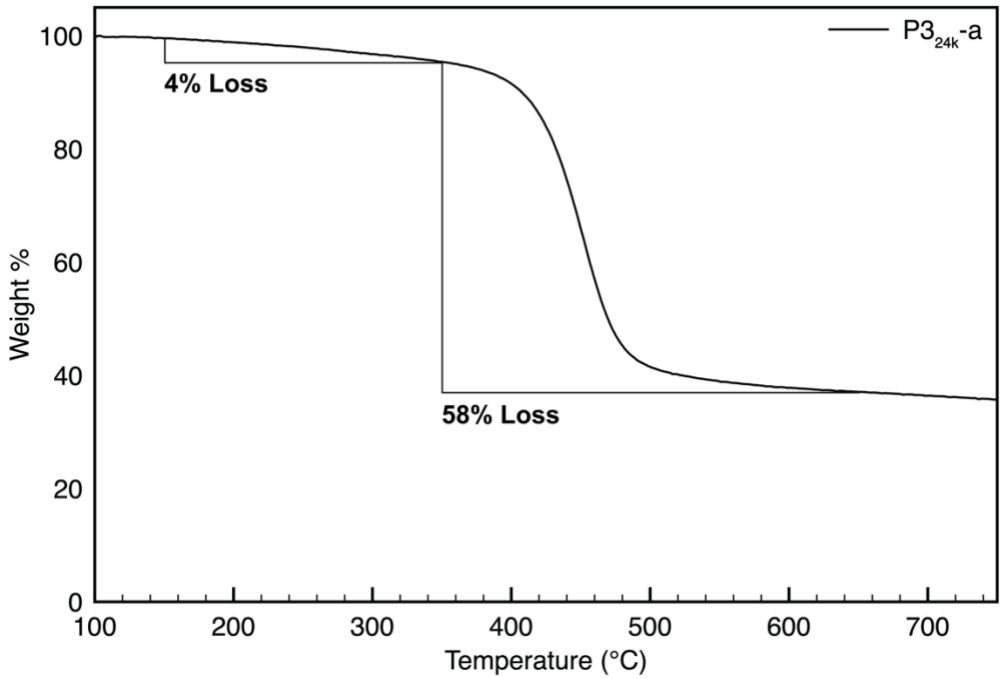

Figure S60. TGA thermogram of **P3$_{24k}$-a**.

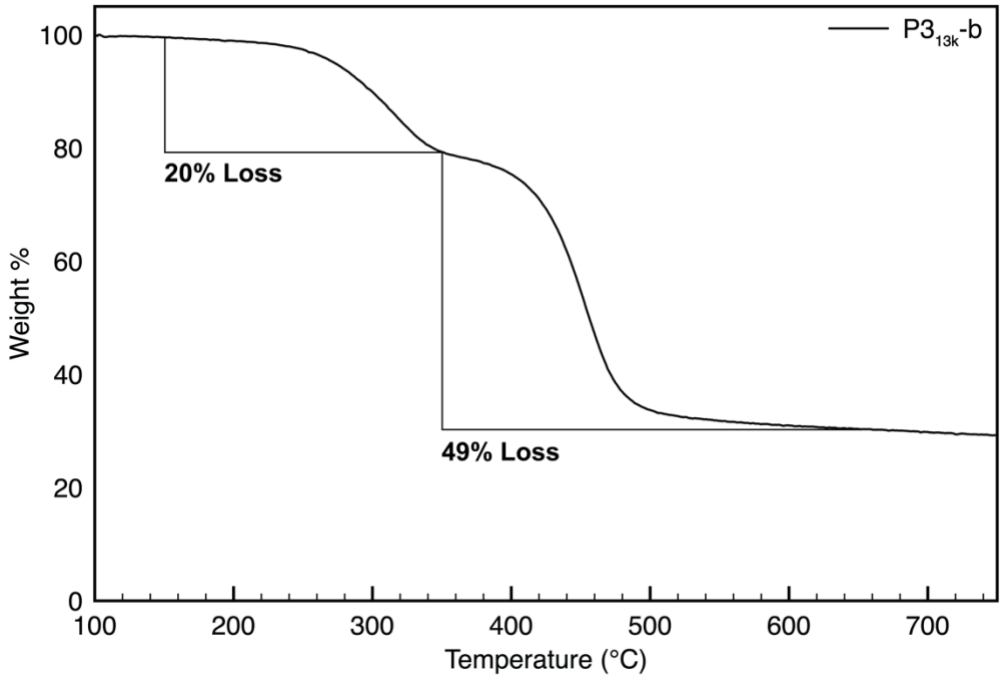

Figure S61. TGA thermogram of **P3$_{13k}$-b**.

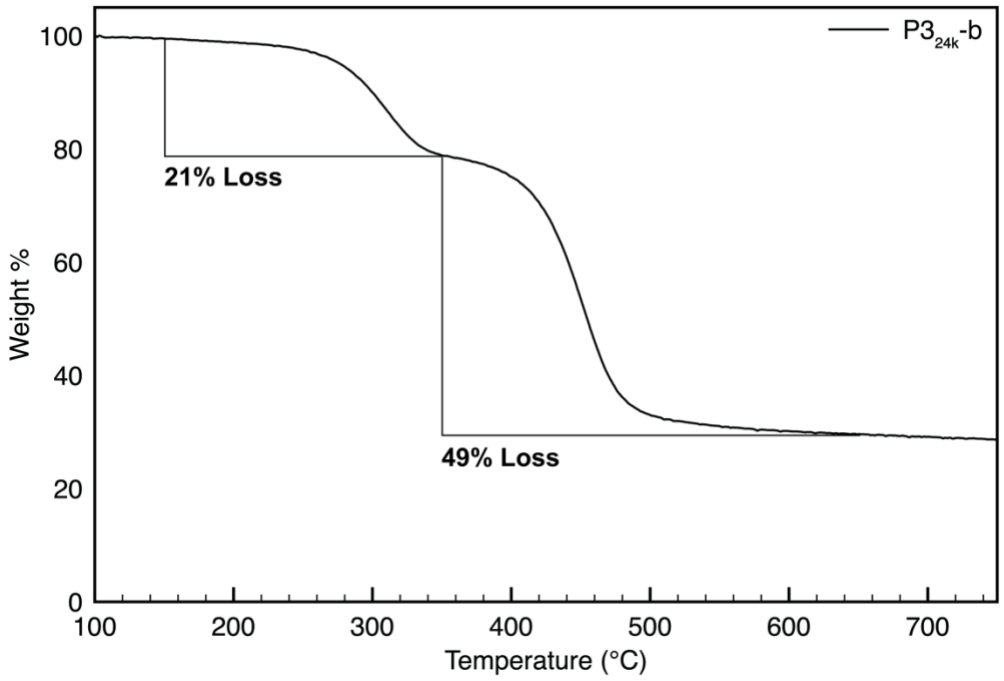

Figure S62. TGA thermogram of **P3$_{24k}$-b**.

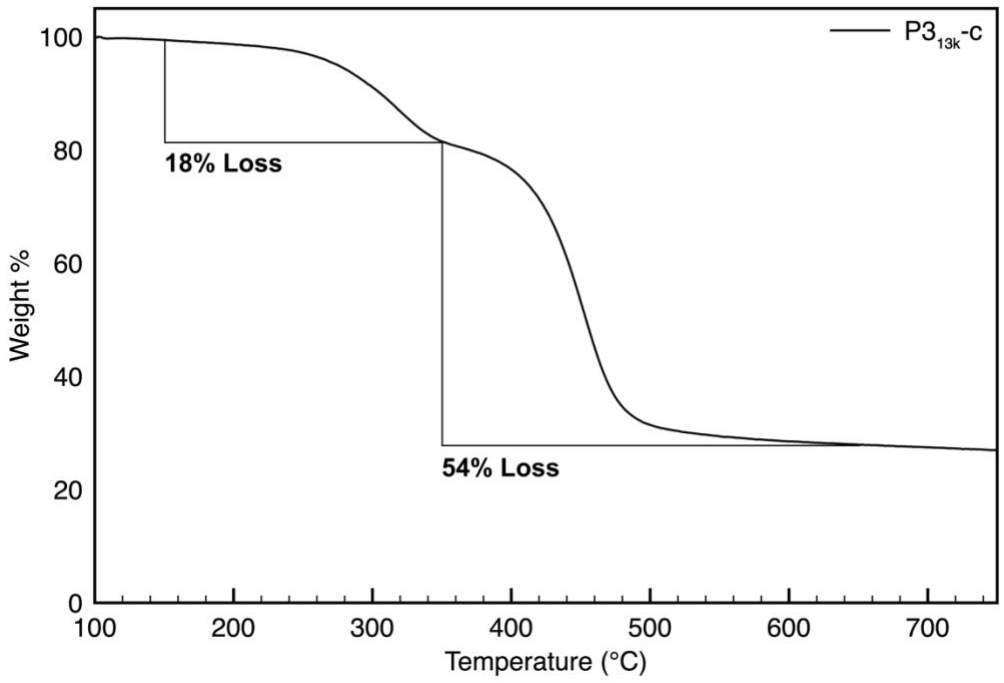

Figure S63. TGA thermogram of **P3$_{13k}$-c**.

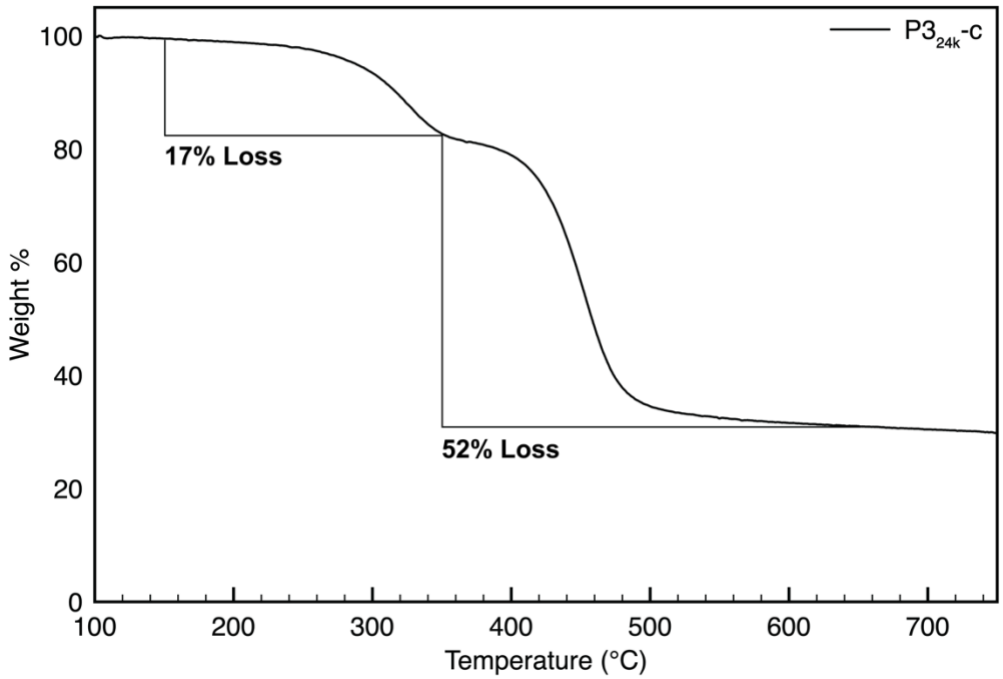

Figure S64. TGA thermogram of **P3$_{24k}$-c**.

General Procedure for Preparing Polymer-SWNT Dispersion Samples

The dispersion samples were prepared following literature precedence.[257] The respective polymer (7.5 mg) and 10 wt% HiPco SWNT in ethanol (50 mg) were added to a 20 mL scintillation vial with tetrahydrofuran (10 mL). The mixture was sonicated using a probe sonicator for 30 min. The resulting black suspension was 8346× *g* for 30 min and the supernatant was carefully isolated and passed through a cotton filter. Excess polymer in the dispersion was removed by passing the solution through a 0.2 µm pore diameter Teflon membrane and rinsing with tetrahydrofuran until the filtrate contained no color or fluorescence when excited with a hand-held 365 nm UV lamp. The thin film leftover on the membrane was redispersed with tetrahydrofuran (10 mL) and characterized by PL mapping, AFM, UV-Vis-NIR, and Raman spectroscopy.

UV-Vis-NIR Spectra

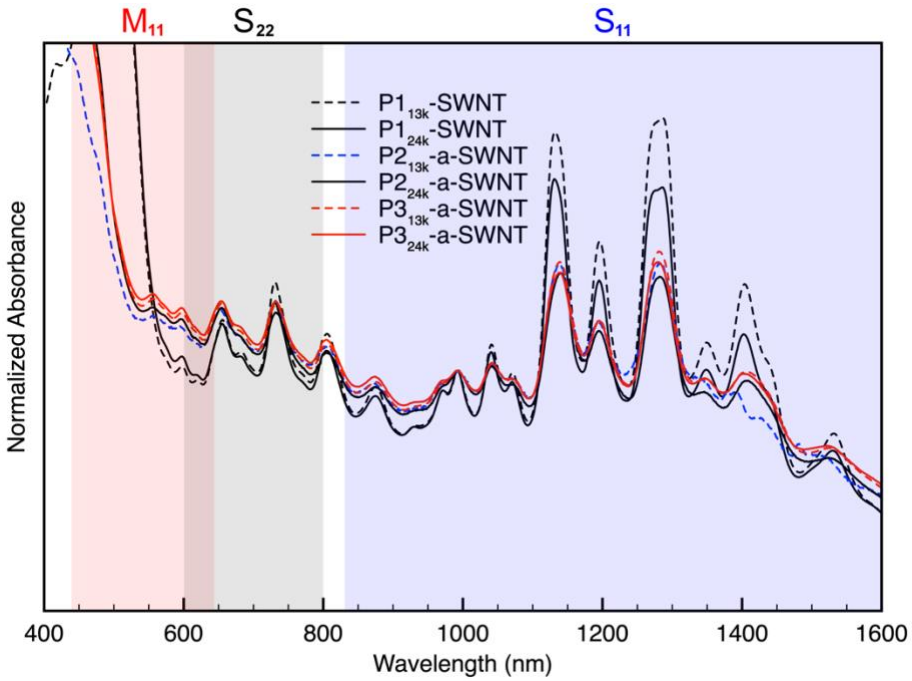

Figure S65. UV-Vis-NIR absorption spectrum overlay of normalized **P1$_{13k}$-SWNT**, **P1$_{24k}$-SWNT**, **P2$_{13k}$-SWNT-a**, **P2$_{24k}$-SWNT-a**, **P3$_{13k}$-SWNT-a**, **P3$_{24k}$-SWNT-a** data.

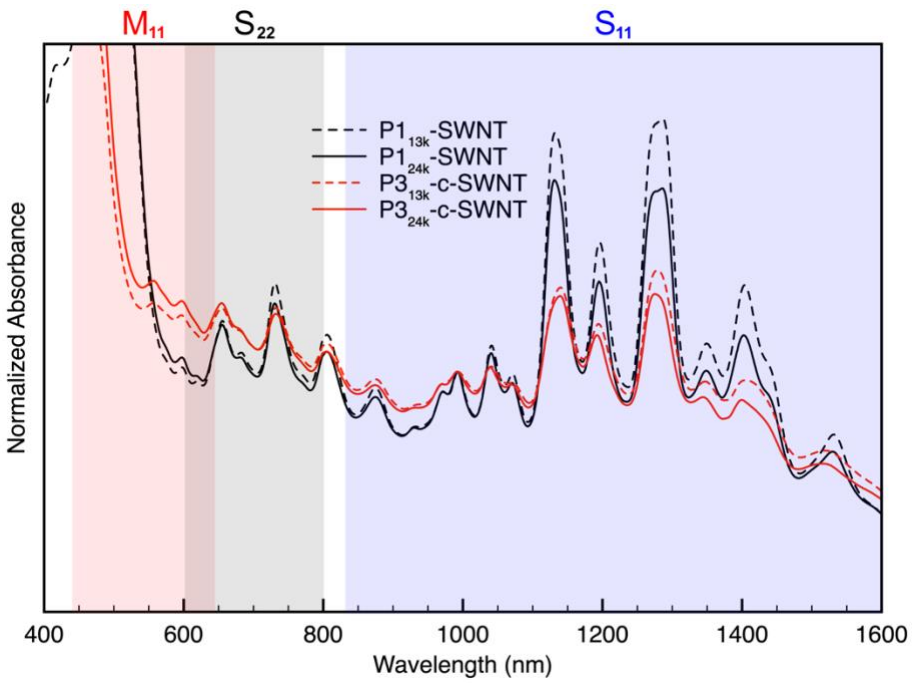

Figure S66. UV-Vis-NIR absorption spectrum overlay of normalized **P1$_{13k}$-SWNT**, **P1$_{24k}$-SWNT**, **P3$_{13k}$-SWNT-c**, **P3$_{24k}$-SWNT-c** data.

Images of Polymer-SWNT Dispersions

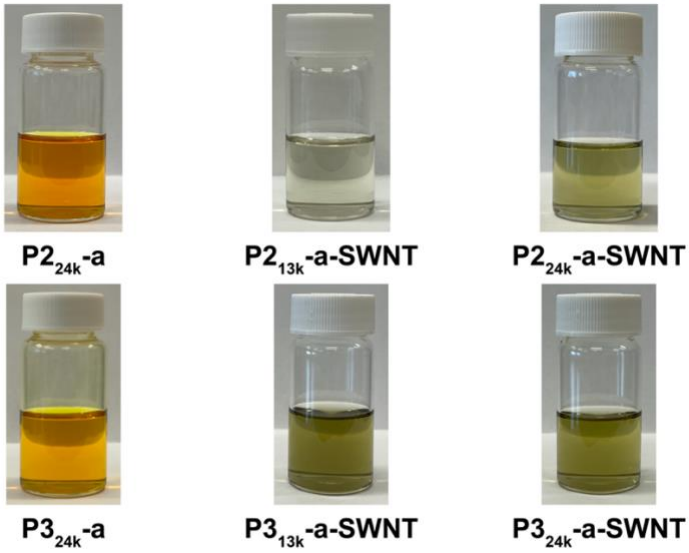

Figure S67. Image of the hydroxyl-containing 24 kDa polymers in THF and the resulting dispersions.

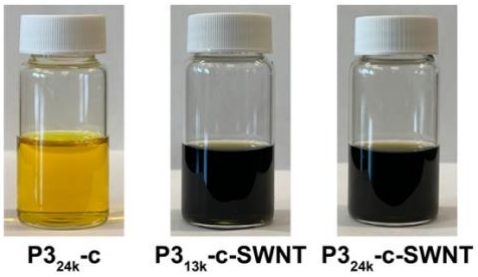

Figure S68. Image of the TEG-containing 24 kDa polymers in THF and the resulting dispersions.

Raman Spectra

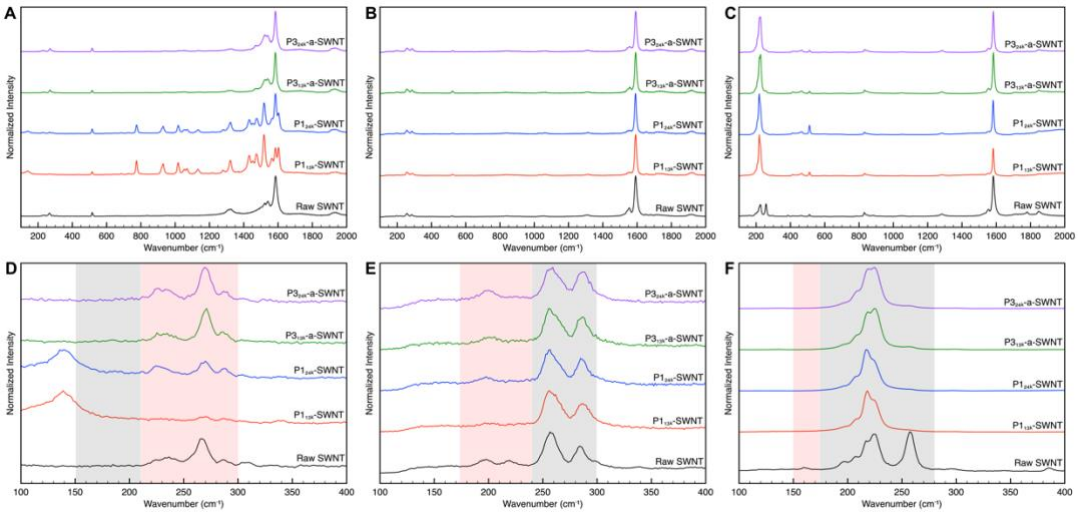

Figure S69. Full Raman spectra of raw SWNTs (black), **P1$_{13k}$-SWNT** (red), **P1$_{24k}$-SWNT** (blue), **P3$_{13k}$-a-SWNT** (green), **P3$_{24k}$-a-SWNT** (purple) at A) λ_{ex} = 532 nm B) λ_{ex} = 633 nm, and C) λ_{ex} = 785 nm. The same spectra of the RBM region at D) λ_{ex} = 532 nm E) λ_{ex} = 633 nm, and F) λ_{ex} = 785 nm.

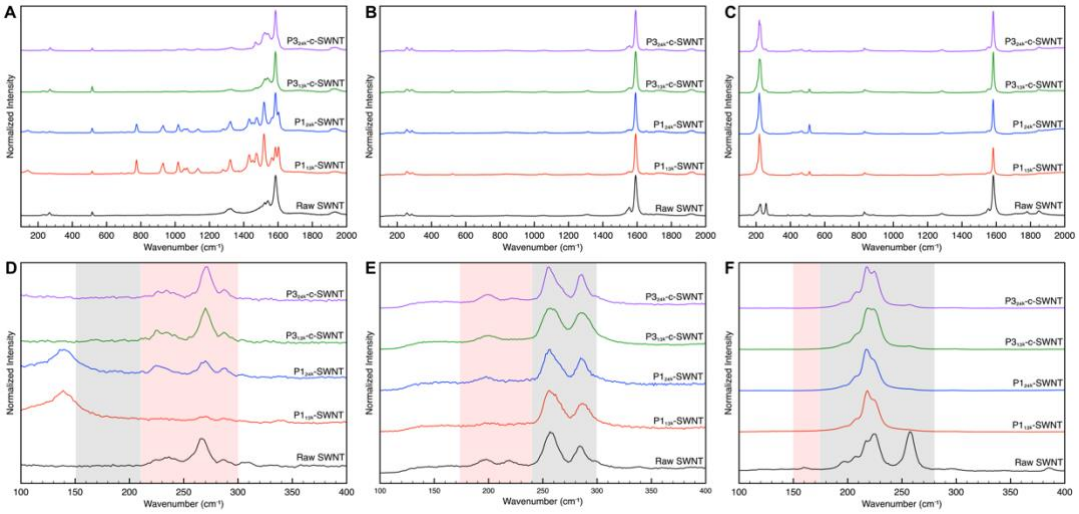

Figure S70. Full Raman spectra of raw SWNTs (black), **P1$_{13k}$-SWNT** (red), **P1$_{24k}$-SWNT** (blue), **P3$_{13k}$-c-SWNT** (green), **P3$_{24k}$-SWNT-c** (purple) at A) λ_{ex} = 532 nm B) λ_{ex} = 633 nm, and C) λ_{ex} = 785 nm. The same spectra of the RBM region at D) λ_{ex} = 532 nm E) λ_{ex} = 633 nm, and F) λ_{ex} = 785 nm.

AFM Images

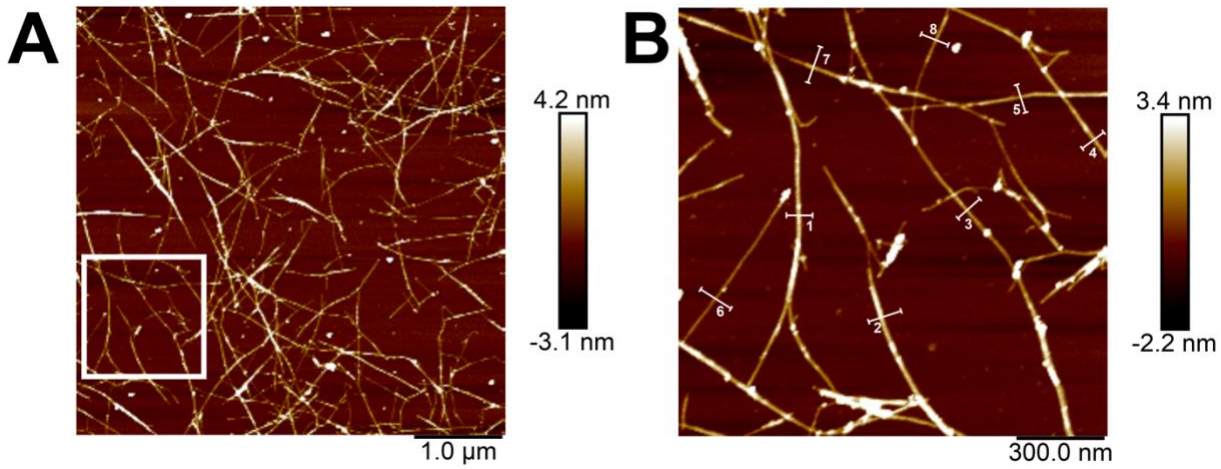

Figure S71. AFM images of **P1$_{13k}$-SWNT** at two magnifications, with the scale bar representing A) 1.0 µm and B) 300 nm. The white box denotes B.

Table S3. Height profiles across bisecting white lines of **P1$_{13k}$-SWNT** (Figure S71).

Index	Height (nm)
1	3.0258
2	3.2345
3	1.9050
4	2.0781
5	2.0093
6	1.2017
7	2.4702
8	1.8210
Average	2.2182 ± 0.6656

Table S4. Height profiles across bisecting white lines of **P1$_{24k}$-SWNT** (Figure 3.5A).

P1$_{23k}$-SWNT	**Height (nm)**
1	1.6310
2	2.3447
3	1.5986
4	2.6359
5	2.1816
6	0.6881
7	4.3634
8	3.9649
Average	2.4260 ± 1.2288

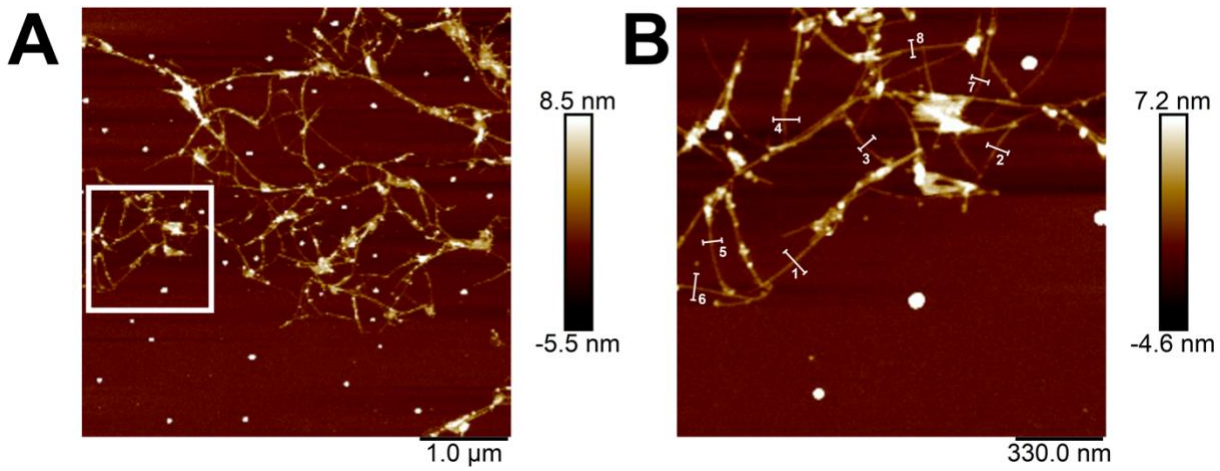

Figure S72. AFM images of **P3$_{13k}$-a-SWNT** at two magnifications, with the scale bar representing A) 1.0 µm and B) 330 nm. The white box denotes B.

Table S5. Height profiles across bisecting white lines of **P3$_{13k}$-a-SWNT** (Figure S72).

Index	Height (nm)
1	2.1668
2	1.5527
3	1.7887
4	1.8770
5	1.9672
6	1.6413
7	1.5246
8	1.8841
Average	1.8003 ± 0.2197

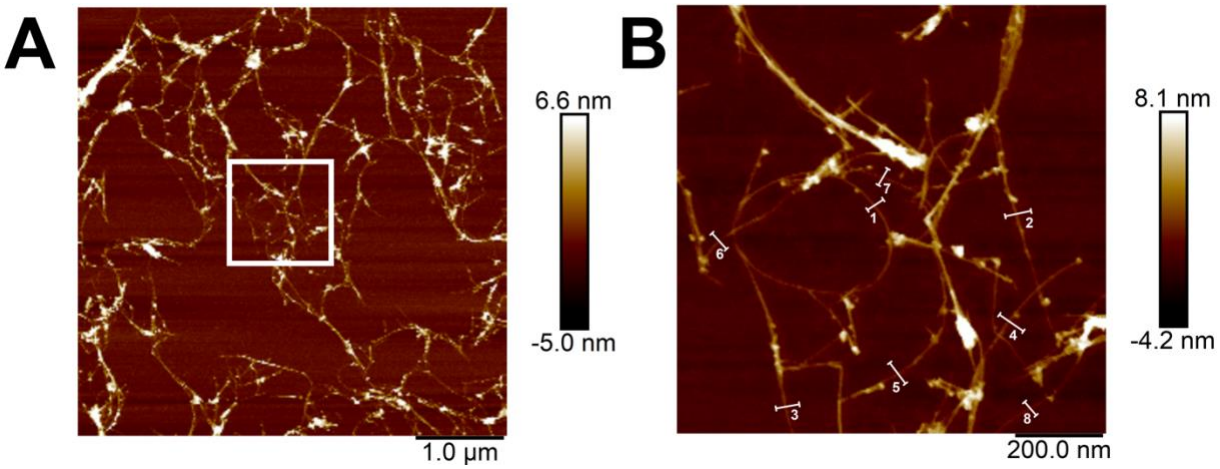

Figure S73. AFM images of **P3$_{24k}$-a-SWNT** at two magnifications, with the scale bar representing A) 1.0 µm and B) 200 nm. The white box denotes B.

Table S6. Height profiles across bisecting white lines of **P3$_{24k}$-a-SWNT** (Figure S73).

Index	Height (nm)
1	2.2690
2	2.1077
3	1.6969
4	1.7674
5	1.4704
6	1.2262
7	1.4875
8	1.4436
Average	1.6836 ± 0.3546

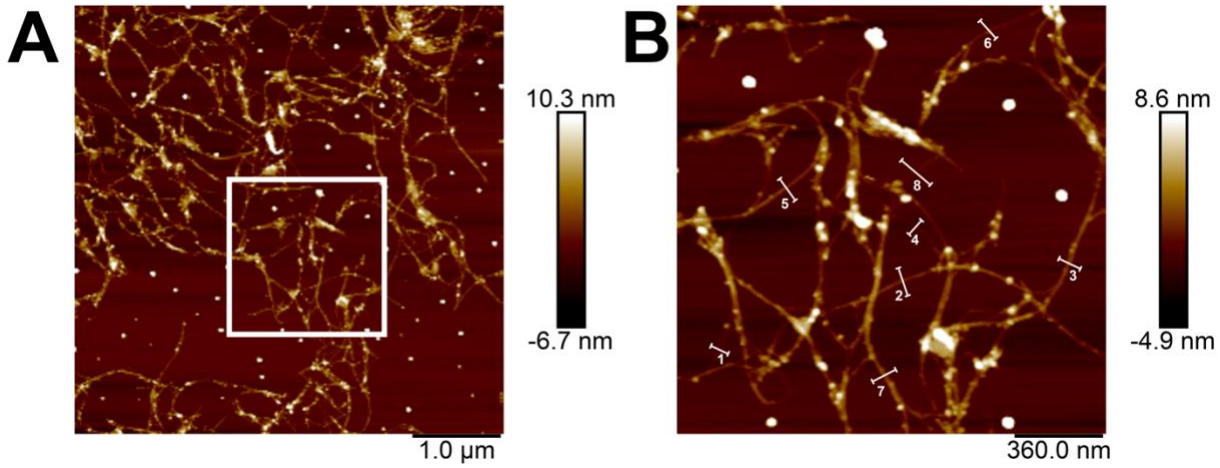

Figure S74. AFM images of **P3$_{13k}$-b-SWNT** at two magnifications, with the scale bar representing A) 1.0 µm and B) 360 nm. The white box denotes B.

Table S7. Height profiles across bisecting white lines of **P3$_{13k}$-b-SWNT** (Figure S75).

Index	Height (nm)
1	2.3977
2	2.7656
3	2.5626
4	1.9603
5	1.8281
6	1.3207
7	2.6312
8	2.0024
Average	2.1836 ± 0.4902

Table S8. Height profiles across bisecting white lines of **P1$_{24k}$-b-SWNT** (Figure 3.5B).

P3$_{23k}$-b-SWNT	Height (nm)
1	2.0883
2	1.4319
3	3.3716
4	1.7313
5	2.9174
6	1.4606
7	1.4247
8	1.3885
Average	1.97679 ± 0.7669

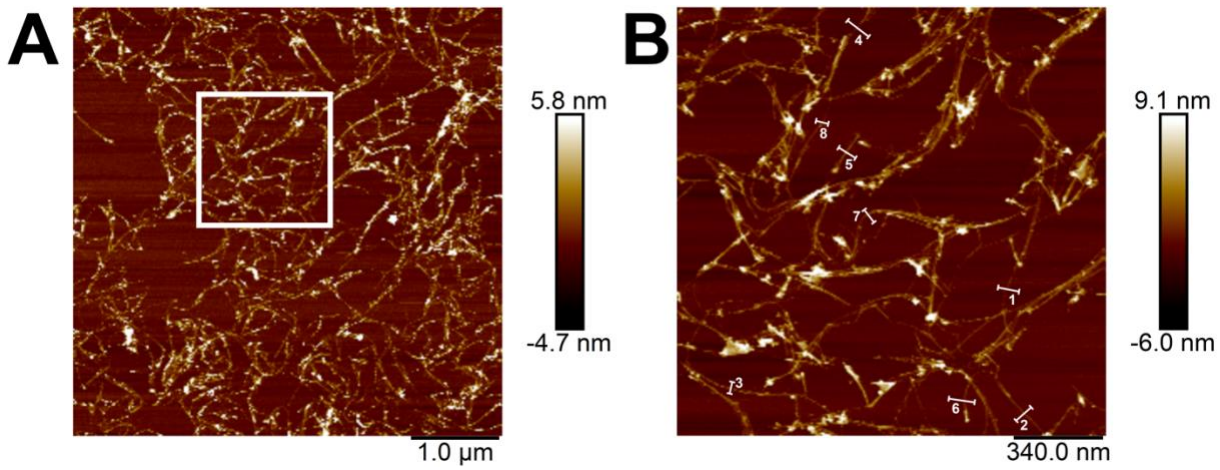

Figure S75. AFM images of **P3$_{13k}$-c-SWNT** at two magnifications, with the scale bar representing A) 1.0 µm and B) 340 nm. The white box denotes B.

Table S9. Height profiles across bisecting white lines of **P3$_{13k}$-c-SWNT** (Figure S76).

Index	Height (nm)
1	2.1675
2	1.8451
3	2.4060
4	2.1382
5	2.0762
6	2.0860
7	2.0850
8	1.6618
Average	2.05822 ± 0.2216

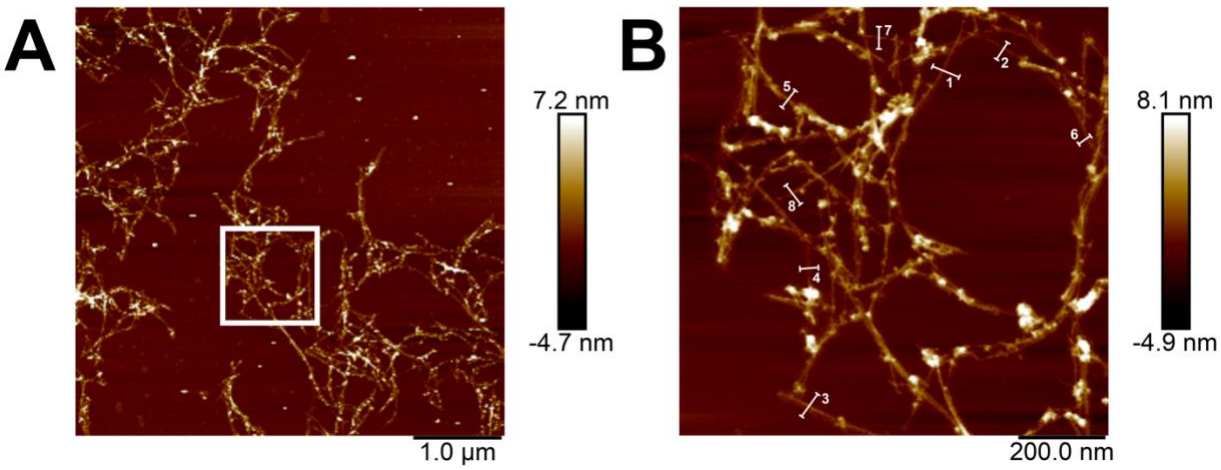

Figure S76. AFM images of **P3$_{24k}$-c-SWNT** at two magnifications, with the scale bar representing A) 1.0 µm and B) 200 nm. The white box denotes B.

Table S10. Height profiles across bisecting white lines of **P3$_{13k}$-c-SWNT** (Figure S77).

Index	Height (nm)
1	1.4592
2	2.3418
3	1.9563
4	1.7404
5	2.0947
6	2.1872
7	2.0498
8	2.0432
Average	1.9841 ± 0.2738

Photoluminescence Maps

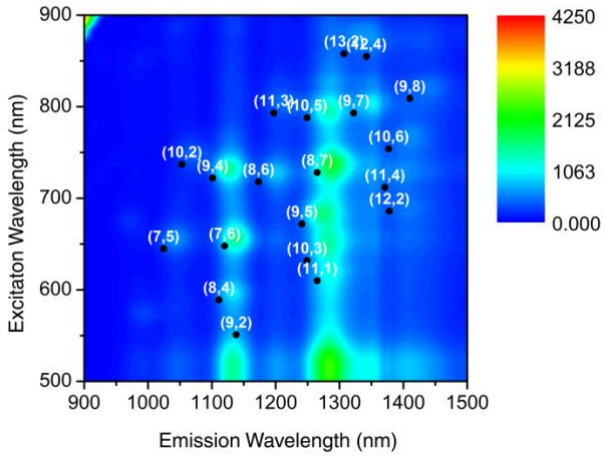

Figure S77. Photoluminescence mapping of **P1$_{13k}$-SWNT** in THF.

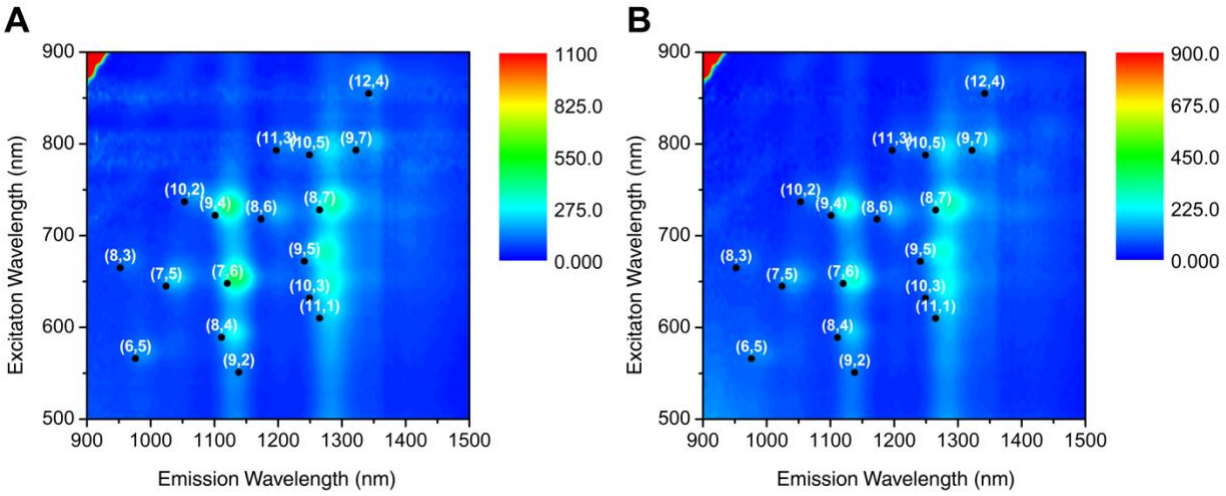

Figure S78. Photoluminescence mapping of A) **P3$_{13k}$-a-SWNT** and B) **P3$_{24k}$-a-SWNT** in THF.

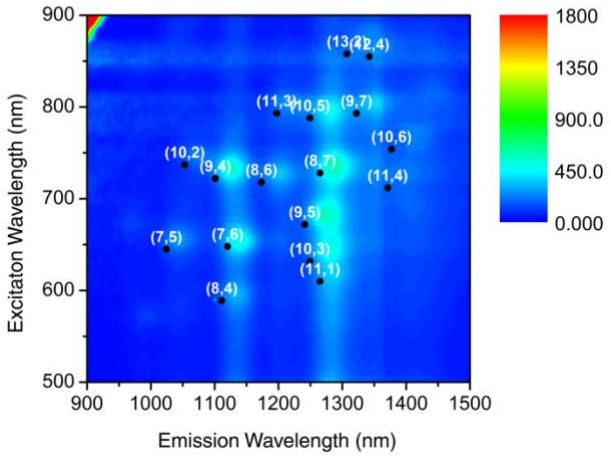

Figure S79. Photoluminescence mapping of **P3$_{13k}$-b-SWNT** in THF.

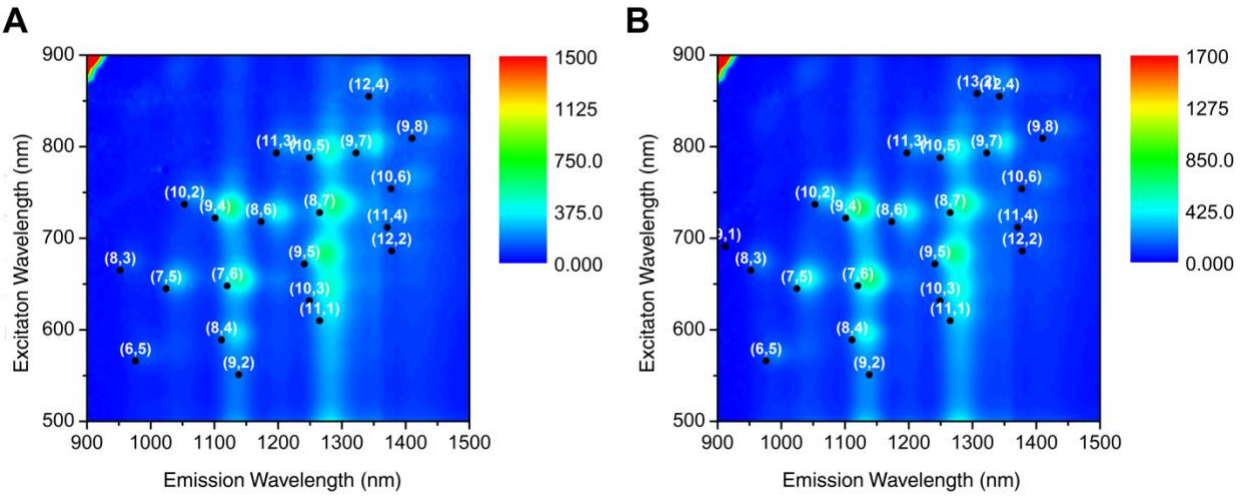

Figure S80. Photoluminescence mapping of A) **P3$_{13k}$-c-SWNT** and B) **P3$_{24k}$-c-SWNT** in THF.

General Procedure of Post-Dispersion Click with 9a

To a prepared dispersion of **P1$_{xxk}$-SWNT** in THF, **9a** (5.4 mg, 13.6 μmol - 1.5 eq to assumed 7.5 mg of polymer in solution) was added. The reaction was monitored using the Cary 5000 spectrometer in dual beam mode. For **P1$_{13k}$-SWNT**, the reaction was carried out in a 10 mm quartz cuvette equipped with a magnetic stir bar at rt. The reaction of **P1$_{24k}$-SWNT** was carried out in a 20 mL scintillation vial equipped with a magnetic stir bar and 200 μL aliquots of the solution were sampled, diluted with 600 μL of THF, and measured in a 10 mm quartz cuvette to prevent oversaturation of the detector. The dispersion was characterized by PL mapping, AFM, UV-Vis-NIR, and Raman spectroscopy.

General Procedure of Post-Dispersion Oxidation:

To the clicked dispersion of **P1$_{xxk}$-SWNT** with **9a**, 2,3-dichloro-5,6-dicyano-1,4-benzoquinone (DDQ) (2.1 mg, 9.4 μmol - 1.5 eq to assumed 7.5 mg of polymer in solution) was added and stirred for 6 h at rt in a 20 mL scintillation vial equipped with a stir bar. The dispersion was rinsed of excess DDQ by passing the solution through a 0.2 μm pore diameter Teflon membrane and rinsing with tetrahydrofuran until the filtrate contained no color or fluorescence when excited with a hand-held 365 nm UV lamp. The thin film leftover on the membrane was redispersed with tetrahydrofuran (10 mL) and characterized by PL mapping, AFM, UV-Vis-NIR, and Raman spectroscopy.

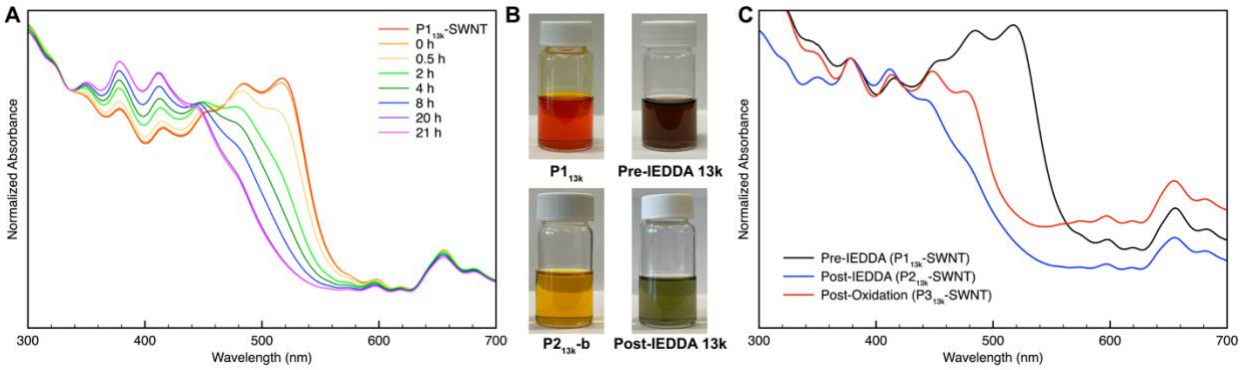

Figure S81. A) Monitoring reaction of post-dispersion modification **P1$_{13k}$-SWNT** with **9a** *via* UV-Vis, B) images of the polymers and polymer-SWNT sample pre- and post-IEDDA, and C) UV-Vis absorption spectrum overlay of the dispersion pre-IEDDA, post-IEDDA, and post-oxidation normalized at 378 nm.

Raman Spectra of Post-Dispersion Click with 9a and Oxidation

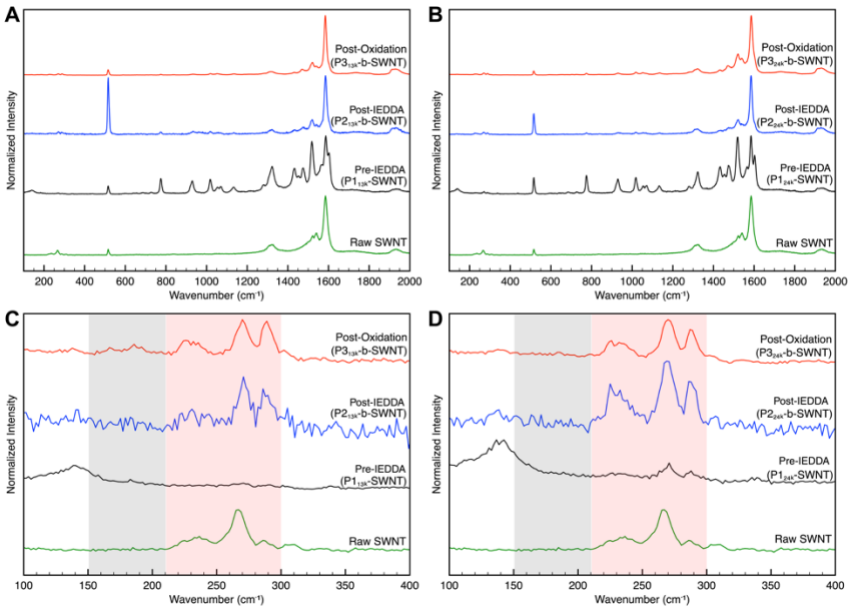

Figure S82. Full Raman spectra of raw SWNTs, pre-IEDDA, post-IEDDA, and post-oxidation on A) **P1$_{13k}$-SWNT**, B) **P1$_{24k}$-SWNT**, and RBM region of C) **P1$_{13k}$-SWNT** D) **P1$_{24k}$-SWNT**, excited at 532 nm.

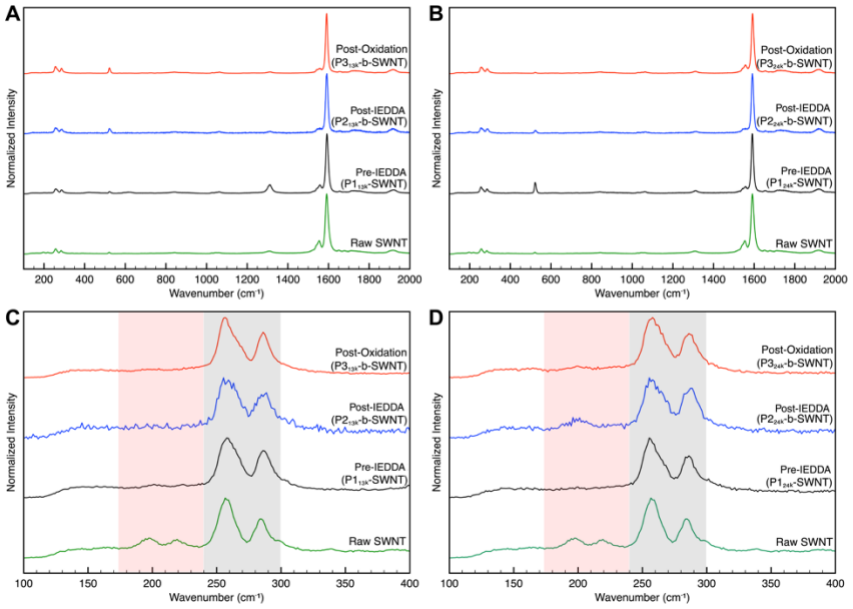

Figure S83. Full Raman spectra of raw SWNTs, pre-IEDDA, post-IEDDA, and post-oxidation of A) **P1$_{13k}$-SWNT**, B) **P1$_{24k}$-SWNT**, and RBM region of C) **P1$_{13k}$-SWNT** D) **P1$_{24k}$-SWNT**, excited at 633 nm.

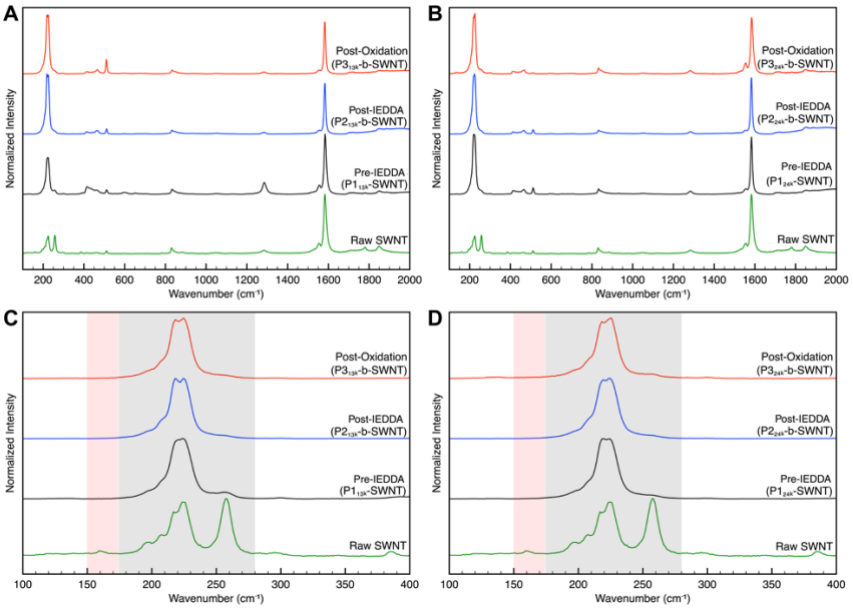

Figure S84. Full Raman spectra of raw SWNTs, pre-IEDDA, post-IEDDA, and post-oxidation of A) **P1$_{13k}$-SWNT**, B) **P1$_{24k}$-SWNT**, and RBM region of C) **P1$_{13k}$-SWNT** D) **P1$_{24k}$-SWNT**, excited at 785 nm.

AFM Data of Post-Dispersion Click with 9a and Oxidation

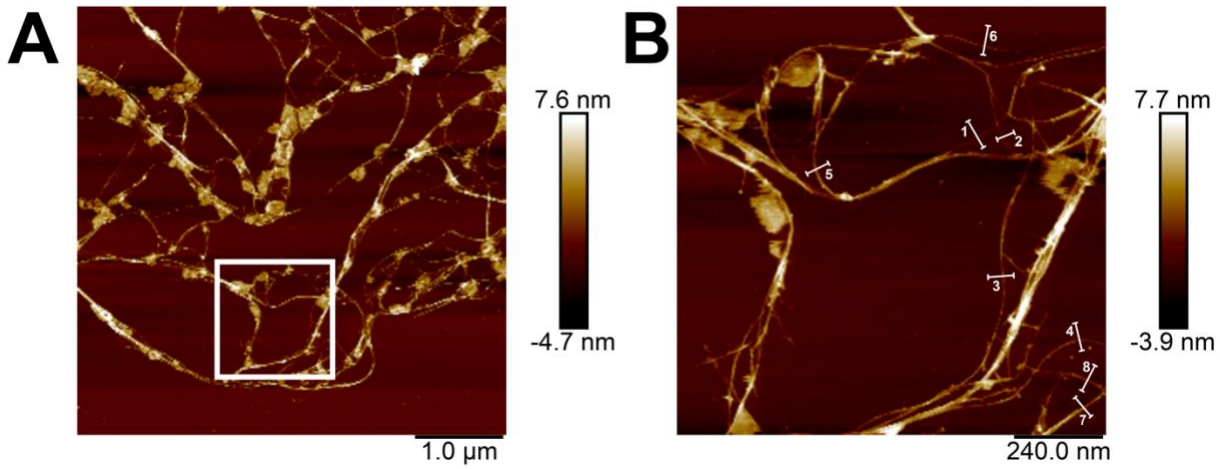

Figure S85. AFM images of post-dispersion clicked sample (**P3$_{13k}$-b-SWNT)** at two magnifications, with the scale bar representing A) 1.0 µm and B) 240 nm. The white box denotes B.

Table S11. Height profiles across bisecting white lines of **P3$_{13k}$-b-SWNT** (Figure S85).

Index	Height (nm)
1	3.2576
2	2.9743
3	2.8664
4	2.1432
5	2.9113
6	2.0707
7	2.6276
8	2.4048
Average	2.6570 ± 0.4212

Table S12. Height profiles across bisecting white lines of **P3$_{24k}$-b-SWNT** (Figure 3.8).

Index	Height (nm)
1	3.3098
2	2.1613
3	3.1051
4	2.9521
5	3.6064
6	2.6214
7	2.5593
8	1.6998
Average	2.7519 ± 0.6229

Photoluminescence Maps of Post-Dispersion Click with 9a and Oxidation

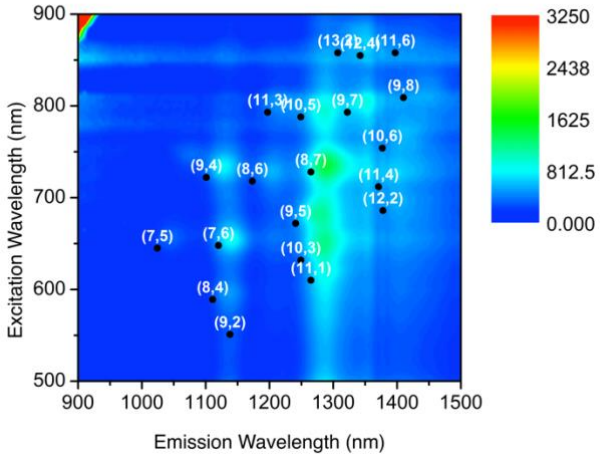

Figure S86. Photoluminescence mapping of post-dispersion click on **P1$_{13k}$-SWNT** (**P3$_{13k}$-b-SWNT**) in THF.